University of Alberta

Impact of gypsum supersaturated solution on the flotation of sphalerite

by

Meijiao Deng

A thesis submitted to the Faculty of Graduate Studies and Research
in partial fulfillment of the requirements for the degree of

Doctor of Philosophy
in
Chemical Engineering

Department of Chemical and Materials Engineering

Fall 2013
Edmonton, Alberta

Abstract

Gypsum supersaturation in process water is known to have detrimental effects on flotation performance of sulphide minerals. The motivation of this research is to develop a better understanding of the impact of gypsum supersaturation in process water on sphalerite flotation. For this purpose, this thesis focused on the impacts of gypsum supersaturation in process water on the surface properties of silica and sphalerite minerals, the interactions between flotation reagents and sphalerite, and the interactions between silica and sphalerite minerals in various types of process water.

Results from this study indicate that the adverse impact of gypsum supersaturation in process water on sphalerite flotation is mainly due to high calcium concentration in the gypsum supersaturated process water. This study shows that gypsum precipitates do not form or coat on silica and sphalerite mineral surfaces in the gypsum supersaturated solutions under the conditions studied. However, both silica and sphalerite mineral surfaces are coated by calcium after being conditioned in a gypsum supersaturated solution, resulting in identical surface charge between silica and sphalerite. The high calcium concentration in the gypsum supersaturated process water is found to retard the activation of sphalerite by copper and hence the subsequent xanthate adsorption. The adsorption of calcium ions is identified to compete with copper species for the reactive surface sites of sphalerite, resulting in the reduction in

copper and xanthate uptake and hence flotation recovery of sphalerite. Hetero-aggregation between gangue minerals (quartz or silica for example) and sphalerite minerals is induced in the gypsum supersaturated process water. Direct colloidal force measurement using an atomic force microscopy (AFM) shows attractive force profile between silica and sphalerite minerals in both gypsum supersaturated solution and calcium chloride solution containing a similar calcium concentration to that of the gypsum supersaturated solution. The extent of slime coating of silica nanoparticles on sphalerite surfaces is found to increase with the increase in calcium concentration. The retardation of sphalerite activation and subsequent xanthate adsorption, in combination with slime coating of gangue mineral particles results in poor recovery and selectivity in sphalerite flotation process.

Removing calcium ions by sodium carbonate addition can significantly offset the detrimental effect of gypsum supersaturated process water on the flotation performance of sphalerite. Micro-flotation of silica and sphalerite mixture minerals shows that the flotation recovery and selectivity of sphalerite are clearly improved after treating the gypsum supersaturated solutions with sodium carbonate.

Acknowledgements

I would like to express my sincere gratitude and appreciation to:

- My supervisors, Professor Zhenghe Xu and Professor Qingxia (Chad) Liu for imparting their support and guidance upon me during the course of this study.
- Professors Qi Liu and Hongbo Zeng for their generous help.
- All the research staff, personal and in particular Dr. Stephen Brienne of the Applied Research Technology (ART) Centre of Teck Resource Ltd. who were involved in the TDS project.
- Dr. Dimitre Karpuzov, Dr. Shihong Xu and Dr. Anqiang He, from the Alberta Centre for Surface Engineering and Science (ACSES) of the University of Alberta, for the provision of laboratory equipment and services.
- Dr. Allen Pratt, from CANMET Mining and Mineral Sciences Laboratories, Natural Resources Canada, for providing sphalerite samples and advice on XPS surface analysis.
- Mr. James Skwarok, Ms. Lisa Carreiro, Ms. Patricia Siferd, Ms. Shaiu-yin Wu, Ms. Jie Ru, Ms Ni Yang and Dr. David Harbottle for always being very accommodating and resourceful.
- Dr. Shengqun Wang and Dr. Luijie Yang for sharing their atomic force measurement (AFM) experience with me.
- Dr. Louxiang Wang, Ms. Natalie Kuznicki, Ms. Chendi Wu, Ms. Teresa Bisson, Ms. Erin Bobicki, Mr. Junmeng Li and all other fellow group members of the Oil Sands Research Group and C^{5}MPT.
- Teck Resource Ltd. and Natural Sciences and Engineering Research Council of Canada (NSERC) for continuing financial support.

Finally, to the special people of my life, my mother, father, Lee Plumb and other family, I extend my gratitude for your enduring support and understanding. It is to you that I dedicate this work.

Table of contents

Chapter 4 Impact of Gypsum Supersaturated Solution on the Uptake of Copper and Xanthate on Sphalerite 97

List of tables

List of figures

Chapter 1 Introduction

1.1 Water in mineral flotation

Flotation is one of the most widely used methods for ore beneficiation. In flotation, mineral particles are introduced to water, in which valuable minerals are separated from gangue minerals or other valuable minerals. In flotation circuits, water represents 80 - 85% of the volume of mineral pulp. The quality of the water, which is controlled by the source of water, dissolved minerals, and chemicals and surfactants deliberately added in the flotation process, plays an important role in the flotation process. In general, the better the water quality the more efficient is flotation.

Water consumption by mineral processing industry accounts for a very small proportion of the total water consumption. However, due to the limited freshwater resource and environmental regulations, the recycle of 'used' water become a common practice in mineral flotation. The use of recycle water normally leads to the built-up of salts and other surfactants, which alters the process water quality. The use of recycle water in flotation has significant effects on flotation recovery and selectivity. Specific effects of recycle water on the flotation performance of sulphide and non-sulphide minerals have been reported by many workers [1-20]. For instance, flotation of sulphides is affected in various degrees by the cationic and anionic species in process water [8]. The presence of certain heavy metal ions (e.g., Fe $^{2+}$ and Pb $^{2+}$) could have adverse impact on flotation as they precipitate sparingly soluble hydroxides and metal xanthates [13-15]. Meanwhile, organic matters present in the process water may affect flotation if the compounds are surface active or function as dispersants, flocculants or depressants. Generally, flotation in fresh water and recycle water produces different selectivity and recoveries. The use of plant recycle water usually decreases selectivity and recovery while increases reagent consumption [1, 2, 4, 5, 14, 17].

The reasons for reduced mineral flotation plant performance due to water recycling can be summarized as following:

1) The use of recycle water leads to the accumulation of organic and inorganic compounds in the process water as well as increased microbiological activities [3, 7, 12, 14, 18, 21].
2) The unrecognized and uncontrolled compounds may adsorb or precipitate on mineral surface, interfere with the adsorption of activators and collectors, and consume flotation reagents due to precipitation, resulting in the loss of recovery[1, 10 4, 5, 8, 10, 16, 17, 22-25].
3) Solid-liquid interfacial properties of mineral particles can be significantly affected by the conformation of adsorbed and precipitated layers [26-28].

4) Chemical reactions may occur between recycle water constituents and the chemical species present on the surface of mineral particles, which can play an important role in the adsorption of reagents [3, 15, 18, 21, 24].
5) The chemical and microbiological constituents of recycle water can have a significant effect on liquid-gas interfacial properties, which can strongly influence froth height, strength and stability during flotation [6, 22].
6) Dissolved chemical species such as calcium, magnesium, iron, copper, lead, zinc, nickel, sulphates, phosphates and carbonates can have a strong effect on the electrokinetic properties of oxide and sulphide minerals at certain pH ranges [4, 5, 16, 20, 29].
7) Interactions between minerals present in the ore can be altered due to the changed surface properties of mineral particles, leading to undesirable hetero-aggregation between valuable minerals and gangue minerals or slime coating. In addition, non-selective coatings on both valuable minerals and gangue can result in the loss of separation efficiency (selectivity) [1, 2, 5, 8, 23, 30].
8) Recycling of water also tends to accumulate very fine suspended particles. Excessive amounts of slimes in the process water can also have an adverse effect on mineral beneficiation processes [10].

1.2 Gypsum supersaturation in sulphide mineral flotation

In sulphide mineral flotation plants, in particular those practicing water recycling, high concentrations of calcium and sulphate ions are frequently experienced. In some process water, the calcium concentration exceeds 1000 ppm [31], and sulphate concentration can be as high as 2500 ppm [27, 28]. Calcium ions are mainly from the dissolution of calcium-containing minerals and the deliberate addition of lime as a pH modifier, pyrite depressant and water treatment reagent. The high concentration of sulphate in the process water of many sulphide flotation plants is mainly attributed to the oxidation of sulphur species and the addition of sulphate-containing chemicals. A few examples of gypsum supersaturation in process water of sulphide mineral flotation plants are given in the following.

1) Red Dog lead-zinc mine

In operation since 1989, Red Dog is a lead-zinc sulphide mine located in north western Alaska, approximately 145 kilometres north of Kotzebue. Operated by Teck Alaska Incorporated, a U.S. subsidiary of Teck Resources Limited, Red Dog has a production capacity of over 580,000 tonnes per annum of zinc contained in concentrate. It is one of the largest zinc mines in the world, both in terms of reserves and annual zinc production. The mine consists of: an open pit mine, a mill for processing ore, waste rock disposal areas, tailings impoundment, and support facilities. The mine uses conventional mining techniques to extract an average of 9800 tons of ore per day. The ore is pre-washed and then subjected to froth flotation where lead and zinc were recovered sequentially. Figure 1-1 schematically illustrates the lead-zinc flotation separation process at Red Dog. The ore is firstly crushed to - 150 mm in the primary crusher. The crushed ore is then feed to the grinding mills with fresh water and recycle water where the ore is further reduce to 80% - 65 µm. The slurry is then subjected to the lead flotation circuit where lead sulphide minerals are separated and zinc sulphate ($ZnSO_4$) is used to depress the zinc sulphide minerals (mostly sphalerite). The tailing from the lead flotation circuit is then reground to 80% - 20 µm and sent to the zinc flotation circuit where copper sulphate ($CuSO_4$) is used to activate the zinc sulphide minerals. The final tailing after the zinc flotation circuit is discharged to the tailing impoundment.

Red Dog mine recycles water from the tailings impoundment back into the flotation process. Prior to recycle back to the mill, water reclaimed from the tailings impoundment was treated using high density sludge (HDS) process where lime and flocculants are used (Appendix). Both reclaimed tailing water without HDS treatment (reclaim water) and HDS treated water (process water) contain high total dissolved solids (TDS) (~4000 ppm) which are supersaturated with respect of calcium and sulphate ions. The calcium and sulphate ion concentrations of Red Dog's reclaim water and process water are reported to 560 ppm (calcium) and 2861 ppm (sulphate), and 840 ppm (calcium) and 2466 ppm (sulphate), respectively. The pH of the HDS processed water and reclaimed tailings water are about 10 and 5.2, respectively, and the flotation separation process is conducted under near neutral pH (6.5 ~ 7). The HDS water treatment has been shut down since 2008 and water reclaimed from the tailings pond was directly recycled back to the mill. The plant survey in 2008 showed high TDS (3800 ~ 4100 ppm) and high concentrations of calcium (640 ~ 720 ppm) and sulphate (2400 ~ 2800 ppm) ions in the whole flotation circuits, which is most likely due to the recycled tailings water. Poor flotation recovery and selectivity has been noticed in the zinc circuit, though the flotation performance of the lead circuit has not been affected. It has been speculated that the poor flotation performance in the zinc circuit was attributed to the supersaturation of gypsum in the process water.

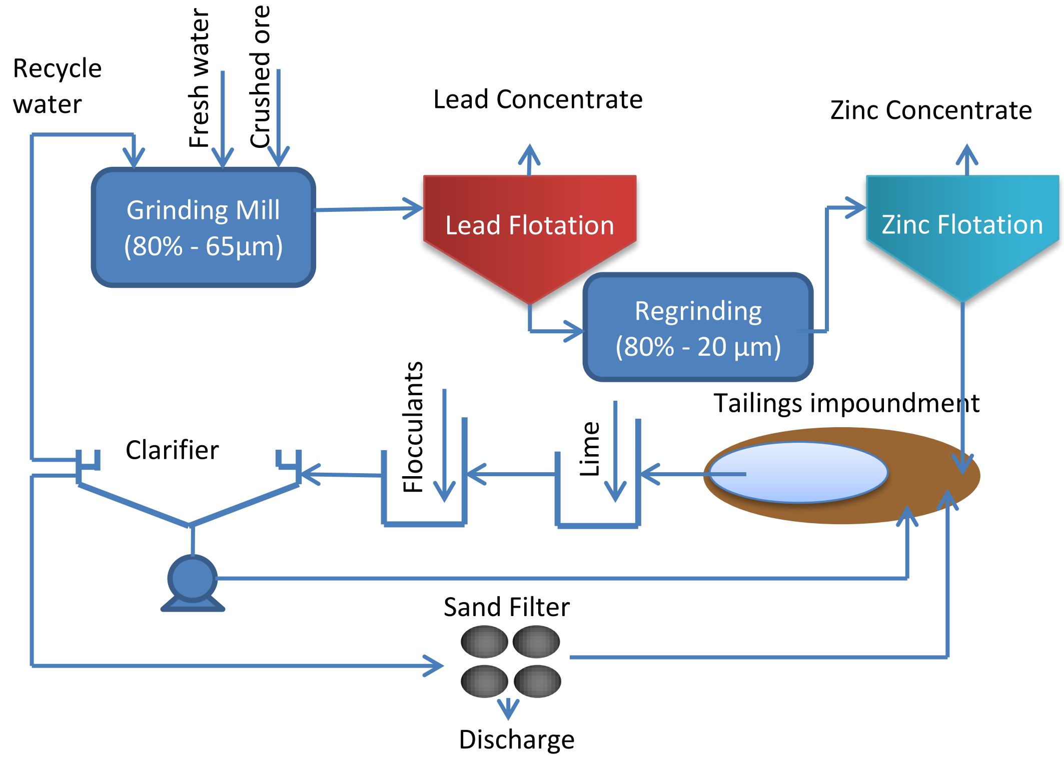

Figure 1-1 Schematic illustration of lead-zinc flotation separation process.

2) Hilton concentrator

The Hilton deposit of Mount Isa Mines Limited is located twenty kilometers north of Mount Isa, in north-western Queensland, Australia. The lead and zinc in the Hilton ore occur as galena and sphalerite. Pyrrhotite is the predominant iron sulphide minerals in the hanging wall, whereas pyrite is the predominant iron sulphide mineral in the footwall ore. Non-sulphide gangue minerals include silica, alumino-silicates, and dolomite. The concentrator produces separate products of lead, zinc and a combined lead/zinc concentrate. The plant flowsheet is shown in Figure 1-2. Lead and zinc flotation at Hilton concentrator is carried out under alkaline conditions where lime is added to adjust pH and depress the sulphide gangues such as pyrrhotite and pyrite. The calcium and sulphate concentrations in the flotation pulp are around 600 ppm and 2800 ppm, respectively. Poor flotation response has been reported in both lead and zinc circuit, which has been related to the gypsum supersaturation in the process water.

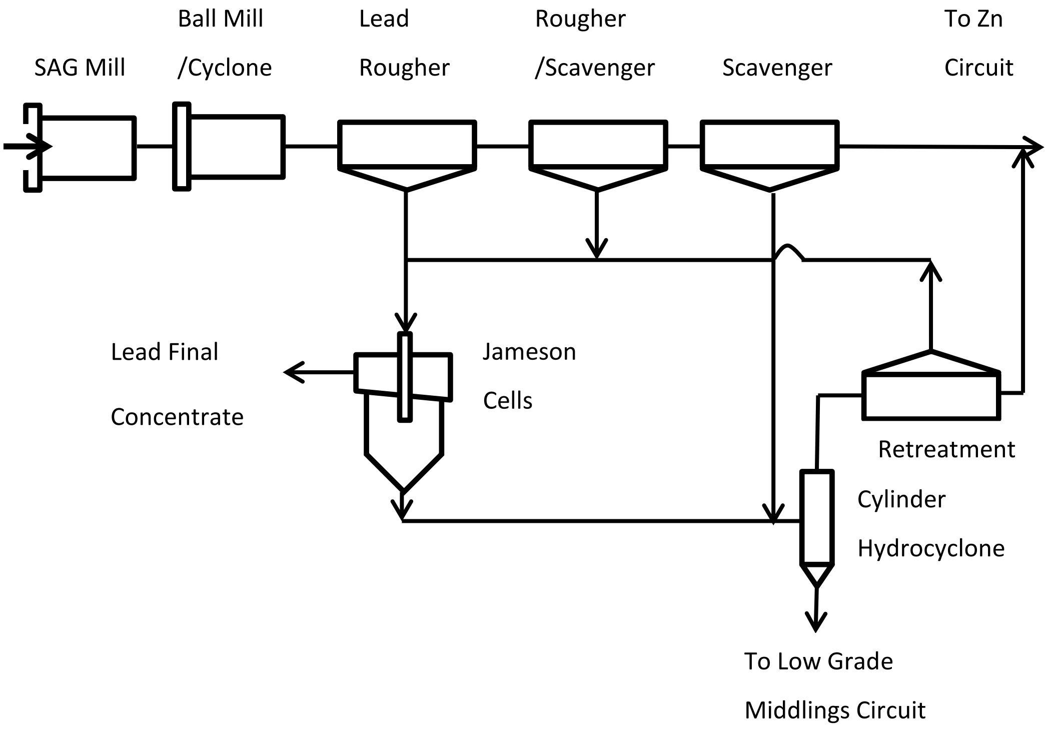

Figure 1-2 Hilton concentrator flowsheet [28].

1.2.1 Adverse impact of gypsum supersaturation in process water on sulphide mineral flotation

High concentrations of calcium and/or gypsum supersaturation in the process water can have significant effects on the flotation performance of sulphide minerals. It has been reported that while lime was used to adjust the pulp pH to a value of 11 in order to depress pyrite it caused problems in the flotation of galena [32]. Flotation of chalcopyrite was depressed in an alkaline pH when lime was used as a pH modifier or when calcium ions were present in the pulp [33]. An extensive investigation of the Hilton concentrator (Mount Isa Mines, Australia) suggested that flotation rate of galena was retarded due to the precipitation of gypsum from the process water [28]. A reduction in selectivity in sphalerite flotation has also been reported at Brunswick Mining Concentrator which has been related to the slime coating of gypsum precipitates. Flotation recovery and selectivity problems of sphalerite at the lead-zinc concentrator has been speculated to be attributed to the gypsum supersaturated process water. The high concentrations of calcium and sulphate ions in mineral process medium (water) have been a persistent concern in sulphide mineral flotation practice. The previous studies mainly focused on the following aspects: 1) effect of calcium ions; 2) $CaSO_4$ scaling on mineral surface; 3) Soda ash addition.

1) Calcium effect

James and Healy investigated the adsorption of calcium and cobalt ions on silica substrate surface [34]. They found that the adsorption of calcium ions onto a silica substrate surface increased abruptly within the pH range of 9 to 10. Gandin and Charles observed an increase in the adsorption density of calcium ions onto a pyrite surface with increasing dissolved oxygen concentration, pH and calcium ion concentration [35]. The adsorption of calcium ions at the ZnS-H_2O interface was studied by Moignard et al. [36] using direct adsorption and micro-electrophoresis techniques. Moignard's study showed that the adsorption of calcium at ZnS-H_2O interface was pH dependent with a significant adsorption commencing at approximately pH 7 and increasing up to pH 11. The adsorption of calcium on mineral surface altered the surface charge of the minerals and the interactions between mineral-flotation reagents, and mineral-mineral particles. Moignard [36] showed that the zeta potential of zinc sulphide particles became less negative in the presence of calcium ions and this effect became more prominent with increasing calcium ions concentration. Similar effects were observed on silica[37], sphalerite[20, 38] and galena [4] minerals.

It was suggested by Moignard [36] that the uptake of calcium ions at ZnS-H_2O interface might hinder the activation of sphalerite. However, the study carried out by Dr. Finch's group at McGill University illustrated no change of copper and xanthate uptake in the presence of calcium (500 ppm) and magnesium (120 ppm) ions [39]. Their pure mineral flotation results indicated that the sphalerite flotation recovery was only reduced at pH above 10 in the presence of calcium ions. It is noticed that, in that study, the sphalerite mineral was conditioned in calcium solution and then transferred to the flotation reagents solutions (in the absence of calcium). This procedure may not be able to represent the real flotation system since in the real flotation practice all ions present in the process medium at the same time. It is possible that the adsorbed calcium ions desorb from the interface, underestimating its adverse impact on the uptake of copper or xanthate on sphalerite.

Meanwhile, the presence of calcium ions impacts the surface charge of minerals, which influences the interactions between minerals. The impact of calcium ions on the interactions between silica and sphalerite at various pHs has been investigated [40]. The results suggested the enhancement of hetero-aggregation of silica and sphalerite at a high pH in the presence of calcium ions while they were well dispersed in the absence of calcium ions. The interaction forces between sphalerite and silica particles were reported to be attractive below pH 8 and decrease with increasing solution pH, and finally become repulsive at pH 10 [41]. The addition of calcium ions has been reported to enhance the attraction force between the two minerals at pH 6 while reducing the repulsive force at pH 10.

2) Gypsum scaling

Another possible factor that gypsum supersaturation in the process water has adverse impact on the flotation performance of sulphide minerals is surface coating of gypsum either by nucleation or hetero-aggregation. Gypsum precipitates were detected on the surface of galena sample from the Hilton concentrator [26, 27]. It has been implied that the flotation rate of galena was retarded due to the presence of an overlayer of precipitated gypsum. The precipitates were speculated to deposit on mineral surface due to hetero-coagulation. Lauder et al. [42] studied the significance of water quality on the flotation performance of sphalerite at Hilton concentrator. He concluded that the sphalerite flotation performance was diminished by the deposition of gypsum onto the surface of the sphalerite. Cullinan [43] found that the flotation of fine size galena mineral was affected after grinding in calcium sulphate supersaturated process water. The adverse effect of calcium sulphate supersaturated process water on fine galena flotation increased with finer particle size. The fine galena flotation was also affected by the pulp temperature. A higher temperature during grinding promoted fine galena depression in the presence of calcium sulphate saturated water. It was concluded by Cullinan that calcium sulphate might precipitated onto galena surface during grinding. Xu and Finch inquired silica and sphalerite mineral surface properties in Ca-SO_4-CO_3 system using zeta potential measurement and surface analysis techniques [30, 37, 38]. However, their results demonstrated no trace of gypsum precipitates on mineral surfaces. They found that the zeta potentials of silica and sphalerite in calcium and Ca-SO_4 solutions were similar. The adsorption of calcium in the electric double layer on mineral surface was believed to be responsible for the lower recovery and poor selectivity of sulphide mineral flotation in the gypsum saturated process water.

3) Soda ash addition

The adverse impact of gypsum supersaturation can be offset by the addition of sodium carbonate or bicarbonate. Grano and his coworkers [26] have shown that the flotation response of galena in the lead roughing and scavenging sections of Hilton Concentrator has been improved significantly with the addition of 4 kg/t of soda ash to the SAG mill. Surface analysis revealed that the concentration of calcium on galena mineral surface decreased during the soda ash plant trial. However, the concentration of sodium carbonate should also be controlled [32].

Further increase in carbonate concentration could lead to the formation of a lead basic carbonate, $Pb_3(OH)_2(CO_3)_2$, which results in the decomposition of the hydrophobic lead xanthate. Significant improvement in zinc recovery and grade, with improved selectivity of sphalerite versus pyrite, was also observed by Lauder at the Hilton Concentrator when approximate 3 to 4 kg/t of soda ash were added to the downstream regrind tower mill [42]. The addition of soda ash increased the pulp pH and reduced the levels of calcium in solution [27, 42]. Due to the solubility difference between calcite ($K_{sp} = 10^{-8.3}$ at 298 K) and gypsum ($K_{sp} = 10^{-4.6}$, at 298K) [44], the formation of calcite favours over that of gypsum in the presence of carbonate. The carbonate reacts with calcium to form calcite which precipitates from solution, as shown in the following Equation:

$$Ca^{2+} + CO_3^{2-} \rightarrow CaCO_3 \downarrow \tag{1-1}$$

Sui et al.[38] confirmed the preferential formation of insoluble calcite over calcium sulphate at carbonate concentrations greater than 10^{-2} M and at a calcium concentration of 3×10^{-2} M (Table 1-1).

Through zeta potential determinations, Sui et al.[38] showed that increasing carbonate usage made the zeta potential of the sphalerite more negative, approaching those of the sphalerite samples in a simple supporting electrolyte solution under the same pHs. Rashchi et al.[37] observed similar effects in their study of silica in the presence of carbonate and calcium ions. The effect of carbonate addition on the changes in the zeta potential of silica was attributed to the formation of calcite precipitates which scavenged calcium ions. The removal of calcium ions enhanced the interaction of collector and activating agents with mineral surfaces which therefore improved the floatability of the minerals, as was shown in a plant testing of soda ash addition to a zinc rougher circuit [45]. It was noted by Grano [27] that calcite precipitates and galena mineral particles were mutually repelled. In other studies, however, calcium carbonate did not appear to disperse completely as some precipitates remained on the mineral surfaces [37, 38].

Table 1-1 Percentage distribution of calcium upon addition of CO_3 for initial $[Ca] = 3 \times 10^{-2}$ M and $[SO_4] = 5 \times 10^{-2}$ M [38].

Form of Ca	Concentration of CO_3 M		
	3×10^{-3}	3×10^{-2}	1×10^{-1}
As free metal ions	27.7	1.6	0
Precipitated with CO_3^{2-}	9.8	96.7	99.8
Precipitated with SO_4^{2-}	41.5	0	0
Bound with SO_4^{2-}	18.2	1.5	0
Bound with NO_3^-	2.8	0.2	0
Total	100.0	100.0	99.8

1.3 Objectives

Considerable studies have been carried out in order to understand flotation performance of sulphide minerals in the gypsum supersaturated process water.

However, mechanisms of the depression action of gypsum supersaturation on sulphide minerals are still not clear. The objective of this research work is to develop a better understanding of the impact of gypsum supersaturated process water on the flotation performance of zinc sulphide minerals. Laboratory prepared gypsum supersaturated solutions are used to represent the gypsum supersaturated process water. Sphalerite and silica are used to represent the zinc sulphide minerals and silicate gangue minerals, respectively. This research focuses on the following four phases:

1) Study the impact of gypsum supersaturated process water on the surface properties of sphalerite and silica minerals

In process water with supersaturation of gypsum, crystals of gypsum are believed to precipitate out. The gypsum precipitates may coat on the mineral surface either by nucleation or hetero-aggregation which can alter the surface properties of the minerals, hence affecting the flotation performance of the minerals. In this study the impacts of gypsum supersaturated process water on the surface properties of silica and sphalerite are studies using zeta potential distribution measurement, quartz crystal microbalance with dissipation (QCM-D), and surface characterization techniques such as scanning electron microscopy (SEM), X-ray photoelectron spectroscopy (XPS) and Auger electron spectroscopy (AES). The aim of this phase of study is to answer the following two questions: 1) whether the gypsum crystals nuclear on silica and sphalerite mineral surfaces in the gypsum supersaturated process water or not; 2) If not, whether the gypsum precipitates hetero-aggregate with silica or sphalerite minerals.

2) Study the impact of gypsum supersaturated process water on the interactions between flotation reagents and sphalerite

Sphalerite flotation generally involves activation and then thio collector adsorption. In order to fully understand the adverse effects of gypsum supersaturated process water on the flotation of sphalerite, it is important to recognise the impacts of gypsum supersaturated water on the interactions between flotation reagents and sphalerite mineral. In this study, copper sulphate and sodium isopropyl xanthate (SIPX) are used as activator and collector respectively. The uptake of copper and xanthate on sphalerite surface in gypsum supersaturated solutions and 800 ppm calcium solutions are investigated.

3) Study the impact of gypsum supersaturated process water on the interactions between sphalerite and silica minerals

The interactions between mineral particles play an important role in the mineral flotation separation. The homo-aggregation of fine target mineral particles is desirable while the hetero-aggregation between the target mineral and gangue mineral particles is detrimental for the selective flotation separation. In this study, the impact of the calcium ions, magnesium ions and gypsum supersaturated solutions on the interactions between silica and sphalerite is studied using QCM-D and AFM force measurements. The purpose of this study is to examine systematically the effect of divalent ions (calcium and magnesium) and gypsum supersaturated water on the interactions between zinc sulphide and silica minerals. QCM-D is used to evaluate the deposition behaviour of silica nanoparticles onto ZnS coated quartz crystal surface over a broad range of divalent ions concentrations and gypsum supersaturated solutions. To better understand the interactions between silica and zinc sulphide minerals in the presence of calcium ions, magnesium ions, and gypsum supersaturated solutions, the colloidal forces between a silica particle and a fractured sphalerite mineral surface are measured. AFM results and predictions based on DLVO theory are employed to verify the QCM-D observations.

4) Study the potential approaches to eliminate the adverse impact of gypsum supersaturated process water on the flotation performance of sphalerite

In this study, the following three approaches of eliminating the adverse impact of gypsum supersaturated process water on the flotation of sphalerite are investigated and evaluated: 1) addition sodium carbonate to remove calcium ions and to convert gypsum supersaturated solution to calcite supersaturated solution; 2) increase the dosage of flotation reagents; 3) Conditioning the minerals with flotation reagents prior to exposing in the gypsum supersaturated process water (pre-hydrophobic treatment). Micro-flotation was conducted to evaluate the potential of those approaches in improving the flotation performance of sphalerite in gypsum supersaturated solutions.

1.4 Literature review

1.4.1 Gypsum precipitation

Calcium sulphate precipitation is a well-documented phenomenon encountered in a wide spectrum of industrial processes and applications such as those involving heat exchange [46-48], mineral processing[27, 49], desalination of seawater by reverse osmosis [50, 51] etc. There are three main forms of calcium sulphate: calcium sulphate dihydrate or gypsum ($CaSO_4 \cdot 2H_2O$), calcium sulphate hemihydrate ($CaSO_4 \cdot 1/2H_2O$), and calcium sulphate anhydrite ($CaSO_4$) [52, 53]. The solubility of different forms of calcium sulphate decreases with increasing temperature [54-58] (Figure 1-3), a fact that is responsible for the formation of calcium sulphate scale on heat exchanger surfaces [59]. Studies on calcium sulphate scale mainly focussed on the kinetics of scale formation [60-72] and the influence of external factors [66, 73-82]. The formation of $CaSO_4$ scale is affected by various factors including fluid hydrodynamics, supersaturation level, solution chemistry, surface chemistry and topography as well as temperature [47, 59, 83-85].

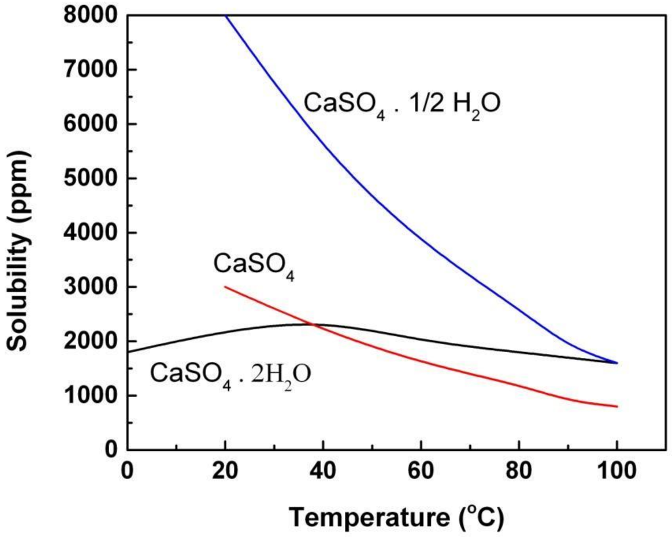

Figure 1-3 Solubility of calcium sulphate in water as a function of temperature (Data from Seidell and Linke[86], Marshall and Slusher[87], and Silcock[88]).

1.4.1.1 Supersaturation and driving force for nucleation

Supersaturation refers to a solution in which the concentration of solute exceeds the saturation value at a given temperature and pressure. Supersaturation can be induced by changing temperature, evaporating of solvent, changing solvent composition, and chemical reaction [89]. Some common expressions describing supersaturation are defined by Equations (1-2) – (1-4) [90]:

$$\Delta C = C - C_S \tag{1-2}$$

$$S = \frac{C}{C_S} \tag{1-3}$$

$$\sigma = \frac{C - C_S}{C_S} = S - 1 \qquad (1\text{-}4)$$

where C is the solute concentration, C_S is the solubility value, ΔC is the concentration driving force, S is the supersaturation states, and σ is the relative supersaturation.

The above definitions of supersaturation assume that the solutions are ideal despite the fact that they consist of mixtures of electrolytes and additional nonelectrolytes. The definitions are only correct for very dilute solutions that the activity coefficients can be assumed to be unity. For the cases deal with solutions with high concentrations, the concentrations must be replaced by activities. In the calcium sulphate systems, the supersaturation states is commonly defined as the ratio of the activity products divided by the thermodynamic solubility product of gypsum (K_{SP}) [60, 91, 92], which was calculated considering the liquid-solid equilibrium between Ca^{2+} and SO_4^{2-} ions and solid $CaSO_4 \cdot 2H_2O$.

$$Ca^{2+} + SO_4^{2-} + 2H_2O \leftrightarrow CaSO_4 \cdot 2H_2O \qquad (1\text{-}5)$$

$$S = \frac{a_{Ca^{2+}}\, a_{SO_4^{2-}}\, a_w^2}{K_{SP}} \qquad (1\text{-}6)$$

where K_{SP} is the thermodynamics solubility product, a_i is the activity product of species i; a_w is the activity of water.

The driving force for the formation of gypsum is the change in the Gibbs free energy (ΔG) for going from the supersaturated solution to equilibrium. For the formation of one mole of gypsum, the change in the Gibbs free energy (ΔG) is given by [90]

$$\Delta G = -RTlnS \tag{1-7}$$

where R is the gas constant and T is temperature in Kelvin.

1.4.1.2 Precipitation kinetics

Traditionally, nucleation is divided into primary homogeneous nucleation, primary heterogeneous nucleation and secondary nucleation. In primary homogeneous nucleation, nuclei are produced in the absence of foreign bodies. Primary heterogeneous nucleation is induced by surfaces other than those of the crystallizing substance. Secondary nucleation may occur in the presence of crystals of the material being crystallized.

1) Homogeneous nucleation

Homogeneous nucleation describes the spontaneous formation of critical nuclei within the supersaturated solution. In homogeneous-primary nucleation, formation of a new solid phase takes place in the absence of any solid phase. According to the classical nucleation theory, the formation of a new phase is initiated by the generation of a very fine embryo within bulk supersaturated solution. A stable nucleus can be formed by the addition of each embryo unit (A) successfully and reach a critical cluster size: $A_1 + A = A_2$, $A_2 + A = A_3 \ldots A_{n-1} + A = A_n$

(critical cluster). Figure 2-4 schematically illustrates the homogeneous formation of the clusters of n molecules.

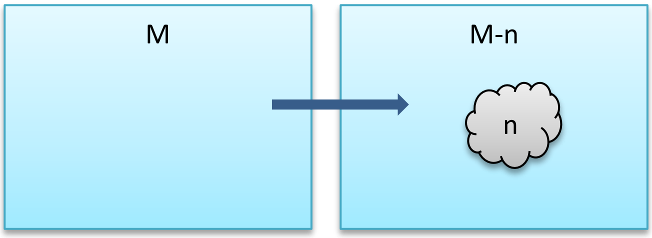

Figure 1-4 Schematic illustration of the homogeneous formation of a cluster of n molecules from a bulk supersaturated solution with M Molecules

The free energy change in the formation of a crystal in a homogeneous solution is usually expressed as Eq. 1-8 [93]:

$$\Delta G^{hom} = -\alpha \frac{L^3 \Delta\mu}{V_m} + \beta L^3 \gamma_{sl} \tag{1-8}$$

where α and β are the volume and geometrical shape factors, respectively, $\Delta\mu$ is the chemical potential difference between the two phases, L is the size of the crystal, V_m is the molecular volume, and γ_{sl} is the interfacial tension between solid and liquid phases. The geometrical shape factor, β ($= 4s^3/27V^2$ where s and V are the surface area and the volume of the nucleus), can be equal to 16π/3, 50, or 4 assuming spherical, rectangular parallelepiped, or cubic-shaped nuclei, respectively. The dependence of Gibbs free energy on L passes through a maximum corresponding to the critical size L*.

$$L^* = \frac{2}{3}\frac{\beta\gamma_{sl}V_m}{\alpha\Delta G} \qquad (1\text{-}9)$$

Substitution of L^* into Eq. 1-8 yields the change in the Gibbs free energy during critical nucleus formation [90]:

$$\Delta G_{crit}^{hom} = \frac{4}{27}\frac{\beta^3 V_m^2 \gamma_{sl}^3}{\alpha^2 k^2 T^2 lnS} \qquad (1\text{-}10)$$

where k is the Boltzmann constant, T is temperature in Kelvins, and S is the supersaturation states.

The nucleation rate, J_{hom} ($cm^{-3}\ S^{-1}$), or the number of nuclei formed per unit time and volume, can be expressed in the form of the Arrhenius reaction velocity equation:

$$J_{hom} = A\exp\left(-\frac{\Delta G_{Crit}^{hom}}{kT}\right) \qquad (1\text{-}11)$$

where A is the pre-exponential factor and k is the Boltzmann constant. Replacing ΔG_{Crit}^{hom} with Eq. 1-10 gives:

$$J_{hom} = A\exp\left(-\frac{4}{27}\frac{\beta^3 V_m^2 \gamma_{sl}^3}{\alpha^2 k^3 T^3 lnS}\right) \qquad (1\text{-}12)$$

Equation 1-12 clearly suggests that the homogeneous nucleation rate increases with increasing supersaturation and temperature, and decreases with increasing surface energy. In practice, precipitation does not occur instantaneously upon the creation of supersaturation in a solution. The period of time between the creation of supersaturation and the formation of the newly created crystals is called induction period.

2) Heterogeneous nucleation

Certain solid bodies (containing heterogeneities, motes, inclusions, etc.) extraneous to the system and promote phase transformation, particularly condensation and crystallization. Heterogeneous nucleation occurs in presence of a suitable foreign body or surface which induces nucleation at degrees of supersaturation lower than those required for spontaneous homogeneous nucleation (Figure 1-5).

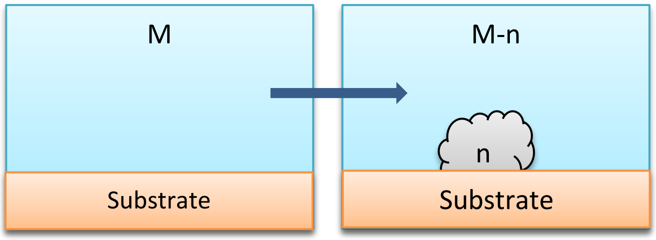

Figure 1-5 Schematic illustration of the heterogeneous formation of a cluster of n molecules on the surface of a substrate from a bulk supersaturated solution with M Molecules.

The overall free energy change associated with the formation of a critical nucleus under heterogeneous conditions is [90]

$$\Delta G_{crit}^{het} = \varphi \Delta G_{crit}^{hom} \qquad (1\text{-}13)$$

where the factor φ can be expressed as [94]

$$\varphi = \frac{(2+\cos\theta)(1-cos\,\theta)^2}{4} \tag{1-14}$$

where θ is the contact angle between the crystalline deposit and the foreign solid surface, corresponding to the angle of wetting in a liquid-solid system (Figure 1-6).

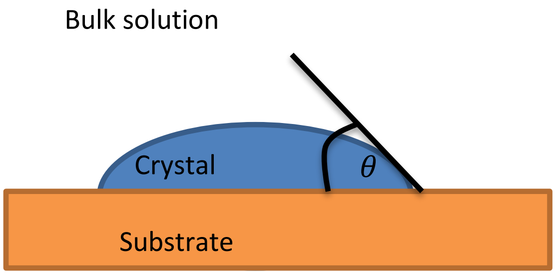

Figure 1-6 Expression of contact angle at foreign surface (substrate)-crystal-bulk solution interface.

Avoiding the contact angle model based only on the wetting of the solid surface, heterogeneous nucleation can be expressed as [95]

$$\Delta G_{crit}^{het} = \frac{\beta V_m(\gamma_{cl})^3}{k^2T^2ln^2S}\frac{\gamma_{sc}-(\gamma_{cl}+\gamma_{sl})}{\gamma_{cl}} = \frac{\beta V_m(\gamma_{cl})^2}{k^2T^2ln^2S}[(\gamma_{sc}-(\gamma_{cl}+\gamma_{sl})] \tag{1-15}$$

where the superscripts l, s, and c refer to the liquid, critical nucleus and catalytic solid, γ_{sc} and γ_{sl} are the interfacial energy between catalytic solids-critical nucleus, and catalytic solids-liquid interface.

And the nucleation rate [95],

$$J_{het} = A\exp\left(-\frac{\Delta G_{Crit}^{hem}}{kT}\right) \tag{1-16}$$

3) Surface and interfacial energy

Surface energy commonly refer to a condensed phase – vapour system, whereas interfacial energy is used to describe two condensed phases, such as liquid – liquid and solid – liquid interfaces. Clearly, interfacial energy plays an important role in the interpreting of precipitation kinetics.

The interfacial energy γ_{ij} between phase i and phase j can be obtained using the van Oss-Chaudhury-Good equation [96]:

$$\gamma_{ij} = \left(\sqrt{\gamma_i^{LW}} - \sqrt{\gamma_j^{LW}}\right)^2 + 2\left(\sqrt{\gamma_i^{+}\gamma_i^{-}} + \sqrt{\gamma_j^{+}\gamma_j^{-}} - \sqrt{\gamma_i^{+}\gamma_j^{-}} - \sqrt{\gamma_i^{-}\gamma_j^{+}}\right) \quad (1\text{-}17)$$

where γ^{LW} is the Lifshitz-van der Waals surface tension component, γ^{+} is the Lewis acid or electron-acceptor parameter, γ^{-} is the Lewis base or electron-donor parameter, which can be calculated from the contact angle measurements.

$$\gamma_l(1 + \cos\theta) = 2\left(\sqrt{\gamma_s^{LW}\gamma_l^{LW}} + \sqrt{\gamma_s^{+}\gamma_l^{-}} + \sqrt{\gamma_s^{-}\gamma_l^{+}}\right) \quad (1\text{-}18)$$

To determine the surface energy component and parameters of a solid, the contact angle must be determined with at least three probing liquids, and two of which must be polar [97-99].

1.4.2 Sphalerite activation and flotation

Sphalerite is a major source of zinc metal. It usually associates with other sulphide minerals such as pyrite, galena, and chalcopyrite. The concentration of sphalerite is commonly accomplished by froth flotation using short chain thiol collectors such as xanthate. Unlike other sulphide minerals, sphalerite responses poorly to short-chain xanthates and other soluble thiol collectors without activation. There are several explanations for the relatively weak interaction between sphalerite and short chain xanthate [100-102]. The most frequently cited reason is the high solubility of zinc-thiol compounds in water in comparison with other metal-thiol compounds (Table 1-2). The flotation of sphalerite with thiol collectors is usually accomplished by activation with heavy metal ions, usually copper ions. The activation products (CuS-like species) can then react with xanthate to form insoluble copper-xanthate species, which make the sphalerite mineral surface hydrophobic.

Table 1-2 Logarithm of the solubility products of some thiol collectors and hydroxides [103].

Ligand	Zinc (ll)	Lead (ll)	Copper (l)
Ethyl xanthate	-8.31	-16.77	-19.28
Butyl xanthate	-10.43	N/A	-20.33
Hexyl xanthate	-12.90	N/A	N/A
Octyl xanthate	-15.82	N/A	-23.06
Ethyl dithiophosphate	-1.82	-11.12	-15.85
Hydroxide	-16.79	-16.09	-14.7

1.4.2.1 Activation mechanisms

The activation of sphalerite has been studied extensively by many researchers over several decades. In 1976, Finkelstein and Allison [104] reviewed the research work related to the activation conducted in 50 years. Twenty years later, Finkelstein [105] gave another thorough survey on the same topic and updated the literatures. Chandra and Gerson [106] also presented a comprehensive literature review on the fundamentals of copper activation of sphalerite and pyrite in 2009. These three papers have been used as primary source for the literature survey summarized in the following.

1) In acidic conditions

It is generally accepted that the copper activation of sphalerite in acidic pH follows an ion exchange mechanism with copper replacing surface zinc ions resulting in copper sulphide-like surfaces. The overall activation reaction is generally represented by the following equation [103]:

$$ZnS_{(s)} + Cu^{2+}_{(aq)} \rightarrow CuS_s + Zn^{2+}_{(aq)} \qquad (1\text{-}19)$$

The adsorption of Cu^{2+} results in an approximately 1:1 release of Zn^{2+} into the solution [105, 107]. Cu^{2+} on the sphalerite surface is subsequently reduced to Cu^{+} with the resulting oxidation of the surface sulphide. The thiol collectors then react with the copper sulphide species formed on the surface, increasing the flotation response. Sphalerite activation by copper at acidic conditions is believed to be a two-stage process, with the first stage follows logarithmic law and the second stage follows parabolic law [103, 108, 109].

2) In neutral and alkaline conditions

Previous studies on the mechanisms of sphalerite activation in neutral and alkaline conditions lead to obscured conclusions due to the involvement of copper hydrolysis products. Girczys et al. [110] proposed the following activation mechanism for sphalerite at neutral and alkaline conditions:

At neutral pH:

$$Zn\text{–}OH_{surface} + Cu(OH)^{+}_{aq} \leftrightharpoons Zn\text{–}O\text{–}Cu^{+}_{surface} + H_2O \tag{1-20}$$

At alkaline pH:

$$ZnS + 2OH^{-} \leftrightharpoons \left|Zn(OH)_2 + S\right|^{2-}_{surface\ state} \tag{1-21}$$

$$\left|Zn(OH)_2 + S\right|^{2-}_{surface\ state} + Cu^{2+}_{aq} \leftrightharpoons Zn(OH)_2 + CuS_{surface} \tag{1-22}$$

This mechanism has been criticised by Ralston and Healy, who believed that the activation of sphalerite in alkaline conditions is better represented by the following reactions [111]:

(1) A rapid bulk precipitation of $Cu(OH)_{2(ppt)}$ followed by adsorption/coagulation on the ZnS surface and/or a rapid surface $Cu(OH)_2$ nucleation resulting in a

ZnS surface partially or completely covered by $Cu(OH)_2$. Some hydrolysis of Zn^{2+} to $Zn(OH)^+$ is expected.

$$Cu_{aq}^{2+} + 2OH^- \leftrightharpoons Cu(OH)_{2(ppt)} \tag{1-23}$$

(2) A slow surface reaction between $Cu(OH)_2$ and ZnS . Zn_{aq}^{2+} is formed when the pH is not high enough to form $Zn(OH)_2$ solids. When the pH is high enough, $Zn(OH)_2$ will be formed.

$$Cu(OH)_{2(ppt)} + ZnS_s \leftrightharpoons (Zn, Cu)S_s + Zn_{aq}^{2+} + 2OH^- \tag{1-24}$$

$$Cu(OH)_{2(ppt)} + ZnS_s \leftrightharpoons (Zn, Cu)S_s + Zn(OH)_{2s} \tag{1-25}$$

or

(3) A slow dissolution of $Cu(OH)_2$ to yield ${Cu_{aq}}^{2+}$ followed by a simple exchange reaction (i.e. Eq. 1-19)

$$Cu(OH)_{2(ppt)} \leftrightharpoons Cu_{aq}^{2+} + 2OH^- \tag{1-26}$$

Prestidge et al. [112] studied the activation of synthetic sphalerite at pH 9 using different concentrations of copper nitrate. Using conventional XPS, they found that the sphalerite surface were coated with $Cu(OH)_2$ at high copper concentrations. Similar results were also found by Gerson et al. [113] and Fornasiero and Ralston [114]. According to Prestidge et al.[112], the activation of sphalerite in alkaline conditions can be represented as following:

$$nZnS_{(s)} + xCu(OH)_{2(ppt)} \rightarrow (ZnS)_n \cdot xCu(OH)_{2(surface)} \tag{1-27}$$

The Cu (ll) from the hydroxide may then exchange with the Zn(ll) from the sulphide.

$$(ZnS)_n . x\ (Cu(OH)_{2(surface)} \rightarrow\ Zn_n - xCu_x\ \cdot xZn(OH)_{2(surface)} \qquad (1\text{-}28)$$

The resulting Cu(ll) sulphide then undergoes redox disproportionation to form Cu(l) sulphur products which may then form Cu(l)-xanthate upon collector addition [114].

Some researchers [115, 116] believe that the copper hydroxide on the surface directly interacts with the xanthate. The resulting product then decomposes to form Cu(l)-xanthate and dixanthogen on the surface.

$$Cu(OH)_{2(surface)} + 2EX^-_{aq}\ \rightarrow\ Cu(EX)_{2(surface)} + 2OH^-_{aq} \qquad (1\text{-}29)$$

$$2Cu(EX)_{2(surface)}\ \rightarrow 2CuEX_{surface} +\ (EX)_{2(surface)} \qquad (1\text{-}30)$$

1.4.2.2 Factors affecting the flotation and activation of sphalerite

Factors such as copper concentration, activation time, pH, surface charge, extent of pre-oxidation, water and surface contaminants, pulp potential and galvanic interactions are important for copper activation of sphalerite and the sequent flotation.

1) Typical copper concentrations used for activation and flotation studies of sphalerite are in the range from 1×10^{-6} M to 1×10^{-4} M [111, 116-119]. The copper

concentration needed to achieve maximum flotation response depends on the activation conditions, origin of the mineral samples and available surface area for activation. Fornasiero and Ralston [114] found that the flotation response of sphalerite decreased with increased copper concentration, with the maximum reduction at pH 8.5 - 10.

2) Increasing activation time leads to an increase in copper uptake on sphalerite with subsequent increase in the release of Zn^{2+} [117]. However, increased copper uptake may not be beneficial for the surface xanthate adsorption [116]. Meanwhile, increase time delay between copper addition and xanthate addition decreases the amount of collector adsorbed onto the sphalerite surface at high pH (9.2) but not at neutral or mildly acidic pH [118].
3) The flotation of sphalerite is highly pH-dependent. It has been shown that the activated sphalerite had lower water contact angles in neutral pH region than in acidic and basic solutions [120]. Through flotation tests, Steininger [121] demonstrated that the flotation of activated sphalerite is suppressed at the pH range of 6 to 9, depending on the amount of $CuSO_4$ added. Steininger [121] observed that the pH range of depression increased with the increased $CuSO_4$ addition. Similar results were found by Laskowski and his co-workers [111].
4) Natural sphalerite normally contains iron. The presence of iron decreases the band gap of sphalerite and affects its reactivity 125. Previous studies have shown that the iron content in the sphalerite minerals influenced the activation and subsequent flotation behaviour of sphalerite; however,

contradictory results have been reported. Chandra and Gerson 106 summarized the activation and flotation studies of sphalerite with different iron and lead content conducted over the past two decades, as shown in Table 1-3.

Table 1-3 Effect of iron and lead content on the activation of sphalerite [106].

Sample (size µm)	Fe content %	Pb content %	Activator (time)	Collector	pH	Conclusion	Ref
Synthetic (N/A)	0 5 40	Not present	$^{64}CuSO_4$ (N/A)	N/A	8	Increase in Fe causes decrease in Cu adsorption	122
Synthetic (N/A)	0 5 40	Not present	$CuSO_4$ (20 min)	Ethyl xanthate	6 8 10	Increase in Fe reduces xanthate adsorption due to lower Cu adsorption	123
Natural (N/A)	33* 115*	0.2* 24*	$CuSO_4$ (1 h)	N/A	9.2	Cu uptake by high Fe sample was less than for the low Fe sample	114
Natural (125-200)	0.38 12	0.04 0.20	$CuSO_4$ (N/A)	SIPX	N/A	Fe rich sphalerite adsorbed more Cu and preferentially binds to xanthate	122
Natural	Fe rich	N/A	$CuSO_4$ (1 min)	SIPX	10 12	Fe inhibited initial Cu activation but catalyzed covellite formation upon xanthate addition	114
Natural -45	0.3 12.5	0.07 0.24	$CuSO_4$ (2 min)	SIPX	11	Fe was detrimental to copper activation and reduced collector adsorption	124
Natural Fresh (110) surface	0.02 to 14.79	N/A	$CuSO_4$ (1 h)	N/A	5	Fe enhance Cu adsorption	125

* Values reported as atomic ratios (×10^3) of metallic impurity elements to zinc
SIPX: Sodium isopropyl xanthate

5) The sphalerite surface preparation for activation and the pro-oxidation of the surface can affect the uptake of copper and sequence xanthate adsorption. Solecki et al. [122] showed that the surface oxidation prior to activation has a significant effect on copper adsorption onto the sphalerite. He found that the uptake of copper and xanthate on unoxidized sphalerite surfaces was much higher than oxidized sphalerite surfaces for both high and low iron content. Gigowski et al. [102], on the other hand, found that copper activation of sphalerite surfaces was more influenced by iron content rather than by the degree of surface oxidation.

6) Sphalerite activation and flotation involves electrochemical reactions. Maust and Richardson [102] are the pioneers who took into consideration of the electrochemical nature of the activation process. They proposed that theoretically for a particular metal ion to be an activator, it must act as an electron acceptor so that it can be reduced as following: $M^{n+} + e \rightarrow M^{(n-1)+}$.

7) Contaminants on mineral surface and in process water can also have significant effects on the sphalerite activation process. Surface slime coating or metal ions adsorption could block the reactive sites on sphalerite mineral

surface which can influence the activation efficiency and mineral hydrophobicity.

1.5 Organization of this thesis

This thesis consists of seven chapters.

Chapter 1: This chapter provides the background and the objectives of this study. Water recycling in mineral flotation process and gypsum supersaturation in sulphide mineral flotation are briefly introduced. Previous studies on the impact of gypsum supersaturation in process water on the flotation performance of sulphide minerals, activation and flotation of sphalerite, and the kinetics of gypsum precipitation are reviewed.

Chapter 2: This chapter describes the materials and research techniques used in this study. The fundamentals and operation procedures of experimental work are provided.

Chapter 3: This chapter focus on the impact of gypsum supersaturated solution on the surface properties of silica and sphalerite pure minerals. The effect of calcium ions, sulphate ions and gypsum supersaturated solution on the zeta potential distributions of silica and sphalerite is investigated. Changes in surface properties of silica and sphalerite minerals before and after conditioning in a gypsum supersaturated solution are examined by SEM, XPS, AES and QCM-D.

Results presented in this chapter answer the questions of whether gypsum precipitates form on mineral surfaces or in the bulk gypsum supersaturated solution, and whether the minerals hetero-aggregate with gypsum particles in the gypsum supersaturated solution.

Chapter 4: This chapter discusses the impact of gypsum supersaturated solution on the interactions between flotation reagents and sphalerite minerals. The impact of calcium ions, gypsum supersaturated solution and gypsum suspension on the uptake of copper and xanthate on sphalerite is studies.

Chapter 5: This chapter examines systematically the effect of divalent ions (calcium and magnesium) and gypsum supersaturated water on the interactions between zinc sulphide and silica minerals using QCM-D deposition measurement and AFM direct force measurement. The impact of calcium ions, magnesium ions, and gypsum supersaturated water on the flotation selectivity of sphalerite from silica was discussed.

Chapter 6: This chapter explores the potential approaches to eliminate the adverse impact of gypsum supersaturated solution on the flotation performance of sphalerite. There methods are examined and evaluated using micro-flotation tests.

Chapter 7: This chapter summarizes the overall conclusions, major contributions of this work and suggestions for future work.

Chapter 2 Materials and Experimental Techniques

2.1 Materials and reagents

High purity sphalerite and silica minerals were used to represent the zinc sulphide and silicate gangue minerals, respectively. The sphalerite mineral samples were purchased from Ward's Natural Science Establishment. X-ray fluorescence (XRF) spectrometer analysis indicate that the sphalerite sample contained 66.36% Zn, 32.27% S, and trace amounts of Fe (0.25%), Al (0.26%) and Si (0.06%). The sphalerite sample was crushed to - 4.75 mm and then dry ground to - 45 μm and stored in deep freezer at -20 °C. Silica particles of three size fractions (15 nm, 5 µm and 40 µm, 98% pure) were purchased from US Silica. Silica microspheres from Polysciences Inc. (Warrington, PA, USA) were used for the modifying of AFM tips. A two-component epoxy (EP2LV, Master Bound, Hackensack, USA) was used to glue the silica microspheres to the tip of AFM cantilevers. Silica wafer with (001) orientation was purchased from NanoFab (University of Alberta, Canada). The silica wafers were cut into 15 mm × 15 mm squares. A mixture of 70 vol% sulfuric acid and 30 vol% hydrogen peroxide solution of 85 °C was used to clean the silica wafers, followed by a thorough washing with Milli-Q water and ethanol. Quartz crystal sensors with coating of either ZnS or silica were purchased from Q-Sense. Prior to the experiments, the

ZnS sensors were cleaned with diluted HCl solution (pH 2) in a sonication water bath for 30 min following with thoroughly rinsing with Milli-Q water. Silica sensors were exposed under UV O-zone for 15 min followed by cleaning in 2% sodium dodecyl sulphate (SDS) solution in a sonication water bath for 30 min and then rinsed with Milli-Q water for at least three times.

The following reagents used in the experiments were A.C.S. reagent grade: hydrochloric acid, HCl (Fisher Scientific); sodium hydroxide, NaOH (Fisher Scientific); copper sulphate, $CuSO_4 \cdot 5H_2O$ (Fisher Scientific); calcium carbonate, $CaCO_3$ (Sigma Aldrich); calcium sulphate, $CaSO_4$ (Acros Organics); calcium sulphate dihydrate, $CaSO_4 \cdot 2H_2O$ (Fisher Scientific); sodium carbonate, Na_2CO_3 (Sigma Aldrich); potassium chloride, KCl (Fisher Scientific), Sodium dodecyl sulphate (SDS, Sigma Aldrich). Sodium isopropyl xanthate (SIPX: $(CH_3)_2$-CH_2-O-CS_2Na) from Prospec Chemicals, Canada was used as collector. The commercial grade SIPX was purified by dissolving in warm acetone (40°C), recrystallization and washing with acetone for three times. The purified SIPX was stored in deep freezer at - 20°C. Commercial grade calcium sulphate hemi-hydrate from US Gypsum Corporation was used as supplied. Milli-Q water prepared with an Elix-5 with a Millipore-UV plus unit (Millipore, Canada) was used throughout the experiments.

2.2 Solution and suspension preparation

2.2.1 Solution preparation

Laboratory gypsum saturated or supersaturated solution, calcite saturated solution, and simulated process water were prepared.

The gypsum saturated solution was prepared by dissolving 4 grams of calcium sulphate in 1L of Milli-Q water that was adjusted to pH 10. The mixture was stirred with a magnetic stirrer at room temperature for one hour, and was then filtered with a 1.6 μm filter to remove undissolved solids. The solids were collected and dried for the determination of the total dissolved solids concentration. The total dissolved solids concentration of the prepared solution determined by this method is around 2500 ppm. Atomic absorption analysis indicated that the solutions contained about 600 ppm calcium, which translates to 2580 ppm gypsum (solubility of gypsum in water is 2400 ppm at 25℃ [58]).

A similar procedure was used to prepare the gypsum supersaturated solution with calcium sulphate hemi-hydrate ($CaSO_4 \cdot 1/2H_2O$). In this case, 10 grams of calcium sulphate hemi-hydrate was dissolved in 1L of Milli-Q water. The pH value of the solution was maintained at 10. The mixture was stirred at room temperature for 30 min, and was then filtered with a 1.6 μm filter to remove undissolved solids. Atomic absorption analysis results indicate that the calcium concentration in the gypsum supersaturated solution is 845 ppm, which translates to 3612 ppm gypsum as compared to the solubility of gypsum in water to be 2400 ppm at 25℃ [58]. The calcium concentration in this laboratory gypsum supersaturated solution is similar to that in the process water of a Pb-Zn Mine (840 ppm).

Calcite-saturated solutions were prepared using an approach similar to that described above. 0.5 g of calcium carbonate (solubility in water: 12 mg/L at 25 ℃, 20 mg/L at 100 ℃) was added to 1 L Milli-Q water and then heated to 100 ℃. The mixture was stirred for one hour before being subjected to hot filtration to remove un-dissolved solids. The calcium concentration of the calcite saturated solution determined by AAS was 20 ppm. A fresh solution was prepared for each day of testing. The pH of calcite saturated solution was adjusted to pH 10.

The simulated process water was created by adding calcium sulphate hemi-hydrate (3.6157 g), potassium sulphate (0.0751 g), magnesium sulphate pentahydrate (0.5983 g) and sodium sulphate (0.1854 g) in 1 L Milli-Q water. The solution was allowed to mix for 30 minutes at room temperature. The pH was adjusted to 10 and maintained using NaOH. The solution was then filtrated with a 1.6 μm filter. The composition of the simulated process water is shown in Table 2-1.

Calcium and magnesium solutions were made by dissolving calcium chloride and magnesium sulphate pentahydrate in Milli-Q water respectively.

Table 2-1 Main composition of the simulated process water

	pH	Ca	K	Mg	Na	SO_4
		ppm				
Simulated Process Water	9.7	870	37	66	72	2400

Stock solutions of 10^{-2} M copper sulphate pentahydrate and 10^{-2} M SIPX were prepared in DI water. The stock solutions were diluted with other prepared solutions such as DI water, 10^{-2} M KCl, 800 ppm calcium, gypsum supersaturated solution, to make 1.25×10^{-5} M copper and 1.25×10^{-5} M SIPX concentration. The pH of the solutions was adjusted to 6.5.

All solutions were prepared freshly prior to each set of experiments.

2.2.2 Suspension preparation

Stock suspensions of silica, sphalerite, and gypsum were prepared. The silica stock suspension was prepared by adding 1 gram of silica (- 5 μm or 15 nm) to 50 mL Milli-Q water. For preparation of sphalerite stock suspension, 1 gram of fine sphalerite (- 45 μm) was further ground to - 5μm and then transferred to a beaker with 50 mL Milli-Q water. A fresh sphalerite stock suspension was prepared for each testing. The gypsum stock solution was prepared by adding 1 gram of calcium sulphate dihydrate ($CaSO_4\cdot2H_2O$, - 2 μm or - 265 nm) in 50 mL gypsum saturated solution.

2.3 Zeta potential measurement

2.3.1 Principle of zeta potential measurement

Electrokinetic phenomena are a group of effects that are observed in disperse systems and in capillaries. There are four distinct effects depending on the way in which motion is induced. Electro-osmosis and electrophoresis are the electrokinetic phenomena that entail the movement of one phase relative to another under the influence of an applied electric field. The production of a sedimentation potential, or the Dorn effect, and the production of a streaming potential are the electrokinetic phenomena of a potential difference in the direction of the relative movement of phases that is due to mechanical forces. Any of these electrokinetic phenomena can be used to determine the zeta potential or electrokinetic potential [126, 127].

Measurement of the velocity of the particles under a known external field gives information about their net electric charge, or their surface potential with respect of the bulk of the suspending phase. This technique is called electrophoresis. When the solid remains stationary and the liquid movies in response to an applied electric field this is called electro-osmosis. It occurs when the solid is in the form of a capillary or a porous plug which is filled with liquid. The applied field acts upon the charges in the liquid, and as they move in response to the field they drag the liquid along with them. Measurement of the velocity of the liquid, or the volume of liquid transported per unit current flow gives information about the net surface charge or the electrical potential in the neighbourhood of the wall. Instead of applying an electric field to cause liquid to move through a capillary of porous plug, one can force the liquid through a pressure gradient. The excess charges near the wall are carried along by the liquid and their accumulation down-stream causes the build-up of an electric field which drives an electric current back against the direction of the liquid flow. The measured potential difference across the capillary or plug is called the streaming potential. Finally, if a suspension of charged particles is allowed to settle, the resulting particle motion causes the development of a potential difference between the upper and lower parts of the suspension, which gives rise to the sedimentation potential.

2.2.3 Zeta potential distribution measurement with Zetaphoremeter

Zeta potential distributions were measured using a ZETAPHOREMETER IV equipped with a rectangular quartz electrophoresis cell, a pair of reversible hydrogenated palladium electrodes, laser illumination, and a digital video capture system operated through a Canon microscope. The ZETAPHOREMETER IV measures the zeta potential of colloidal particles by electrophoresis technique. The microscope offers a very sharp 1.07 μm depth of focus for accurately viewing particles in a stationary layer with little background interference. The system also employs sophisticated image analysis software which allows for accurate location of the stationary layers, measurement of electrophoretic mobility, and computation of the corresponding zeta potential distributions. The system outputs histograms of zeta potential distributions computed from mobility measurements using the Smoluchowski equation [128].

Zeta potential distribution measurements have been recently used to study the interactions between two different particles by comparing the zeta potential distribution of the mix of the two different components with that of the single material system [129-132]. Figure 2-1 schematically illustrates the zeta potential distribution analysis technique in explaining the interactions between two distinct particles in a binary system. As shown in Figure 2-1a, each suspensions of particle A and B gives a zeta potential distribution of their own with corresponding peaks at ζ_A and ζ_B when measured separately. When mixing the two particles together under the same conditions, the measured zeta potential distributions of the mixture depend on the characteristics of the interactions between the two types of particles. If there is no aggregation between particle A and B, a zeta potential distribution with two peaks centered at almost the same position of the individually measured zeta potential distributions of particle A and B is anticipated (Figure 2-1b). In the case that particle A and particle B strongly aggregates, a single zeta potential distribution peak would be observed (Figure 2-1c and 2-1d). The position of the peak depends on the particle A to particle B ratio. In the case of weak aggregation between particle A and B, a zeta potential distribution with tri-modal peaks or a broad distribution is anticipated as shown in Figure 2-1e and 2-1f. The advantage of the zeta potential distribution measurement technique is that tests are performed in situ, avoiding complex changes that arise when the minerals are dried, as required for most ex situ characterizations. In this study, zeta potential distribution measurements were applied to study the impact of gypsum supersaturation in process water on the mineral surface properties, interactions between minerals and gypsum scaling on mineral surfaces. It has to be noted that the capability of using zeta potential distribution measurement to evaluate the interactions between two different types of particles is limited by the electrokinetic characteristics of the particles as well as the physicochemical conditions that the measurement is taken. Distinct zeta potentials between the two particles are required to successfully apply the zeta potential distribution measurement for interpreting the interactions.

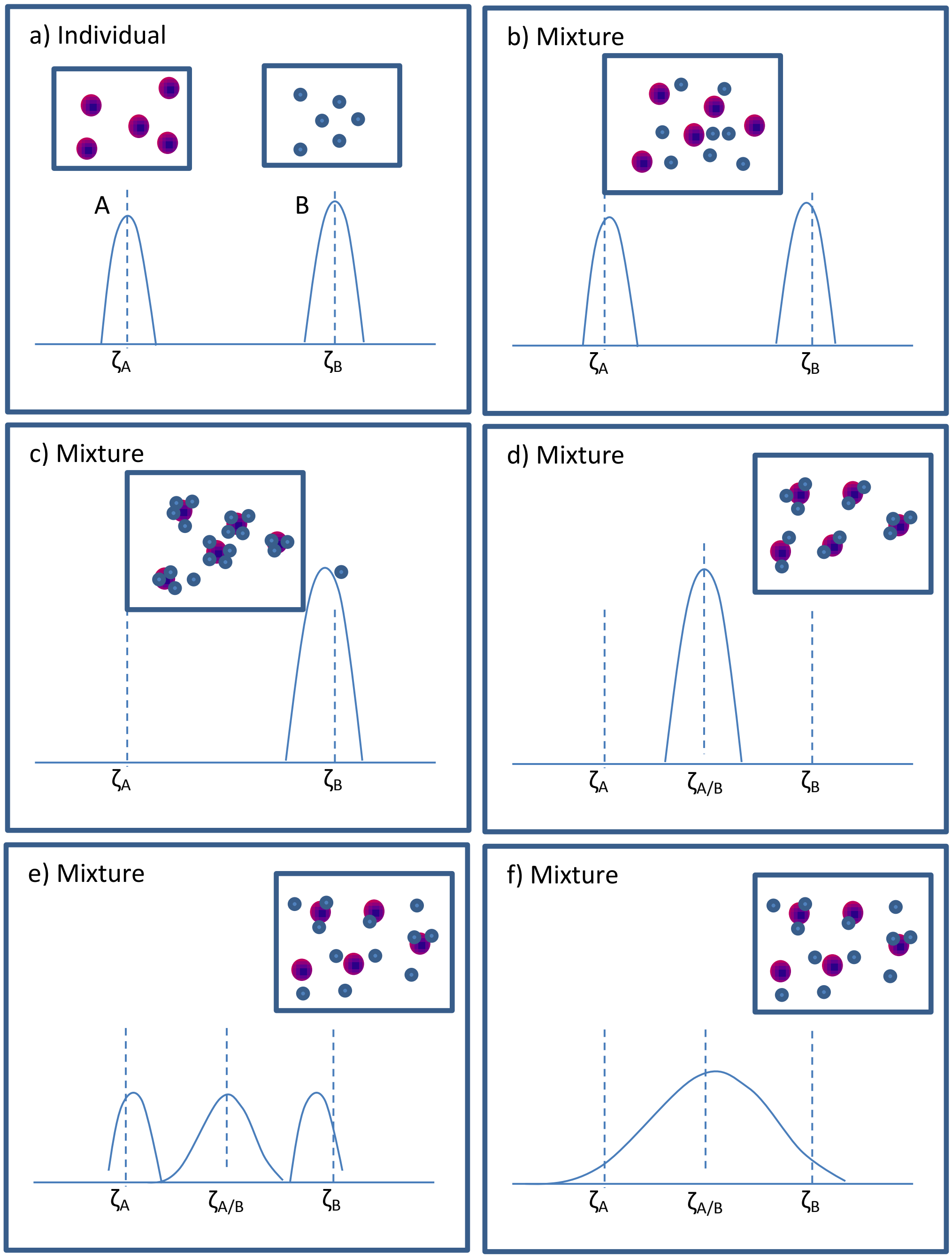

Figure 2-1 Schematic zeta potential distributions in the study of colloidal interaction in a binary system (a, individual zeta potential distributions of particle A and B; b, zeta potential distributions of particle A and particle B mixture without hetero-aggregation; c, Strong hetero-aggregation between

particle A and B with particle A fully coated by particle B; d, Strong hetero-aggregation between particle A and B with insufficient particle A to fully cover particle B; e & f, weak hetero-aggregation between particle A and B).

For a particular zeta potential distribution measurement, the stock suspensions were diluted with solution of interest. The suspensions for zeta potential distribution measurements were prepared to an optimal concentration on the order of 0.1 to 1 g solids per liter suspension, equivalent to 20 to 150 particles per view field that could be tracked accurately by the software during a mobility measurement. All suspensions were analyzed at room temperature to minimize convective effects in the electrophoresis cell. To ensure representative measurements, the cell was flushed and replenished with the same suspension for every second measurement. At least five mobility measurements in each direction were recorded for each sample.

2.4 Surface characterization techniques

2.4.1 Scanning electron microscopy (SEM)

SEM is essentially a high magnification microscope which enables the investigation of specimens with a high resolution down to 25 Angstroms or better. The basic principle of SEM is that a focused beam of electrons are generated by a suitable source, typically a tungsten filament of a field emission gun. The electron beam is accelerated through a high voltage and pass through a system of apertures and electromagnetic lenses to produce a thin beam of electrons which scans the surface of the specimen by means of scan coils. Signals derived from the electron-sample interactions reveal information about the sample including topography, chemical composition (using EDS, Energy Dispersive X-Ray Spectroscopy), crystalline structure and crystal orientations (using EBSD, diffracted backscattered electrons). Specimens can be observed in high vacuum, low vacuum and in Environmental SEM specimens can be observed in wet condition. A JAMP-9500F equipped with electron guns for Secondary Electron Microscopy was used in this study.

2.4.2 X-ray photoelectron spectroscopy (XPS)

XPS, also known as Electron Spectroscopy for Chemical Analysis (ESCA), is a widely used surface analysis technique. In XPS, the sample is placed in an ultrahigh vacuum environment and irradiated with soft X-rays photons (1-2 keV). The X-ray excitation of the inner shell electrons of target atoms induces direct emission of photoelectrons. The energy of photoelectrons is characteristic of the target material, and the measurement of the energy spectrum (number of count vs kinetic/binding energy) provides valuable information about the top 2-20 atomic layers, depending on the material studied. Peak position and peak area are used to evaluate the composition, while the peak shape gives unique information about the chemical shifts or chemical bonds of the elements. The XPS spectrometer AXIS 165 was used in this study.

2.4.3 Auger electron spectroscopy (AES)

AES is another commonly used surface analytical technique for obtaining the chemical composition of solid surfaces. In AES the sample of interest is irradiated with a high energy (2 - 10 keV) primary electron beam. This bombardment results in the emission of backscattered, secondary, and Auger electrons that can be detected and analyzed. The backscattered and the secondary electrons are used for imaging purposes similar to that in SEM. The Auger electrons are emitted at discrete energies that are characteristic of the elements present on the sample surface. When analyzed as a function of energy, the peak positions give information of the elements and the chemical states present on the sample surface. All elements in the periodic table, except hydrogen and helium, can be detected, and the depth of analysis is in the range of 3 - 5 nm or top 2-20 atomic layers. The secondary electron images yield information related to surface topography if a scanning primary beam is used. As the electron beams can be focused to a very small probe size, excellent spatial resolution (0.5 µm) can be achieved.

Auger point analysis and scanning analysis can be performed with a spatial resolution down to 250 nm. When ion gun is used for sputtering of top layers, depth profiles can be run automatically and maps and line scans of Auger electron distributions can be generated. JAMP 9500F was used for the AES analysis.

2.4.4 Sample preparation for surface analysis

The typically sample preparation procedure for surface analysis is as following: 1) conditioning the mineral samples of either silica or sphalerite in the solutions of interest for 30 min; 2) collecting the particle samples by filtration; 3) rinsing the collected particle samples with ethanol and drying them in a vacuum oven at room temperature; 4) Keeping the samples in a freezer prior to mounting onto the SEM, XPS, and/or AES sample holder for analysis.

2.5 Quartz crystal microbalance with dissipation (QCM-D)

2.5.1 Working principle of QCM-D

QCM-D is a surface sensitive technique developed by Q-Sense, which enables real-time measurements of molecular adsorption and/or interactions on various surfaces. The latest QCM-D model, Q-Sense E4, used in this study consists of the following main parts: sensor crystal, four flow modules which hold sensor crystals, chamber platform which is the base for the flow modules, electronic unit where the signals are generated and data is collected before being sent to the computer. The computer is equipped with software QSoft 401 which simultaneously acquires and displays QCM-D measurements. Figure 2-3 shows the typical QCM-D experimental setup with Q-Sense E4.

Figure 2-2 Typical QCM-D experimental setup with Q-Sense E4

The working principle of the QCM-D is based on the piezoelectric properties of the quartz crystal which is sandwiched by a pair of gold electrodes. When an AC voltage is applied to the electrodes, the quartz crystal oscillated at a specific resonance frequency which is highly sensitive to the total mass of the crystal. A decrease in resonance frequency will be observed if an extra mass is added on the crystal. The mass adsorbed on the crystal surface can be calculated by measuring the reduction of the resonance frequency of the crystal. If the adsorbed layer is thin, rigid and evenly distributed, the decrease in frequency is proportional to the mass of the adsorbed film through Sauerbrey relation [133]:

$$\Delta m = -\frac{C \cdot \Delta f}{n} \tag{2-1}$$

where C is the mass sensitivity constant equal to 17.7 ngcm^{-2}Hz^{-1} when f = 5 MHz, n is the overtone (n = 3, 5, 7, or 9) of the resonance frequency of the applied voltage across the electrodes. It is also possible to estimate the thickness (d) of the adsorbed layer:

$$d = \frac{\Delta m}{\rho} \tag{2-2}$$

where ρ is the effective density of the adsorbed layer.

In most situations however, the adsorbed layer is not rigid or viscoelastic which is not fully couple to the oscillation of the crystal, hence the Sauerbrey relation (Eq. 2-1) will underestimate the mass loaded on the sensor surface. A viscoelastic adsorbed layer will dampen the oscillation of the quartz crystal sensor. The damping of energy dissipation (D) of the sensor's oscillation gives information of the structure properties (viscoelasticity) of the adsorbed layer on the sensor surface. The energy dissipation (D) occurs when the driving voltage to the quartz crystal sensor is shut down and the energy from the oscillating crystal dissipates from the system which is defined as:

$$D = \frac{E_{lost}}{2\pi E_{stored}} \tag{2-3}$$

where E_{lost} is the energy dissipated during one oscillation cycle and E_{stored} is the total energy stored in the oscillator.

The Sauerbrey relation (Eq. 2-1) [133] is only valid when the adsorbed mass causes low dissipation in frequency shifts between different overtones and/or the ratio of dissipation and frequency changes ($-\Delta D_n/\Delta f_n$) is small [134-136]. Manufacturer of QCM-D (Q-Sense) suggests the threshold $-\Delta D_n/\Delta f_n$ value of 1×10^{-7} Hz^{-1}, while Reviakine et al. [134] proposed a value of 4×10^{-7} Hz^{-1}. For high dissipation values or $-\Delta D_n/\Delta f_n$ ratios, the Sauerbrey equation (Eq. 2-1) is believed to underestimate the adsorbed mass [137, 138], and models taking into account of the viscoelastic properties of the adsorbed layer has been proposed [135, 136, 139-144].

QCM-D E4 system simultaneously measures frequency and dissipation changes at multiple overtones, which enables the modeling of viscoelastic properties and the calculation of the correct thickness of films that do not obey the Sauerbrey relation. With the Q-Sense E4 system, seven frequencies and seven dissipation values per sensor are measured, providing a well-determined model of the particular film properties. Moreover, the different overtones give information about the homogeneity of applied layers. As the detection range out from the sensor surface decreases with increasing overtone number, abnormal frequency behavior suggests vertical variations in film properties. The fact that the detection range from the sensor surface decreases with increasing frequency is also used by the modeling software (QTools) to calculate an accurate thickness of films that do not fully couple to the oscillation of the sensor. Another advantage of using higher overtones is the decreasing noise to signal ratio, which is good when extra-high sensitivity is desired.

2.5.2 Use of QCM-D in this study

QCM-D has been widely used to monitor the deposition kinetics of polymers [145-147], DNA [148, 149], proteins [150, 151], and nanoparticles [137, 152, 153] or microparticles [154]. In this study, QCM-D was used to monitor the gypsum scale on silica and zinc sulphide surface, and the adsorption kinetics of copper and xanthate on zinc sulphide surface. The interaction between minerals was also investigated using QCM-D. For a typical QCM-D experiment, a clean quartz sensor with coatings of interest was carefully mounted in the flow module with the active surface facing the testing solutions. The flow module was mounted on the chamber platform and a solution of interest was pumped into the flow module with an IPC-N peristaltic pump (Ismatec, Switzerland) at a flow rate of 150 µL/min. A background (baseline) solution was firstly introduced into the system to obtain a stable baseline. The testing solution or suspension of interest was then pumped into the flow module until reaching equilibrium. The baseline solution was pumped into the system to remove loosely adsorbed or deposited layers. The temperature of the system was controlled by a built-in heating and cooling thermoelectric device in the flow module. All QCM-D experiments were carried out at 22.00 ± 0.02°C. The QCM-D chamber was placed upside down throughout the experiments. Frequency and dissipation shifts were continuously recorded during the entire experiment.

2.6 Surface force measurement (AFM)

2.6.1 Principle of AFM force measurement

The atomic force microscopy (AFM) is one of a family of scanning probe microscopes which has grown steadily since the invention of the scanning tunnelling microscope (STM) by Binning and Rohrer in the early eighties [155]. It was developed to overcome a drawback of STM which is that it can only image and measure conducting or semiconducting surfaces [156]. Generally, an AFM consists of a piezo scanner, a cantilever with a sharp tip (probe), a laser beam source, a split photodiode and a detector-feedback electronics system.

Figure 2-3 illustrates the working principle of AFM for colloidal force measurement. As shown in the Figure 2-3a, a probe particle is attached onto the tip of an AFM cantilever and a sample substrate is mounted on the AFM translation stage. A laser beam is focused onto the other side of the cantilever. The reflection of the laser beam is directed to a split photodiode which detects the deflection of the cantilever. A constant output signal is obtained when the sample on the translation stage initially moves towards the particle (Figure 2-3b: a-b), suggesting zero defection of the cantilever or zero force between the two surfaces at large separation distant. An increase or a decrease in the output signal can be obtained when further moving the lower surface towards the upper particle (Figure 2-3b: b-c). An increase in the output signal indicates the cantilever being pushed away from the moving surface, corresponding to a repulsive between the two surfaces. While a decrease in the output signal indicates the cantilever being pulled towards the moving surface, which corresponds to an attractive force between the two surfaces. Further moving the lower surface towards the particle, the lower surface will eventually contact the upper particle and a constant compliance will be observed (Figure 2-3a: c-d). A constant compliance suggests that the lower surface is pushing the upper particle along with the cantilever upwards. The constant compliance allows the cantilever deflection to be calibrated in terms of output signals since the displacement of the piezo translation stage is known. The cantilever deflection can then be calculated as a function of the separation distance between the two surfaces and the interaction force between the two surfaces can be calculated using Hook's Law. The piezo translation stage starts to retract at the end of the extension (Red line in Figure 2-3b). The retracting signal will be identical to the approaching signal if the colloidal force between the two surfaces is purely repulsive (Red solid line in Figure 2-3b). When there is an adhesion between the two surfaces, the cantilever continues to follow the displacement of the piezo translation stage due to the adhesive force holding the particle onto the surface. In this case, the retracting signal will follow the dot line in Figure 2-3b. When the restoring force of the cantilever exceeds the adhesive force, a sudden detachment of the particle from the lower surface occurs and the signal returns to zero value. More detailed description of the principles of the colloidal force using an AFM can be found elsewhere [157, 158].

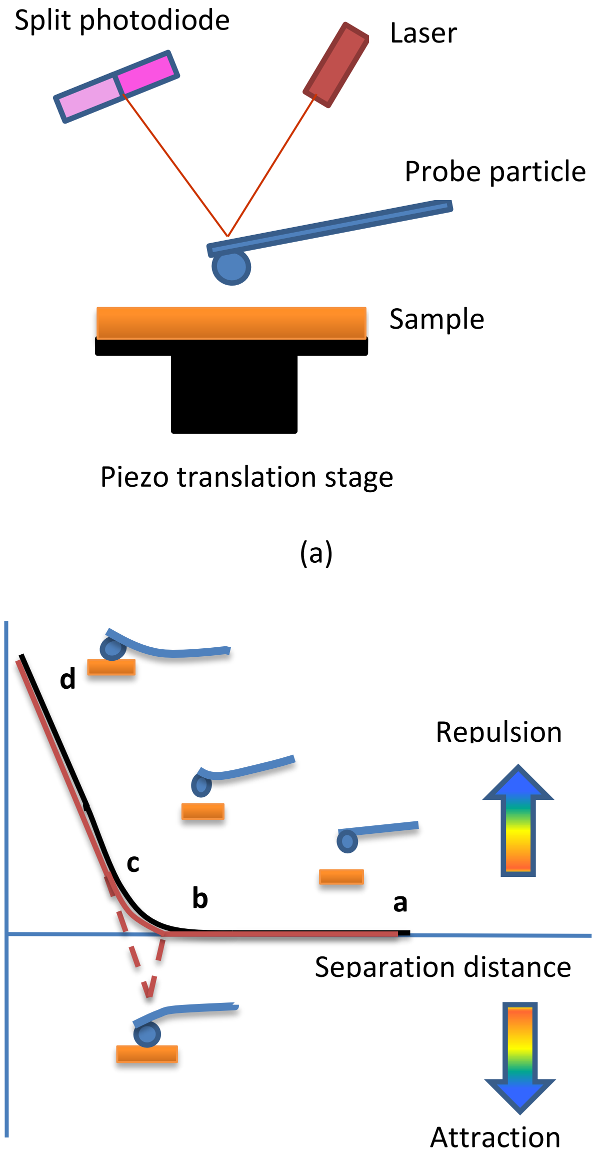

(a)

(b)

Figure 2-3 Schematic illustration of AFM working principle

2.6.2 The use of AFM in this study

A Nanoscope Multimode AFM (Digital Instrument, Santa Barbara, USA) was used to measure the interaction forces between silica and silica, silica and gypsum crystal surface, and silica and sphalerite surfaces (Figure 2-4). Silica wafer with

(001) orientation and fractured sphalerite were used as substrates. Silica microsphere was attached to the short, wide beam cantilever. For a typical AFM force measurement, the substrate was glued onto a magnetic disk and mounted on the piezoelectric translation stage of the scanner. The cantilever substrate was mounted to the vendor- provided liquid cell which was place on the top of the sample surface and sealed with an O-ring. Solution of interest was then injected into the liquid cell and the system was allowed to equilibrate for at least 20 min before the force measurement.

The colloidal interaction forces between a silica probe and a silica wafer substrate or a fractured sphalerite surface were measured in various concentrations of calcium and magnesium solutions and gypsum supersaturated water. The experiment was initiated by injecting 1 mM KCl solution into the fluid cell and the first measurement was made after an equilibration time of 20-30 min. The KCl solution was then replaced with different concentrations of calcium or magnesium or gypsum supersaturated solution. After the measurement for a given solution, the solution was sucked out gently from the fluid cell. The fluid cell was flushed with 1 mM KCl at least three times and then flushed and filled with the next solution. The colloidal forces between a silica particle and a cleaved natural gypsum surface were measured in a gypsum saturated solution follow a similar procedure described above. To ensure representative force profiles, the forces were measured at various locations for a given set of test and at least 10 approaching and retracting force curves were recorded for each location. The experiments were conducted at room temperature and all solutions were filtered with a 0.2 μm filter prior to injecting into the fluid cell. The obtained force profiles were processed using the SPIP software (Image Metrology). For quantitative comparison, the measured interaction forces were normalized by the probe radius. The maximum loading force used in the force measurement was in the range of 5 - 8 mN/m.

Figure 2-4 Nanoscope Multimode AFM (Digital Instrument, Santa Barbara, USA)

2.6.3 Surface preparation

A spherical silica particle (~ 8 μm) was glued onto a short, thick AFM cantilever using a two component epoxy (EP2LV, Master Bound, USA) and set in a vacuum desiccator for more than 24 hours. The prepared AFM probes were exposed under UV-Ozone for at least 15 min prior to their use in the force measurements. The spring constant of the cantilever was calibrated by the thermal tune method in testing liquids. After force measurements, the silica probes were examined under an optical microscope and the size of the silica probes were determined by analyzing the images.

Silica wafers were cut into 15×15 mm square pieces. Fractured sphalerite plane surfaces were used for the AFM force measurement between a spherical silica particle and sphalerite surface. To obtain sphalerite surface, a chunk of sphalerite crystal was fractured and sphalerite grains with a flat fractured surface were carefully chosen under an optical microscope. The chosen grain was then glued onto a cut silica wafer with the flat fractured crystal plane being exposed for the use in the AFM force measurement. The fractured sphalerite surface was washed with diluted HCl (pH 2) to remove any oxidation product and then rinsed with Milli-Q water and ethanol and blow dried with ultra-pure nitrogen before mounted to the AFM apparatus. A typical AFM image of the fractured sphalerite surface is shown in Figure 2-5. As shown in the figure, the fractured sphalerite surface is considerable clean, smooth, and suitable for AFM force measurement. Gypsum surfaces were obtained by cleaving ultra-pure natural gypsum crystal. Figure 2-6 shows a typical AFM image of a cleaved gypsum surface obtained in gypsum saturated solution.

air).

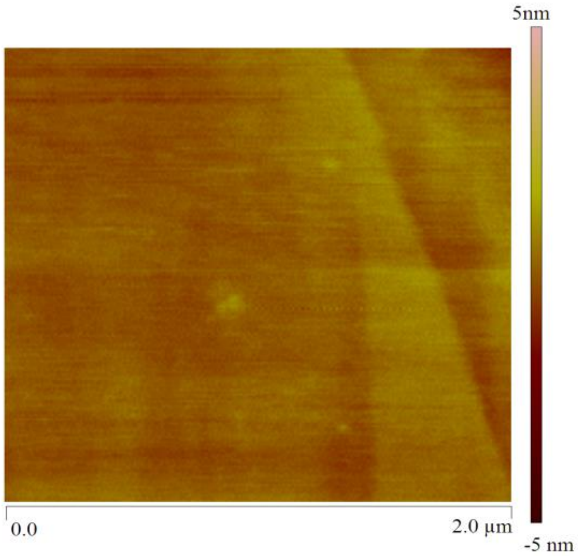

Figure 2-5 A typical AFM image of the fractured sphalerite surface obtained in air: contact mode AFM at a scan rate of 1 Hz (Mean roughness of 2.31 nm).

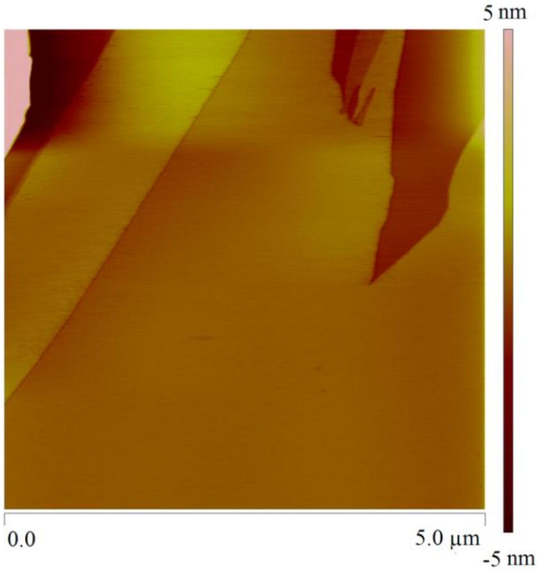

Figure 2-6 A typical AFM image of cleaved gypsum surface obtained in gypsum saturated solution: contact mode AFM at scan rate of 1 Hz (Mean roughness of 4.35 nm).

2.6.4 DLVO fitting

Since the both silica and sphalerite mineral surfaces are hydrophilic, the colloidal interactions between silica – sphalerite and silica – silica do not involve hydrophobic interaction. For such reasons, the colloidal forces obtained from the AFM force measurements were fitted with the classic DLVO (Derjaguin-Landau-Verwey-Overbeek) theory [159]. The van der Waals forces (F_{vdW}) were calculated by Hamaker's method in the form of a sphere of radius R interacting with a flat surface at a distance D [159], shown by the following equation:

$$\frac{F_{vdW}}{R} = -\frac{A}{6D^2} \tag{2-4}$$

where A is the Hamaker constant. The Hamaker constants A for silica/water/silica system and silica/water/sphalerite were taken as 8.5×10^{-22} J [160] and 1.0×10^{-20} J [41], respectively.

The electrical double layer forces were calculated by numerically solving the nonlinear Poisson-Boltzmann (BP) equation (Eq. 2-5) at constant surface potential boundary conditions. The BP equation was solved in the form of interaction force per unit area (F(x), Eq. 2-6), which is integrated to obtain energy per area between two planar plates (U_{EDL}(D)), shown in equation 2-7. The Derjaguin's approximation (Eq. 2-8) was used to calculate the electrical double layer force between a sphere and a flat plate at separation distance D.

$$\varepsilon\varepsilon_0 \frac{d^2\psi}{dx^2} = -e\sum_i z_i n_{i\infty} exp\left(\frac{-z_i e\psi}{k_b T}\right) \quad (2\text{-}5)$$

$$F(x) = k_b T \sum_i n_{i\infty}\left(exp\left(\frac{-z_i e\psi}{k_b T}\right) - 1\right) - \frac{\varepsilon\varepsilon_0}{2}\left(\frac{d\psi}{dx}\right)^2 \quad (2\text{-}6)$$

$$U_{EDL} = -\int_{\infty}^{D} F(x)\,dx \quad (2\text{-}7)$$

$$\frac{F_{EDL}(D)}{R} = 2\pi U_{EDL}(D) \quad (2\text{-}8)$$

Where z_i is the valence of ion i, $n_{i\infty}$ is the number density of ion i in the bulk, ψ is the potential in the electric double layer, e is the electron charge, k_b is the Boltzmann constant, T is the absolute temperature, ε and ε_0 are the relative permittivity of the medium and the permittivity of vacuum, respectively.

2.7 Micro-flotation

A custom built micro-flotation cell was used in this study (Figure 2-7). The detailed information on the cell can be found elsewhere [161]. Basically, the micro-flotation cell contains two parts. The lower part of the cell (part A) consists of a glass chamber with a frit having pores of uniform size (1.6 µm) and a gas inlet. The upper part (part B) consists of a vertical separation vessel and a concentrate receiver vessel. A magnetic stirring bar is placed on top of the frit to agitate the particles while the gas inlet is connected to a gas cylinder (usually N_2) and flow-meter to monitor the gas flow. Conditioning was done outside the cell, and the pulp/slurry was then transferred into the cell and floated for a desired time. For a typical micro-flotation test, 2 g of sphalerite (- 45 μm) or a mixture of silica (1 g, - 40 μm) and sphalerite (1 g, - 45 μm) was conditioned in 200 mL of desired solutions for 30 min. The minerals were conditioned for 5 min with copper sulphate, then conditioned for an additional 5 min with SIPX. Samples were floated for 10 min immediately after the conditioning with high purity nitrogen at a flow rate of 15 ml/min. The flotation was conducted at 1.25×10^{-5} M SIPX with 0 or 1.25×10^{-5} M copper sulphate. For the tests of the effect of pro-hydrophobic treatment on the flotation behavior of silica and sphalerite minerals, the mineral solids were conditioned with copper sulphate and SIPX in 200 mL Milli-Q water for 10 min. The solids were then collected by filtration and transferred to 200 mL solution of interest and conditioned for another 20 min before being transferred to the micro-flotation cell. The solids in the froth and pulp were collected, dried and weighted.

For single mineral flotation, the flotation recovery was calculated as following equation:

$$R\ (\%) = \frac{Wt.\ of\ concentrate}{Wt.\ of\ concentrate + Wt.\ of\ tailing} \tag{2-9}$$

For a mixed mineral flotation, the content of both concentrate and tailing was analysed with XRF. The flotation recovery of mineral A and mineral B is calculated as following: for example, for a mixed mineral A and mineral B flotation, if you have a1% (Wt.) of mineral A and b1% (Wt.) of mineral B in the concentrate, and a2% (Wt.) of mineral A and b2% (Wt.) of mineral B in the tailing,

$$R\ mineral\ A\ (\%) = \frac{Wt.\ of\ concentrate \times \mathrm{a1\%}}{Wt.\ of\ concentrate \times \mathrm{a1\%} + Wt.\ of\ tailing \times \mathrm{a2\%}} \tag{2-10}$$

$$R\ mineral\ B\ (\%) = \frac{Wt.\ of\ concentrate \times \mathrm{b1\%}}{Wt.\ of\ concentrate \times \mathrm{b1\%} + Wt.\ of\ tailing \times \mathrm{b2\%}} \tag{2-11}$$

Where a1% and b1% are the weight percentages of mineral A and B in the concentrate, and a2% and b2% are the weight percentages of mineral A and B in the tailing, respectively.

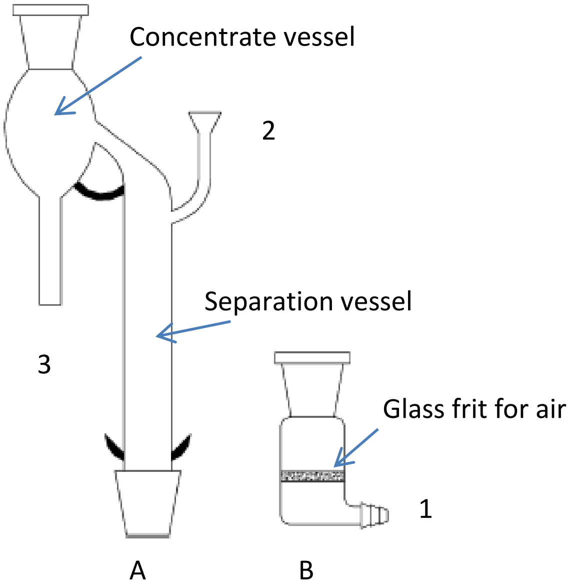

Figure 2-7 Schematic of the micro-flotation cell (1 - gas inlet, 2 - pulp inlet, 3 - concentrate outlet).

2.8 Other techniques

2.8.1 Atomic adsorption spectroscopy (AAS)

AAS is a spectro-analytical technique widely used for the quantitative determination of chemical elements. It employs the absorption of optical radiation (light) by atoms in gas-phase to determine their concentrations. In this study, AAS (Varian 220 FS) was used to determine the concentrations of Ca, Mg, Na, and K in the laboratory prepared calcite saturated solution, gypsum supersaturated solution and simulated process water. The uptake of Cu and the release of Zn were also determined using AAS when copper sulphate was used to the activation of sphalerite.

2.8.2 UV-Vis spectroscopy

UV-Vis-NIR Spectrophotometer determines absorption of ultraviolet, visible and near infrared radiation by samples. It measures attenuation of a beam of light after it passes through a sample or after reflection from a sample surface. UV-Vis spectroscopy is usually applied to molecules or inorganic complexes in solution. In addition to identification of complex molecules, the concentration of an analyte in solution can be determined by measuring the absorbance at some wavelength and applying the Beer-Lambert Law. A Shimadzu UV-3600 was used to determine the uptake of xanthate on sphalerite surface by analysing the concentration of a xanthate solution before and after conditioning with sphalerite mineral particles. The absorbance at wavelength 301 was used in the analysis.

Chapter 3 Impact of Gypsum Supersaturated Solution on Surface Properties of Silica and Sphalerite Minerals

3.1 Introduction

Water quality is a critical parameter in mineral flotation [14, 15, 22, 23]. Many current mineral flotation plants recycle the tailings water in the process to reduce the demand of fresh water and minimize the discharge of tailings water [21]. However, the recycle of the tailings water can have adverse effects on the process water quality and ultimately impact the flotation performance of minerals [14, 24, 25].

In sulphide mineral flotation plants especially those practicing water recycling, the process water usually contains high concentrations of calcium and sulphate ions. In some mines, the calcium concentration in the process water can exceed 1000 ppm [31], and sulphate concentration can be as high as 2500 ppm [27]. At Pb-Zn Mine, for example, the process water could contain high total dissolved solids (up to 4000 ppm) which are supersaturated with respect to the solubility of calcium sulphate. The concentration of calcium and sulphate ions in the process water of Pb-Zn Mine could be as high as 800 ppm and 2800 ppm, respectively.

The high concentrations of calcium and sulphate ions in the process water can cause problems in the sulphide mineral flotation practice. Problems in galena flotation recovery were noted when lime was used to adjust the pH to depress pyrite [32]. The flotation of chalcopyrite was also reported to be depressed in an alkaline pH when lime was used as a pH modifier or when calcium ions were introduced in the pulp [33]. An extensive investigation into the problem of galena flotation recovery at the Hilton concentrator (Mount Isa Mines, Australia) suggested that the flotation rate of galena was retarded due to surface coating of precipitated gypsum [28]. Cullinan [43] found that the flotation of fine galena pure mineral was depressed when using water of high dissolved salt content, which was gypsum supersaturated. The adverse effect on the fine galena floatability was enhanced by the decrease of particle size and an increase pulp condition temperature.

The adverse effect of high concentrations of calcium and sulphate ions on the flotation of sulphide minerals can be attributed to one or two mechanisms. One possible mechanism is the depression action of calcium ions. In sphalerite flotation, the presence of calcium ions might reduce the exchange rate of activation ions resulting in a deceased recovery [36]. However, Lascelles et al. [39] showed that the presence of calcium (500 ppm) and/or magnesium (120 ppm) ions had no impact on the uptake of copper and xanthate on sphalerite. The presence of calcium ions can enhance the hetero-aggregation between target minerals and gangue minerals [40, 41]. It has been reported that calcium ions decrease the negative surface charge on the mineral surfaces, reducing electrostatic repulsion and the dispersion of mineral particles [32]. Another possible mechanism is the gypsum slime coating on mineral surfaces by either nucleation or hetero-aggregation, retarding the flotation of the desired minerals. It has been implied that the flotation rate of galena was retarded due to the presence of an overlayer of precipitated gypsum [26, 27]. The precipitates were speculated to deposit on mineral surface by hetero-aggregation. However, other investigations on silica and/or sphalerite in gypsum saturated or supersaturated systems showed no trace of gypsum precipitates on mineral surfaces [30, 37, 38]. It should be noted that gypsum is considerable soluble [58] with a solubility in water of 2400 ppm at 25°C. The formation of gypsum precipitates depends on various factors including fluid hydrodynamics, solution chemistry, supersaturation level, surface chemistry and topography of solids as well as temperature [47, 59, 83-85]. Therefore, the sample preparation procedure for the surface analysis is extremely important. In many of the previous studies, the sample rinsing with water was applied after being conditioned in the calcium sulphate solutions. It is possible that the rinsing with water might have washed away the gypsum precipitates resulting in misleading results of surface analysis.

In this study, we focus on the impact of process water of high calcium and sulphate ion concentrations on the surface properties of minerals. The aim of this study is to develop a fundamental understanding of the adverse effect of gypsum supersaturated process water on the flotation performance of sphalerite. An in-house prepared gypsum supersaturated solution is used to represent the gypsum supersaturated process water. Pure silica and single sphalerite minerals are used to represent the gangue mineral and valuable mineral of a zinc sulphide ore. The surface properties of silica and sphalerite minerals in the gypsum supersaturated solution are investigated using zeta potential distribution measurement, quartz crystal microbalance with dissipation (QCM-D), and surface analysis techniques such as X-ray photoelectron spectroscopy (XPS), scanning electron microscopy (SEM), and auger electron spectroscopy (AES). The results of this study answer the questions of whether gypsum precipitates form on mineral surfaces or in the bulk gypsum supersaturated solution, and whether the minerals hetero-aggregation with gypsum particles in the gypsum supersaturated solution. The effects of gypsum supersaturated solution on the surface properties and flotation behaviors of silica and sphalerite minerals are discussed.

3.2 Results and Discussion

It has been speculated that gypsum might coat on minerals surfaces by either nucleation or hetero-aggregation in the gypsum supersaturated process water, which might be responsible for the poor recovery and selectivity of sphalerite flotation. In order to fundamentally understand the adverse effect of gypsum supersaturated process water on the flotation of sphalerite, the surface properties of silica and sphalerite minerals in the gypsum supersaturated solution were investigated using zeta potential distribution measurement, XPS, SEM, and AES analysis, and QCM-D experiments.

3.2.1 Surface charge properties of silica and sphalerite minerals in gypsum supersaturated solutions

Suspensions of silica and sphalerite were analyzed in supporting electrolyte solution (10^{-2} M KCl or 25 × 10^{-3} M K_2SO_4), calcium solution (800 ppm Ca), and gypsum supersaturated solutions. At least five mobility measurements in each direction were recorded for each sample, and all zeta potential distributions were measured at pH 10.

3.2.1.1 Zeta potential distributions of silica and sphalerite minerals in gypsum supersaturated solution

In order to understand the effect of gypsum supersaturated solution on the surface charge properties of silica and sphalerite, zeta potential distributions of silica and sphalerite were measured in gypsum supersaturated solutions, and in simple supporting electrolyte solution (10^{-2} M KCl). The zeta potential distribution of gypsum particles in its own supersaturated solutions was also measured. The results are shown in Figure 3-1.

Zeta potential distribution of gypsum in its own supersaturated solution has a peak at around +3 mV. This value is slightly different from the values reported by others for gypsum at similar pH [37, 38], which might be due to the different procedures in sample preparation. The zeta potential distributions of silica and sphalerite in 10^{-2} M KCl have peaks centered at values of -51 mV and -31 mV, respectively (Figure 3-1a, 3-1b). These values are similar to the average zeta potential values reported for silica and sphalerite at similar conditions [30, 37, 38, 40, 162]. However, when the silica and sphalerite particles are dispersed in the gypsum supersaturated solution, the zeta potentials of these two minerals become identical and shift to less negative value of around -10 mV.

The shifts of zeta potential distributions of silica and sphalerite in the gypsum supersaturated solution in comparison with those in 10^{-2} M KCl could be attributed to many factors. One of the factors might be the electrical double layer compression due to excessively high electrolyte concentration of the gypsum supersaturated solutions. As shown in Table 3-1, the conductivity of the gypsum supersaturated solution (as high as 3.3 µS/cm) is much higher than that of 10^{-2} M KCl (around 1.5 µS/cm). The adsorption of high valence of calcium ions may well account for the shifts of zeta potential to less negative values. Partial minerals surface coating with gypsum through either nucleation or coagulation may also contribute to the observed zeta potential shifts.

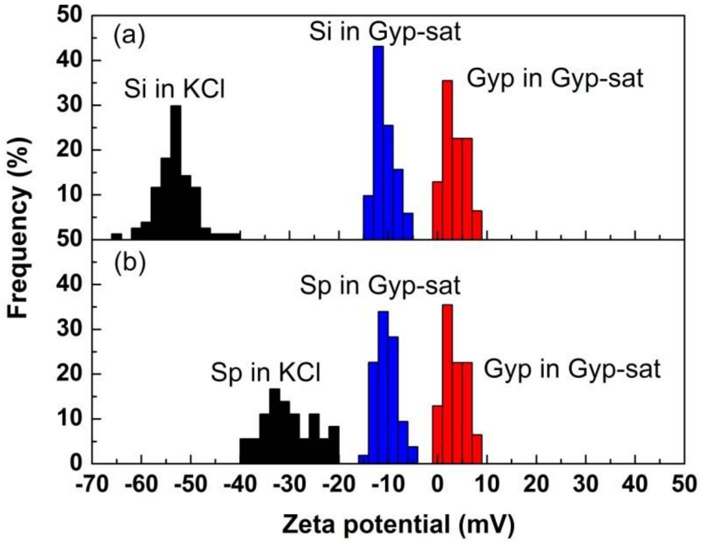

Figure 3-1 Zeta potential distribution of silica (a) and sphalerite (b) in gypsum supersaturated solutions and supporting electrolyte solution (10-2 M KCl) at pH 10.

Table 3-1 Average zeta potential of silica and sphalerite in different solutions of pH 10.

Mineral samples	**10^{-2} M KCl**		**25×10^{-3} M K_2SO_4**		**800 ppm Ca**		**Gyp-sat**	
	Cond. (μs/cm)	ζ (mV)	Cond. (μs/cm)	ζ (mV)	Cond. (μs/cm)	ζ (mV)	Cond. (μs/cm)	ζ (mV)
Silica	1.5	- 55	4.1	- 41	3.6	- 13	3.3	- 10
Sphalerite	1.4	- 31	4.0	- 26	3.8	- 12	3.2	- 10

3.2.1.2 Effect of sulphate on the surface charge properties of silica and sphalerite

In comparison with the 10^{-2} M KCl solution, the gypsum supersaturated solution contains high concentrations of calcium (845 ppm) and sulphate (~ 2400 ppm). In order to understand how much the sulphate ions contribute to the changes of surface charge of silica and sphalerite in the gypsum supersaturated solution, zeta potential distribution of silica and sphalerite was measured in K_2SO_4 solution. A K_2SO_4 with a concentration of 25×10^{-3} M was used to reach a similar sulphate concentration in the gypsum supersaturated solution. The results are shown in Figure 3-2 and Table 3-1.

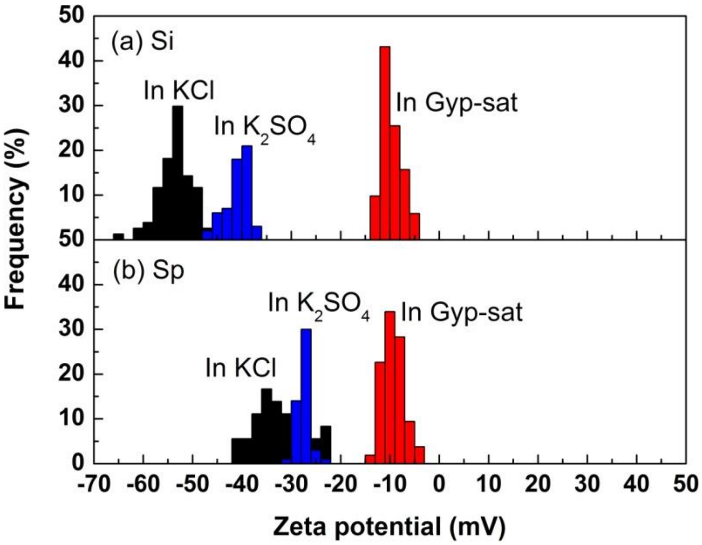

Figure 3-2 Effect of sulphate ions on the zeta potential distributions of silica (a) and sphalerite (b) at pH 10 (K_2SO_4 : 25×10^{-3} M; KCl : 10^{-2} M).

The zeta potential distributions of silica and sphalerite in 25 × 10^{-3} M K_2SO_4 solution shift to slightly less negative in comparison with those in the 10^{-2} M KCl solution, centered at values of - 41 mV and - 26 mV, respectively. The zeta potential shifts are attributed to the electrical double layer compression due to the increased ion concentration. It is interesting to note that silica and sphalerite minerals still carry different surface charges in the 25 × 10^{-3} M K_2SO_4 solution even though the zeta potentials shift toward less negative values. This is dramatically different from the effect of gypsum supersaturated solution, even though both have same sulphate ion concentration. The results clearly indicate the important role of calcium in modifying the zeta potential values of these two minerals.

3.2.1.3 Effect of calcium on the surface charge properties of silica and sphalerite minerals

In order to better understand the effect of gypsum supersaturated solution on silica and sphalerite mineral surfaces, zeta potential distributions of these minerals were measured in the electrolyte solution contains 800 ppm calcium solution. As shown in Figure 3-3 and Table 3-1, calcium has a significant effect on the surface charge of silica and sphalerite. The zeta potentials of both silica and sphalerite shift to about - 12 mV in the presence of 800 ppm calcium which is similar to the calcium concentration of gypsum supersaturated solution (845 ppm), although they are totally different in the KCl solution. The zeta potential of silica and sphalerite in 800 ppm calcium solution of pH 10 is almost identical to the zeta potentials of silica and sphalerite in the gypsum supersaturated solution. In XPS analysis, calcium signals are detected on both silica and sphalerite minerals surfaces conditioned in the 800 ppm calcium solution, as shown in Figure 3-4. These results suggest that the shifts of zeta potential distributions of silica and sphalerite in the gypsum supersaturated solution are mainly attributed to the high calcium concentration in the supersaturated solution.

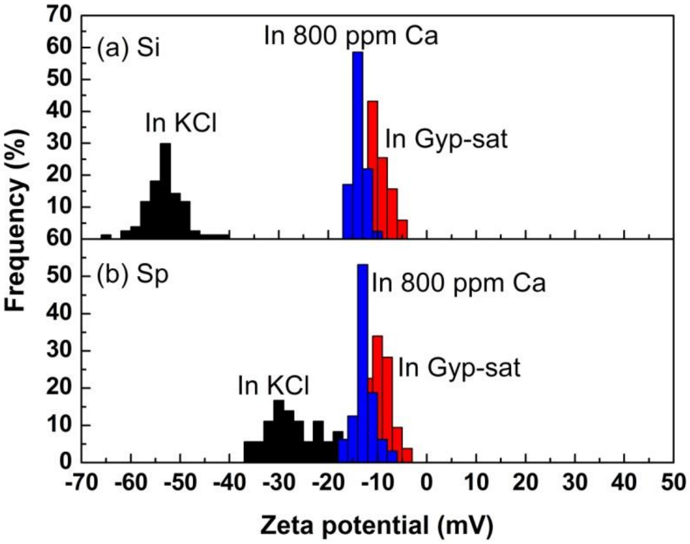

Figure 3-3 Effect of calcium (800 ppm) on the zeta potential distributions of silica (a) and sphalerite (b) at pH 10 (KCl: 10^{-2} M, 800 ppm Ca solution was prepared with $CaCl_2$).

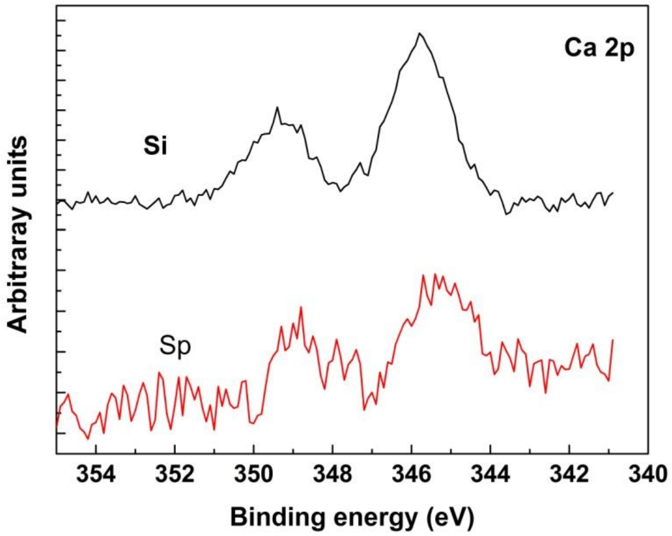

Figure 3-4 XPS narrow scan Ca2p spectra for silica (Si) and sphalerite (Sp) particles conditioned in 800 ppm calcium solution at pH 10.

3.2.2 Gypsum scaling study on silica and sphalerite mineral surfaces in gypsum supersaturated solution

Calcium sulphate scaling is a common problem in a wide range of industrial processes and applications, especially those involving heat exchange [46-48], mineral processing [27, 28, 49], desalination of seawater by reverse osmosis [50, 51] etc. There are three forms of calcium sulphate including gypsum ($CaSO_4 \cdot 2H_2O$), calcium sulphate hemihydrate ($CaSO_4 \cdot 1/2H_2O$), and anhydrite ($CaSO_4$) [52, 53]. The solubility of these three forms all decreases with increasing temperature [54-58], a fact that is responsible for the formation of calcium sulphate scale on heat exchanger surfaces [59]. The formation of calcium sulphate scale depends on various factors [47, 59, 83-85]. It has been long speculated that gypsum might nucleate on mineral surface during the mineral flotation in the gypsum supersaturated process water, which could change the surface properties of the minerals.

In this study, silica and sphalerite samples (1 g) were conditioned in 100 mL gypsum supersaturated solutions at room temperature for 30 min. The solids were then collected by filtration, washed with ethanol and vacuum dried. For comparison, another batch of silica or sphalerite samples was conditioned in Milli-Q water following the same procedure. Precipitates from the gypsum supersaturated solution were also collected for analysis. The samples were characterized using SEM (JAMP-9500F), XPS (Kratos AXIS 165) and AES (JAMP-9500F).

The XPS results of silica and sphalerite minerals with and without conditioning in the gypsum supersaturated solution, and the precipitates from the gypsum supersaturated solution are shown in Figure 3-5. Silica and sphalerite mineral (conditioned in Milli-Q water) surfaces are fairly clean and without any trace of calcium (Ca 2p 345 eV) or sulphate (S 2p 167.5 eV) signals as anticipated. The S 2p peaks of sphalerite at 160.5 eV and 161.5 eV are characteristic of sulphur in sulphide. After conditioned in the gypsum supersaturated solution, calcium and sulphate are detected on both silica and sphalerite minerals. Calcium and sulphate signals are also found on the precipitates collected from the gypsum supersaturated solution, indicating that the precipitates are calcium sulphate. The XPS results suggest that there are calcium sulphate precipitates in both silica and sphalerite mineral systems conditioned in the gypsum supersaturated solution.

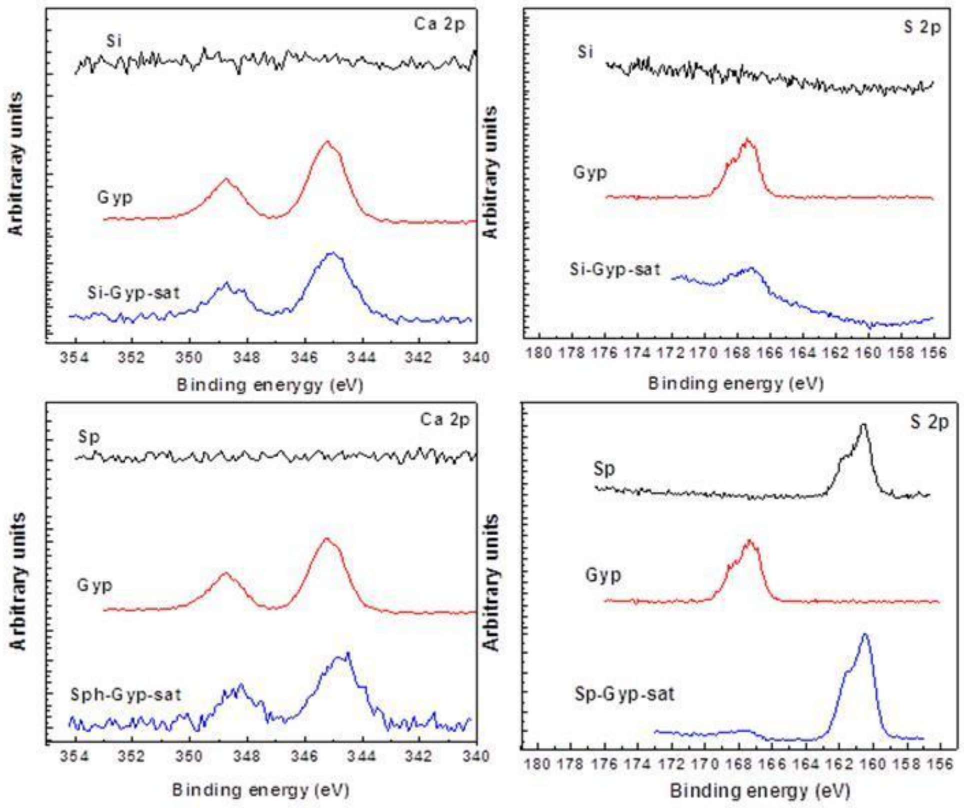

Figure 3-5 XPS narrow scan Ca 2p and S 2p spectra for silica and sphalerite particles without treatment (Si, Sp), conditioned in gypsum supersaturated solution (Si-Gyp-sat, Sp-Gyp-sat), and gypsum precipitates (Gyp) from gypsum supersaturated solution.

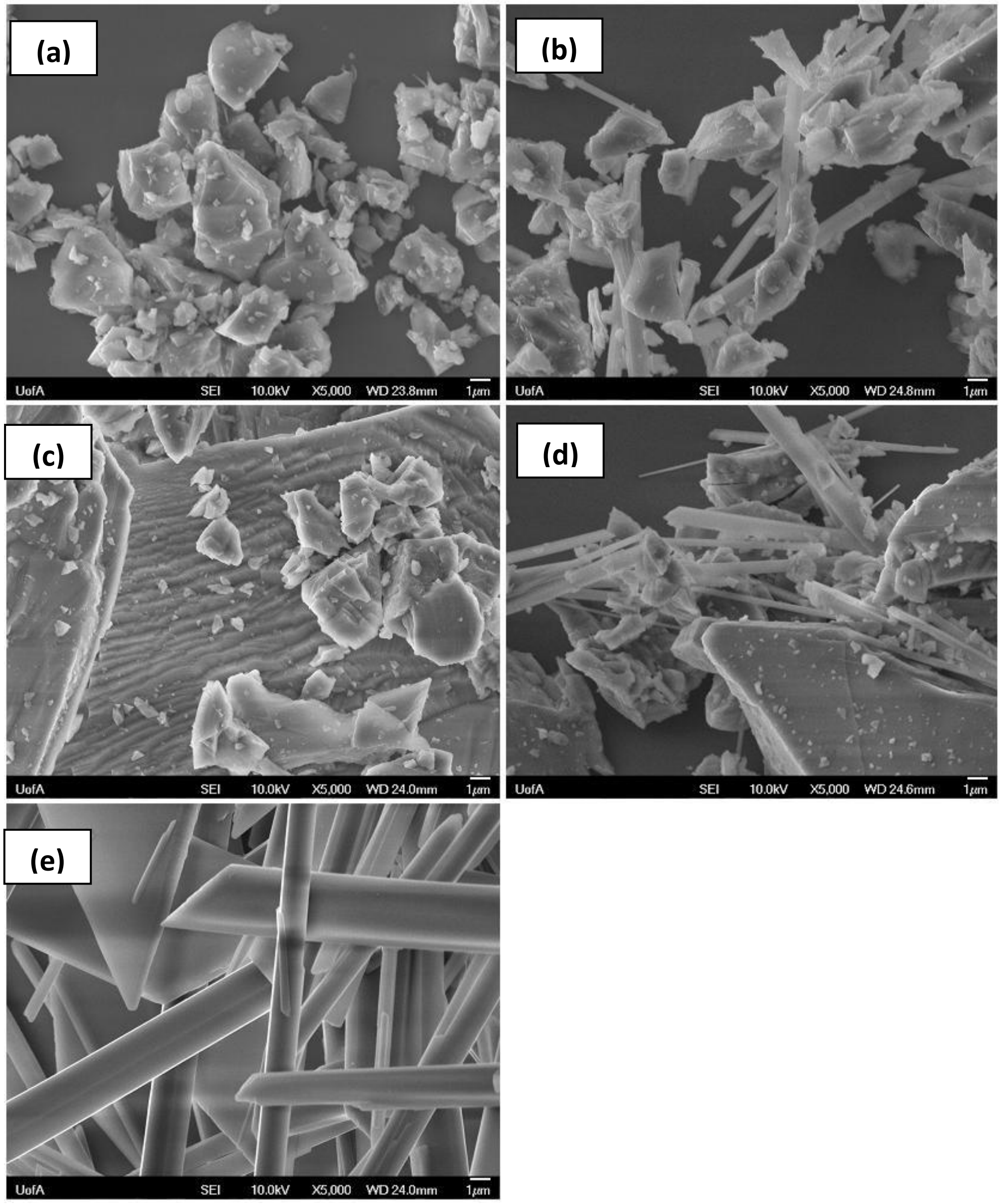

Figure 3-6 Typical SEM micrographs of a) Silica in water, b) Silica conditioned with gypsum supersaturated solution, c) Sphalerite in water, d) Sphalerite conditioned with gypsum supersaturated solution, and e) Gypsum precipitates from gypsum supersaturated solution.

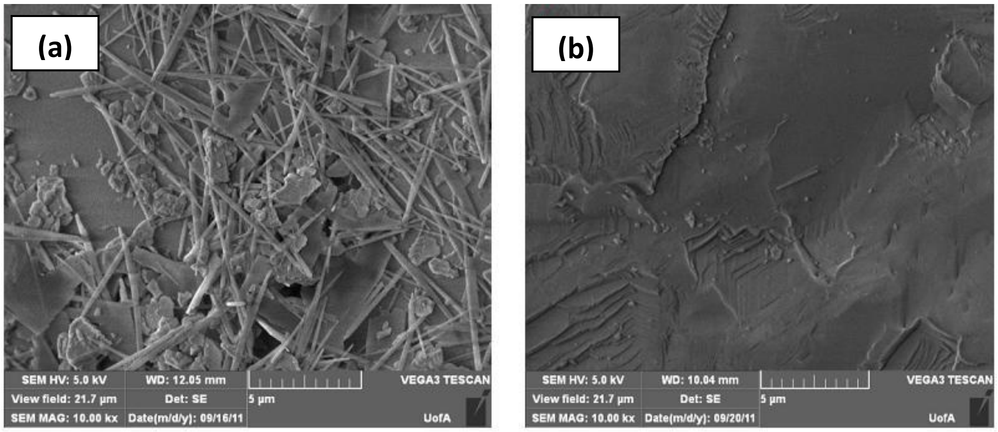

Figure 3-7 Typical SEM micrographs of sphalerite conditioned in gypsum supersaturated solution before (a) and after (b) 5 min sonication in ethanol.

The SEM micrograph of the precipitates from the gypsum supersaturated solution shows that the precipitates are needle shape gypsum crystals (Figure 3-6e). Needle shape gypsum precipitates are also found in the silica and sphalerite minerals conditioned in gypsum supersaturated solutions (Figure 3-6b and 3-6d). However, those precipitates are more likely formed in the bulk gypsum supersaturated solution. As shown in Figure 3-7, the gypsum precipitates can be removed from the sphalerite surface after 5 minutes of sonication in the ethanol solution.

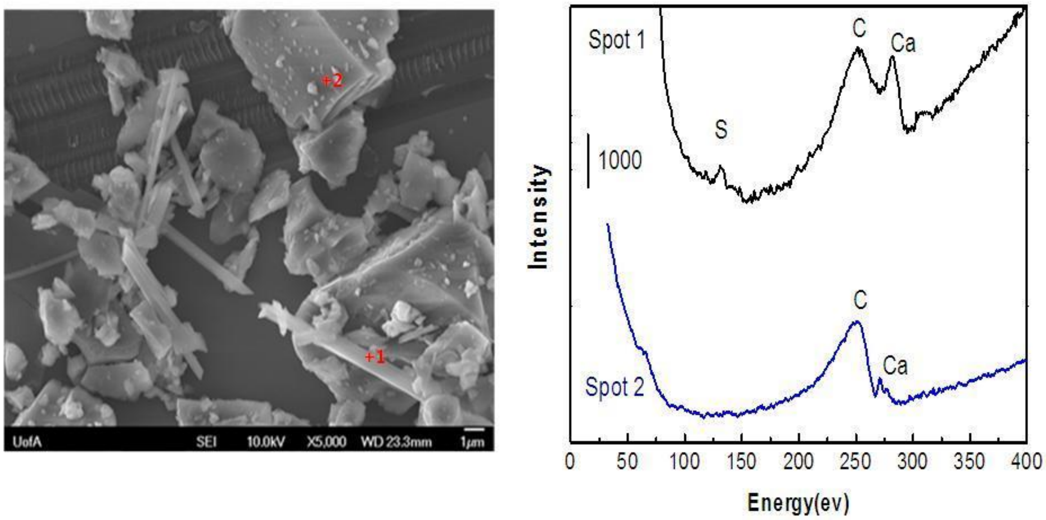

Figure 3-8 Auger narrow scan S LVV and Ca LMM spectra for silica conditioned in gypsum supersaturated solution (Spot 1 right on the gypsum precipitates, and Spot 2 on silica particle).

The surface analysis by Auger spot mapping on silica minerals conditioned in gypsum supersaturated solution further confirms the absence of gypsum precipitates on the mineral surface (Figure 3-8). At spot 1 of gypsum precipitates, both signals of calcium and sulphur are detected. However, at spot 2 where there are no visible needle shape precipitates, only a very weak signal of calcium is detected without the sulphur peak. These findings suggest the formation of gypsum precipitated in the bulk gypsum supersaturated solution, not nucleation on the mineral surfaces.

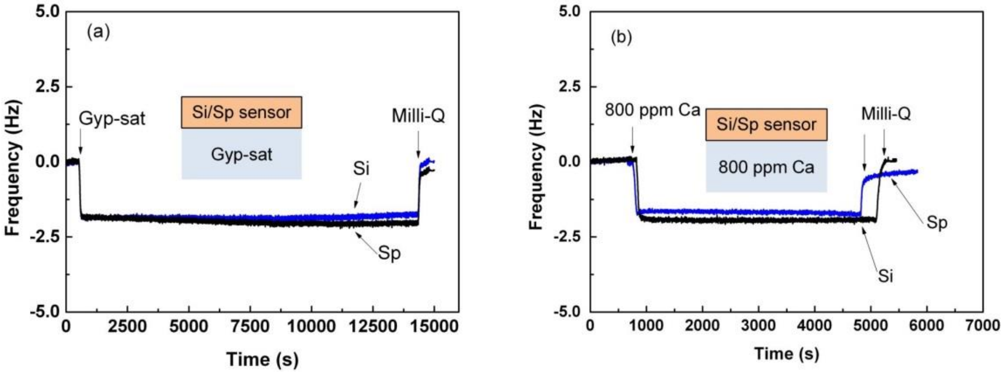

Figure 3-9 Frequency of SiO_2 and ZnS sensors in a) gypsum supersaturated solution and b) 800 ppm calcium solution monitored with QCM-D (baseline solution: Milli-Q water, pH 10).

Gypsum scaling on mineral surfaces was also studied using QCM-D. A freshly prepared gypsum supersaturated solution or 800 ppm calcium solution was introduced into the QCM-D module mounted with a quartz crystal sensor coated with either SiO_2 or ZnS. Milli-Q water of pH 10 was used as a baseline solution for the gypsum scaling and calcium adsorption studies.

As shown in Figure 3-9, the QCM-D frequency changes of SiO_2 and ZnS sensors in the gypsum supersaturated solution are similar to those in the 800 ppm calcium solution. The results indicate that the frequency changes of SiO_2 and ZnS sensor in the gypsum supersaturated solution are mainly attributed to the calcium adsorption on the mineral sensor surface. The calcium ions are physically adsorbed on the SiO_2 and ZnS sensors because the frequency changes are reversible when a baseline solution is introduced in the QCM-D chamber.

3.2.3 Interactions between gypsum particles and silica or sphalerite minerals

Our results indicate that gypsum precipitates form in the bulk gypsum supersaturated solution. However, the gypsum precipitates could still coat on the minerals surfaces by heterocoagulation and hence interfere with mineral flotation. It is therefore interesting to study the interactions between gypsum precipitates and silica or sphalerite particles. In this study, zeta potential distributions of mineral mixtures were measured and the results are shown in Figure 3-10.

The zeta potential distributions of silica-gypsum mixture and sphalerite-gypsum mixture show two distinct peaks. One peak centers at the position of the zeta potential of silica or sphalerite in the gypsum supersaturated solution while the other peak is at the zeta potential of gypsum particles in its own supersaturated solution. These zeta potential distributions results indicate a negligible hetero-aggregation between silica or sphalerite minerals and gypsum particles in the gypsum supersaturated solution.

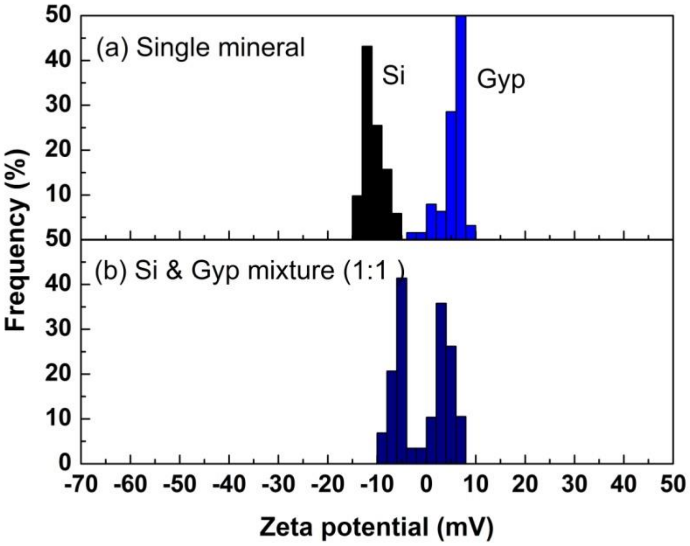

a) Silica and gypsum mixture

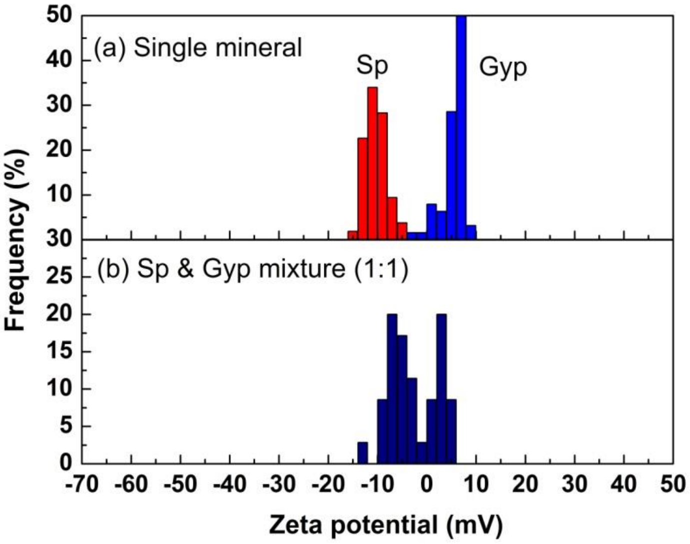

b) Sphalerite and gypsum mixture

Figure 3-10 Zeta potential distributions of a) silica and gypsum mixture, and b) sphalerite and gypsum mixture in gypsum supersaturated solution at pH 10.

The interactions between minerals and gypsum particles were also studied with

QCM-D. A freshly prepared gypsum suspension (0.1 % of -265 nm gypsum particles in gypsum saturated solution) was introduced into the QCM-D module mounted with either SiO_2 or ZnS coated sensor. Gypsum saturated solution was used as a baseline solution. The findings from the QCM-D results are in agreement with the zeta potential distribution measurements. As shown in Figure 3-11, the frequencies of both SiO_2 sensor and ZnS sensor remain constant when a gypsum suspension was introduced in the system. As mentioned before, the frequency shift (Δf) of the QCM-D sensor is related to the adsorption or desorption of a mass onto or from the sensor surface. A constant frequency indicates no gypsum particles deposited onto the SiO_2 or ZnS sensor. The QCM-D results further confirm the absence of hetero-aggregation between minerals and gypsum particles in the gypsum supersaturated solution.

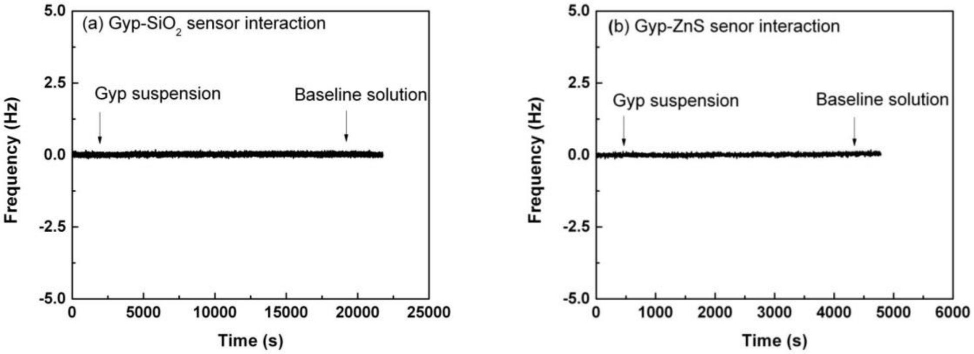

Figure 3-11 QCM-D study on the interactions of (a) SiO_2 sensor or (b) ZnS sensor with gypsum particles in gypsum saturated solution at pH 10 (baseline solution: gypsum saturated solution, gypsum particle size: ~265 nm).

It is well known that particles can coagulate at zero zeta-potentials due to the van der Waals force. However, both results from the zeta potential distribution measurements and QCM-D studies indicate that there is no hetero-aggregation between silica – gypsum and sphalerite – gypsum, even though silica or sphalerite and gypsum carry opposite surface charge. This is because that the magnitudes of the positive and negative surface charge between silica or sphalerite and gypsum are not large enough overcome the repulsive hydration force which has been reported between hydrophilic surfaces [163-168]. As shown in Figure 3-12, hydration force is detected between a silica probe and a cleaved gypsum surface in the gypsum saturated solution of pH 10.

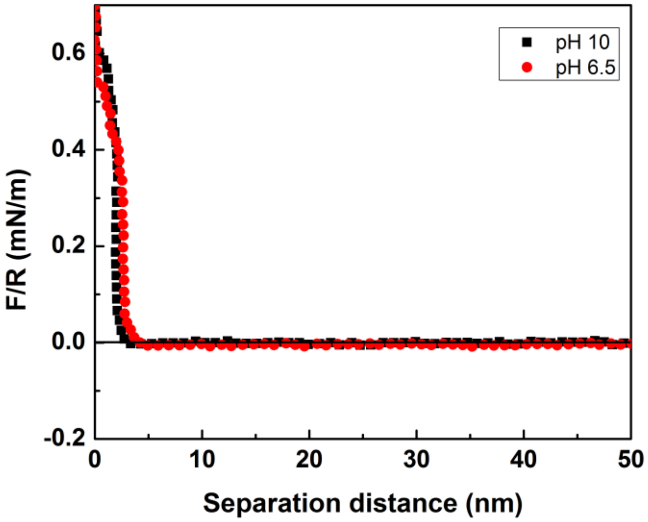

Figure 3-12 Normalized AFM interaction force curve between silica and gypsum surface in gypsum saturated solution of pH 10 and 6.5.

3.2.4 Thermodynamic calculation

Thermodynamically, the formation of gypsum depends on the change in the Gibbs free energy for going from the supersaturated solution to equilibrium. The change in the Gibbs free energy (ΔG) for the formation of one mole of gypsum, or crystalline gypsum is given by Eq. 3-1 [90]

$$\Delta G = -RTlnS \tag{3-1}$$

Where R is the gas constant, T is temperature in Kelvin and S is the supersaturation.

The free energy change during the critical nucleus formation in a homogeneous solution is usually expressed as Eq. 3-2 [90]

$$\Delta G(\text{hom}) = \frac{4}{27}\frac{\beta^3 V_m^2 \gamma_{cl}^3}{\alpha^2 k^2 T^2 lnS} \tag{3-2}$$

Where α and β are the volume and surface shape factors, respectively, V_m is the molecular volume, γ_{cl} is the interfacial energy between critical nucleus and liquid phases, k is the Boltzmann constant. The free energy of formation critical nucleus on the catalyst surface (heterogeneous nucleation) is given by Eq. 3-3 [95]

$$\Delta G(het) = \frac{\beta V_m (\gamma_{cl})^3}{k^2 T^2 ln^2 S}\frac{\gamma_{sc}-(\gamma_{cl}+\gamma_{sl})}{\gamma_{cl}} = \frac{\beta V_m (\gamma_{cl})^2}{k^2 T^2 ln^2 S}[(\gamma_{sc}-(\gamma_{cl}+\gamma_{sl})] \tag{3-3}$$

Where the superscripts l, s, and c refer to the liquid, critical nucleus and catalytic solid, γ_{sc} and γ_{sl} are the interfacial energy between catalytic solids-critical nucleus, and catalytic solids-liquid.

In the presence of minerals, whether the gypsum forms on minerals surfaces or spontaneously grows in the bulk gypsum solution depends on overall changes in Gibbs free energy, which is directly determined by the interfacial energy, γ.

The interfacial energy between mineral and gypsum ($\gamma_{\text{mineral-gypsum}}$) can be estimated from Eq. 3-4 [90, 95, 169-171]

$$\gamma_{mineral-gypsum} = \left(\sqrt{\gamma_{mineral}^{LW}} - \sqrt{\gamma_{gypsum}^{LW}}\right)^2 + 2\left(\sqrt{\gamma_{mineral}^{+}\gamma_{mineral}^{-}} + \sqrt{\gamma_{gypsum}^{+}\gamma_{gypsum}^{-}} - \sqrt{\gamma_{mineral}^{+}\gamma_{gypsum}^{-}} - \sqrt{\gamma_{gypsum}^{+}\gamma_{mineral}^{-}}\right) \tag{3-4}$$

Where the γ^{LW} is the Lifshitz-van der Waals, γ^{+} is the Lewis acid (electron-acceptor), and γ^{-} is the Lewis base (electron-donor) parameters ($Lewis\ acid - base\ \gamma^{AB} = 2(\gamma^{+}\gamma^{-})^{1/2}$), which can be obtained by solving the Young's Eq. 3-5 [90, 169-171] using data from Table 3-2 and 3-3.

$$(1 + \cos\theta)\gamma_{solution} = 2\left(\sqrt{\gamma_{solids}^{LW}\gamma_{solution}^{LW}} + \sqrt{\gamma_{solids}^{+}\gamma_{solution}^{-}} + \sqrt{\gamma_{solids}^{-}\gamma_{soluiton}^{+}}\right) \tag{3-5}$$

The interfacial energy between minerals and solution ($\gamma_{\text{mineral-solution}}$), and gypsum crystal and solution ($\gamma_{\text{gypsum-solution}}$) can be calculated with Eq. 3-6 [95, 170]

$$\gamma_{solids-solution} = \gamma_{solids} - \gamma_{solution}\cos\theta \tag{3-6}$$

Table 3-2 Surface tension components and parameters (mJ m^{-2}) of liquids used in direct contact angle determination, or in wicking at 20 ^{o}C [90, 170, 171]

Liquid	γtotal	γLW	γAB	γ+	γ-
Diiodomethane	50.8	50.8	0	0	0
Ethylene glycol	48.0	29.0	19.0	1.92	47.0
Dimethyl sulfoxide	44	36	8	0.5	32
Formamide	58.0	39.0	19.0	2.28	39.6
Glycerol	64.0	34.0	30.0	3.92	57.4
Water	72.8	21.8	51.0	25.5	25.5

Table 3-3 Contact angles of probing liquids on gypsum, ZnS and SiO_2 at 20 ^{o}C [172]

Probing liquid	Gypsum	ZnS	SiO_2
Diiodomethane	22.1		45.5
Ethylene glycol	22		
Dimethyl sulfoxide	33		14
Formamide		31.5	
Glycerol		45.3	30
Water	0	38.2	0

As show in Table 3-5, the interfacial energy between gypsum and liquid phases ($\gamma_{\text{gypsum-solution}}$) is - 13.83 (mJ m^{-2}), which means spontaneous nucleation of gypsum is always favourable as long as achieving the supersaturation state (lnS>0). On the other hand, the interfacial energy between gypsum-ZnS and gypsum-silica is much higher than the interfacial energy between gypsum-liquid, ZnS-liquid and silica-liquid ($\gamma_{gypsum\text{-}ZnS}$ - ($\gamma_{gypsum\text{-}solution}$ + $\gamma_{ZnS\text{-}solution}$) = 20.14 mJ m^{-2}, $\gamma_{gypsum\text{-}Silica}$ - ($\gamma_{gypsum\text{-}solution}$ + $\gamma_{silica\text{-}solution}$) = 44.94 mJ m^{-2}), indicating that the nucleation of gypsum on silica and ZnS surface is thermodynamically not favourable. The interfacial energy calculation results also suggest that the coagulation between gypsum precipitates and silica/ZnS minerals is thermodynamically undesirable.

Table 3-4 Surface tension components (mJ m^{-2}) of gypsum, ZnS and silica calculated with equation 3-5 and using the date in Table 3-2 and 3-3.

	Surface energy components				
	γ^{Lw}	γ^{+}	γ^{-}	γ^{AB}	γ^{total}
Gypsum	47.14	0.002	47.87	0.62	47.76
ZnS	44.31	0.202	39.31	5.63	49.94
Silica	36.74	0.088	124.85	6.65	43.39

Table 3-5 Interfacial energies (mJ m^{-2}) between minerals-gypsum, minerals - gypsum saturated solution, and gypsum - gypsum saturated solution calculated with equation 3-4 and 3-6 using data in Table 3-4.

$\gamma_{gypsum\text{-}ZnS}$	$\gamma_{gypsum\text{-}solution}$	$\gamma_{ZnS\text{-}solution}$	$\gamma_{gypsum\text{-}ZnS}-(\gamma_{gypsum\text{-}solution}+\gamma_{ZnS\text{-}solution})$
-0.48	-13.83	-6.80	20.14
$\gamma_{gypsum\text{-}Silica}$	$\gamma_{gypsum\text{-}solution}$	$\gamma_{silica\text{-}solution}$	$\gamma_{gypsum\text{-}Silica}-(\gamma_{gypsum\text{-}solution}+\gamma_{silica\text{-}solution})$
2.50	-13.83	-28.61	44.94

3.3 Significance in sphalerite flotation

According to our results, silica and sphalerite minerals carry the same charge in the gypsum supersaturated solution and their surfaces are indiscriminately coated with calcium. Needle shape gypsum precipitates were found to form in the bulk gypsum supersaturated solution. The hetero-aggregation between silica or sphalerite minerals and gypsum particles was found insignificant in the laboratory prepared gypsum saturated or supersaturated solution. However, one should note that the gypsum scaling is controlled by many factors; gypsum scaling on mineral surfaces can still be trigged in the real flotation process due to its much more complex system in comparison with the model gypsum supersaturated solution. For instance, the grinding process in the flotation plant would lead to the increase in mineral surface area and/or temperature. The increase of mineral surface area can introduce sites where surface precipitation of gypsum may occur. The increase of temperature can also result in the gypsum scaling on mineral surface since the solubility of the calcium sulphate decreases with the increase of temperature. The results from this study are obtained from a model gypsum supersaturated solution system where the grinding factor and temperature factors are not evaluated. It would be interesting to further probe the surface properties of silica and sphalerite minerals in the cases of grinding in gypsum supersaturated solutions with the elevation of pulp temperature.

Calcium in the gypsum supersaturated system plays a significant role on the minerals surface properties. The high calcium concentration in the gypsum supersaturated solution is responsible for the identical surface charges between silica and sphalerite. The identical surface properties of silica and sphalerite minerals in the gypsum supersaturated solution might be responsible for the poor flotation recovery and selectivity between those two minerals in real flotation system. First of all, the surface occupation by calcium may retard the exchange rate between activation ions and sphalerite and the subsequent uptake of xanthate collectors on the sphalerite as reported previously [36]. Secondly, calcium ions and gypsum precipitates in the bulk solution may consume some flotation reagents, for example, collector xanthate, as calcium could react with xanthate and generate insoluble calcium xanthate precipitates. Furthermore, the presence of calcium in the gypsum supersaturated solution can enhance the hetero-aggregation between silica and sphalerite, which might be responsible for the poor flotation recovery and selectivity in the flotation separation of sphalerite from silicate gangue minerals. Further investigations on the impacts of gypsum supersaturated solution on the interactions between flotation reagents and silica or sphalerite minerals and the interactions between silica and sphalerite are in progress.

An effective approach to eliminate the detrimental effect of both calcium and gypsum precipitates on the flotation of sphalerite is by adding carbonate (e. g.

soda ash) or bicarbonate to remove calcium ions and convert gypsum precipitates into calcium carbonate precipitates. In the case of Hilton concentrator, the addition of soda ash to the grinding circuit significantly improved the galena flotation [27]. Soda ash has also been used for control of calcium in sphalerite flotation [45]. Surface analysis indicated the reduction of concentrations in both calcium and sulphate on galena with the addition of carbonate and it was speculated that galena and calcium carbonate precipitates were mutually repelled [27]. In other studies, calcium carbonate did not appear to disperse completely as some precipitates remained on the mineral surfaces [37, 38].

3.4 Conclusions

The gypsum supersaturated solution has significant effects on the surface properties of silica and sphalerite minerals. Silica and sphalerite minerals carry identical surface charge in the gypsum supersaturated solution and the zeta potentials of the minerals shift to less negative value in comparison with those in the simple electrolyte solution. Gypsum precipitates are found on silica and sphalerite minerals in the gypsum supersaturated solution; however, the gypsum precipitates form in the bulk gypsum supersaturated solution. The hetero-aggregation between gypsum particles and silica or sphalerite minerals is not significant. The changes of surface properties of silica and sphalerite minerals in the gypsum supersaturated solution are mainly attributed to the high concentrations of calcium in the gypsum supersaturated solution. The zeta potentials of silica and sphalerite minerals are identical in the presence of 800 ppm calcium which is similar to those in the gypsum supersaturated solution. Silica and sphalerite minerals surfaces are indiscriminately coated with calcium in both 800 ppm calcium solution and gypsum supersaturated solution. The identical surface properties of silica and sphalerite in the gypsum supersaturated solution may be responsible for the poor flotation recovery and selectivity of sphalerite in the gypsum supersaturated process water.

Chapter 4 Impact of Gypsum Supersaturated Solution on the Uptake of Copper and Xanthate on Sphalerite

4.1 Introduction

In mineral flotation plants it is a common practice to treat the tailings water and recycle back to the flotation process. The recycle of water can change the quality of process water by accumulating and building up the dissolved ions and flotation chemical additives. Certain ions and residual flotation chemicals in the recycle water could have either positive or negative effect on the flotation process depending on the nature and concentrations of chemicals and mineral systems. Zinc ions from the recycle water, for instance, are beneficial for selective separation of galena from sphalerite in the lead-zinc flotation separation. On the other hand, some ions and chemical additives accumulated in the recycle water can be detrimental to flotation separation [14, 15, 21, 23, 24]. In sulphide mineral flotation operations that practise tailings water recycle, for instance, the process water with the recycle water from the tailings treatment could be often saturated or supersaturated with gypsum. The concentrations of the calcium and sulphate ions up to as high as 800 ppm and 2800 ppm, respectively, are not uncommon, exceeding the solubility limit of gypsum which is 2400 ppm in water at room temperature. The high concentration of calcium and sulphate ions in the process water not only causes scaling problems but also affects the mineral flotation separation. Problems in flotation recovery and selectivity have been reported in the flotation of galena, sphalerite and chalcopyrite in the presence of high concentrations of calcium or calcium and sulphate ions [25, 28, 33, 36, 39, 45].

It has been speculated that gypsum might precipitate out from the gypsum saturated or supersaturated solution and coat on the mineral surface, which might be responsible for the reduced flotation recovery and selectivity. However, our study on silica and sphalerite minerals in the gypsum supersaturated solution system suggested the absence of gypsum coating on mineral surfaces (Chapter 3). Despite the presence of needle-shaped gypsum precipitates in the gypsum supersaturated solution system, the gypsum precipitates neither grew on sphalerite mineral surface nor hetero-aggregated with sphalerite minerals under the typical flotation chemistry conditions. The current chapter focuses on the impact of gypsum supersaturated recycle water on the interactions between flotation reagents and sphalerite mineral.

It is well known that sphalerite mineral responses poorly to thiol collectors due to the relative low stability of zinc-xanthate complexes as compared to other heavy metal xanthates [32, 103]. The flotation of sphalerite mineral with short chain thiol collectors (xanthates) is commonly accomplished by activation with other heavy metal ions, usually copper. The activation of sphalerite with copper has been extensively studied for many years in a number of laboratories [102, 105-108, 111, 114, 117, 118, 173-178]. Many activation mechanisms have been proposed depending on the activation pH where activation occurs. It is generally accepted that under acidic conditions, the activation is through an ion exchange process with copper replacing surface zinc ions leading to copper sulphide-like surfaces. At neutral and alkaline pH, however, a variety of mechanisms have been proposed with the involvement of species from copper hydrolysis. The activation process of sphalerite with copper involves two stages [32]. At the initial stage, the uptake of copper is rapid, which is a weak function of the copper concentration in solution and is controlled by solution diffusion. Once the uptake of copper exceeds three monolayers, the diffusion of copper in the solid state follows the parabolic law. The activation of sphalerite minerals with copper could be affected by surface charge, contaminants in process water or on the mineral surface [106, 125]. The gypsum supersaturation in recycle water might have effect on the copper activation of sphalerite and hence the adsorption of xanthate. Calcium ions have been suggested to specifically interact with ZnS surface [179] and the exchange rate with activating ions has been suspected to be reduced in the presence of calcium [36]. However, others reported no impact of calcium and/or magnesium ions on the uptake of copper and xanthate by sphalerite [39].

In order to avoid the depression action of gypsum supersaturation in recycle water on sphalerite flotation, it is important to understand the impact of gypsum supersaturation in recycle water on the interactions between flotation reagents (copper and xanthate) and sphalerite mineral. In this study, we used a gypsum supersaturated solution to represent the gypsum supersaturated recycle water. The calcium and sulphate concentrations of the gypsum supersaturated solution are similar to those in the recycle water. The purpose of this study is to learn a better understanding of the impact of gypsum supersaturation in recycle water on sphalerite flotation.

4.2 Results and discussion

4.2.1 Zeta potential distribution measurements

The zeta potential distributions of sphalerite in 10^{-2} M KCl solution, 800 ppm calcium solution, and gypsum supersaturated solution in the presence of 1.25×10^{-5} M copper and/or SIPX were measured at pH 6.5. The results are shown in Figures 4-1 to 4-3.

a) In KCl solution

For comparison, the effect of copper and SIPX on the zeta potential distributions of sphalerite mineral in 10^{-2} M KCl supporting electrolyte solution was determined and the results are shown in Figure 4-1. In the supporting electrolyte solution of pH 6.5, the zeta potential distribution of sphalerite exhibits a peak centered at around - 15 mV (Figure 4-1a), which is similar to the average zeta potential value of sphalerite reported under similar conditions [40, 114, 180, 181]. In the presence of 1.25×10^{-5} M copper, the zeta potential distribution of sphalerite shifts to a positive value, with a peak centered at + 18 mV (Figure 4-1b), indicating the specific adsorption of copper species or replacement of zinc by copper ions. The zeta potential distribution shifts back to a negative value (- 10 mV) when dispersing the copper activated sphalerite particles in 1.25×10^{-5} M SIPX solution as shown in Figure 4-1d. The results suggest the successful uptake of copper and SIPX on sphalerite in the simple electrolyte supporting solution, as anticipated. As shown in Figure 1c, the zeta potential distribution of sphalerite in the presence of 1.25×10^{-5} M SIPX is similar to that in KCl solution, confirming that SIPX cannot adsorb on the surface of the sphalerite mineral without the activation of copper ions.

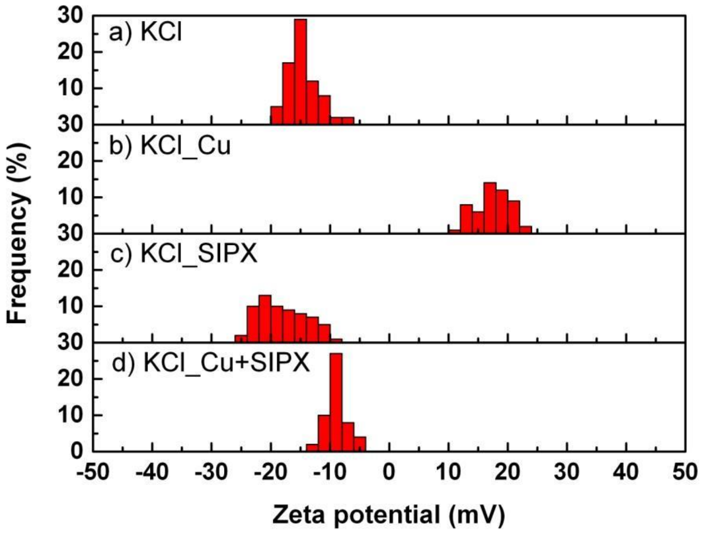

Figure 4-1 Zeta potential distributions of sphalerite in 10^{-2} M KCl solution in the presence of copper and/or SIPX at pH 6.5.

b) In 800 ppm calcium solution

The zeta potential distributions of sphalerite in 800 ppm calcium solutions in the presence of copper and/or SIPX are shown in Figure 4-2. In 800 ppm calcium solution, the zeta potential distribution of sphalerite shifts to slightly less negative value of - 12 mV in comparison with that in KCl solution (- 15 mV). In the presence of 1.25×10^{-5} M copper, the distribution shifts to around 0 mV, indicating the uptake of copper on sphalerite mineral surface. However, the zeta potential shift of sphalerite due to the adsorption of copper in 800 ppm calcium system is much less than that in the KCl system, suggesting that the presence of calcium ions may inhibit the uptake of copper on sphalerite mineral surface. The same as in the KCl system, SIPX cannot adsorb on sphalerite surface without copper activation in the 800 ppm calcium system. However, the addition of SIPX to the copper activated sphalerite suspension in 800 ppm calcium solutions cause a shift in zeta potential distribution from around 0 mV to - 5 mV, indicating a limited adsorption of xanthate on copper activated sphalerite in 800 pm calcium solution.

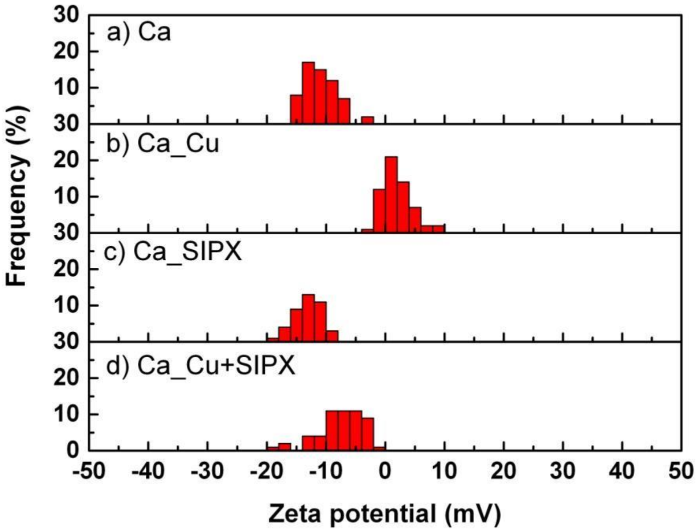

Figure 4-2 Zeta potential distributions of sphalerite in 800 ppm calcium solution in the presence of copper and/or SIPX at pH 6.5.

c) In gypsum supersaturated solution

The effect of copper and SIPX on the zeta potential distributions of sphalerite in the gypsum supersaturated solutions are similar to that in the 800 ppm calcium solutions, as shown in Figure 4-3. The zeta potential of sphalerite in the gypsum supersaturated solution is similar to that in the 800 ppm calcium solution. The shift of zeta potential distribution of sphalerite in the presence of copper in gypsum supersaturated solution is much smaller in comparison with that in the KCl solutions. The results indicate that in the gypsum supersaturated solution system the activation of sphalerite with copper may not be as efficient as that in

KCl system. The inhibited uptake of copper might be attributed to the high calcium concentration in the gypsum supersaturated solution.

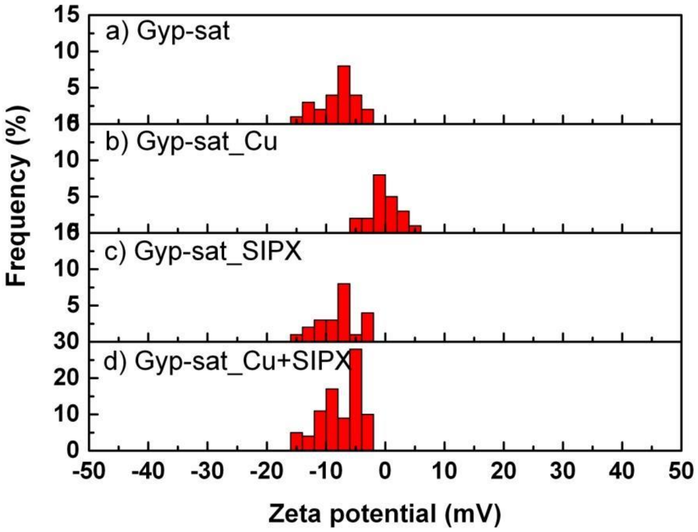

Figure 4-3 Zeta potential distributions of sphalerite in gypsum supersaturated solution in the presence of copper and/or SIPX at pH 6.5.

4.2.2 Copper and SIPX adsorption

AAS (VARIAN 220FS) and UV-Vis-NIR Spectrophotometer (Shimadzu UV-3600) were used to determine the solution concentration of copper and SIPX, respectively. The sphalerite mineral samples (1 g) were dispersed in desired solutions (100 mL) for 30 min prior to conditioning in 1.25×10^{-5} M copper solutions for 5 min. The solids were collected using vacuum filtration and transferred immediately to 100 mL of desired solutions containing 1.25×10^{-5} M SIPX and conditioned for another 5 min. The supernatant was collected after settling of the solids. The concentration of copper in filtrate and the concentration of SIPX in the supernatant were determined from which the uptake of copper and SIPX by sphalerite was determined.

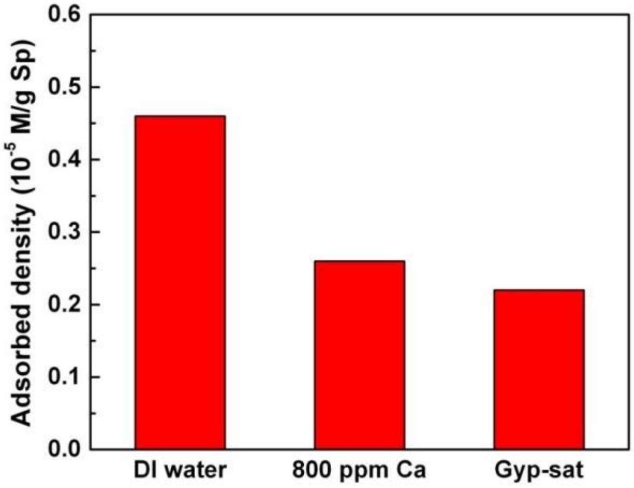

Figure 4-4 Effect of calcium and gypsum supersaturated solution on the uptake of copper on sphalerite at pH 6.5 (Initial Cu concentration: 1.25×10^{-5} M).

The AAS results further confirm that the uptake of copper on sphalerite is retarded in 800 ppm calcium and gypsum supersaturated solution. As shown in Figure 4-4, the amount of adsorbed copper on sphalerite in 800 ppm calcium solution and gypsum supersaturated solution is much less than that in DI water. The reduced uptake of copper on sphalerite mineral surface results in the reduction in the uptake of SIPX in 800 ppm calcium solution and gypsum supersaturated solution (Figure 4-5).

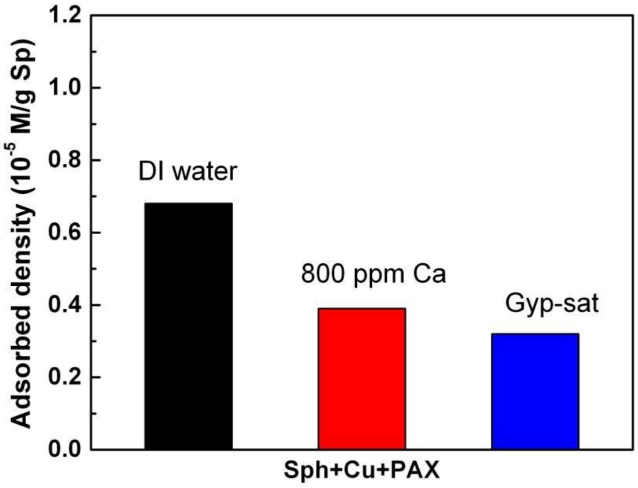

Figure 4-5 Effect of 800 ppm calcium and gypsum supersaturated solution on the uptake of SIPX on copper activated sphalerite at pH 6.5 (Initial SIPX concentration: 1.25×10^{-5} M).

It has also been speculated that calcium ions and gypsum precipitates would react with xanthate and form insoluble product. To exclude this possibility, the xanthate (SIPX) was also added to different concentrations of calcium solutions, gypsum supersaturated solution, and gypsum supersaturated solution with 1 wt% gypsum particles (gypsum suspension). UV analysis results demonstrate that neither calcium ions nor gypsum supersaturated solution consume SIPX or react with SIPX under the tested conditions. As shown in Figure 4-6, calcium concentration has no effect on the SIPX concentration in the solution. The SIPX concentration does not change in the 800 ppm calcium solution, gypsum supersaturated solution, and gypsum suspension (Figure 4-7).

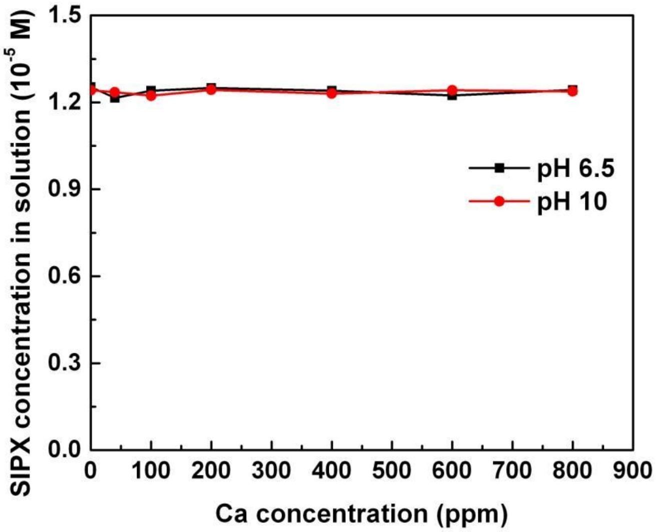

Figure 4-6 Effect of Ca on the SIPX concentration in solution (Initial SIPX concentration: 1.25×10^{-5} M).

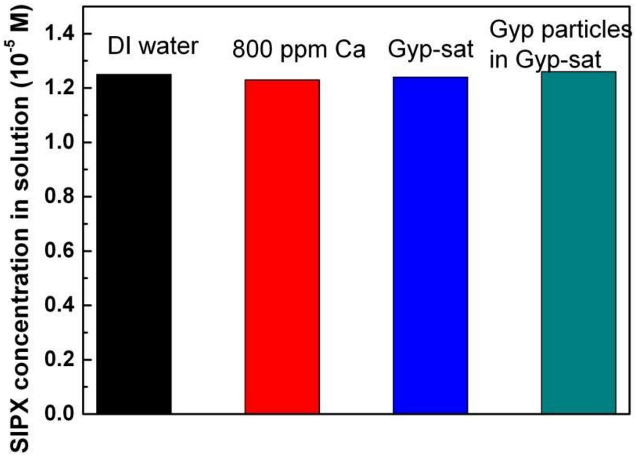

Figure 4-7 Effect of calcium, gypsum supersaturated solution and gypsum particles on the SIPX concentration in solution at pH 6.5 (Initial SIPX concentration: 1.25×10^{-5} M).

4.2.3 QCM-D results

QCM-D is a powerful technique to study the adsorption kinetics of molecular at solid-liquid interfaces. It enables real-time measurements of molecular adsorption and / or interactions on various solid surfaces in solution. In general, the changes in resonance frequency of the quartz crystal are related to the changes in mass on the crystal surface. An increase in mass induces a proportional decrease in resonance frequency. In this study the effect of calcium on the adsorption kinetics of copper and xanthate on a ZnS coated quartz sensor surface is studied using a QCM-D (Q-Sense AB, Göteborg, Sweden). The uptake of copper and SIPX on the ZnS sensor surface as a function of time was monitored in both DI water and 800 ppm calcium solution. The copper and SIPX concentrations used in this study was 1.25×10^{-5} M. For each QCM-D experiment, a stable baseline was first achieved using the DI water for the DI water system and 800 ppm calcium solution for the calcium solution system and then followed by introducing copper solutions. The baseline solutions were injected into the flow module for 3 min when the frequency shift reaches plateau. Subsequent SIPX adsorption test was performed following the same procedure described above. Normalized frequency shifts at third overtone were used to interpret the adsorption kinetics of copper and SIPX on ZnS sensor surface.

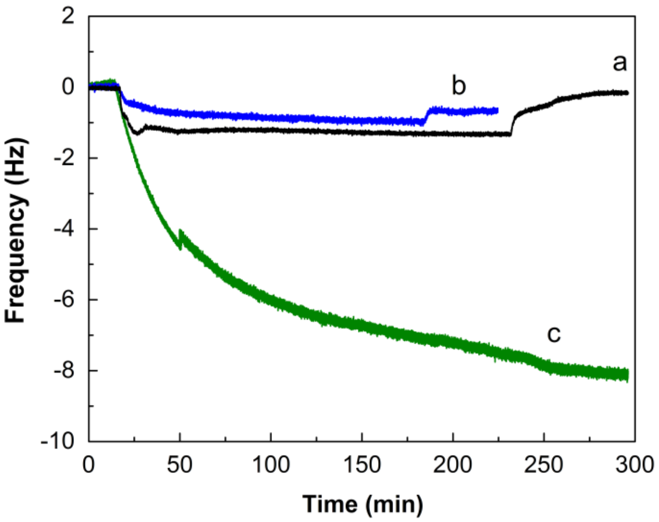

Figure 4-8 QCM-D measurement of the impact of calcium on the uptake of copper on ZnS sensor at pH 6.5. (a – adsorption of calcium (800 ppm calcium solution) on ZnS, b – adsorption of copper on ZnS in 800 ppm calcium solution, c – adsorption of copper on ZnS in DI water).

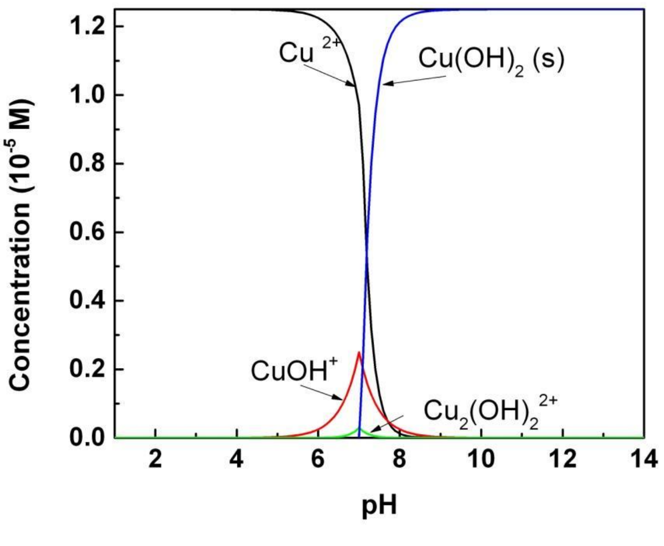

Figure 4-9 Speciation diagram for 1.25×10^{-5} M Cu^{2+}. (Equilibrium data from [182])

Figure 4-8 presents the effect of calcium on the uptake of copper on freshly cleaned ZnS sensor at pH 6.5. The adsorption of calcium on ZnS sensor surface at pH 6.5 is also monitored by QCM-D. As shown in Figure 4-8, a small negative frequency change was observed upon pumping 800 ppm calcium solution into the flow module mounted with ZnS sensor, indicating a limited adsorption of calcium. The frequency shifts back to zero when the flow module was rinsed with DI water at pH 6.5, suggesting that the adsorption of calcium on ZnS at pH 6.5 is reversible. Even though the adsorption of calcium on ZnS is limited and reversible, its effect on the uptake of copper on ZnS surface is substantial. The uptake of copper on ZnS sensor surface is significantly retarded in 800 ppm calcium solution. As shown in Figure 4-8, a rapid drop in frequency is detected when 1.25×10^{-5} M copper in DI water was introduced into the QCM-D flow module, which cannot be restored by rinsing with baseline solution (DI water). However, in 800 ppm calcium solution, the frequency change is much slower and smaller as compared with the condition without calcium ions, indicating retarded adsorption of copper species on ZnS sensor surface. It should be noted that the difference in atomic mass between copper and zinc is not significant. As shown in Figure 4-9, at pH 6.5, the majority Cu species are Cu^{2+} and $CuOH^{+}$. The activation of ZnS by Cu^{2+} is known as an ion exchange mechanism where the uptake of Cu^{2+} results in approximately 1:1 release of Zn^{2+} into the solution [105, 106, 115]. Hence, the recorded frequency change of ZnS sensor is mainly attributed to the adsorption of copper hydrolysis species, most likely in the form of $CuOH^{+}$.

The adsorption kinetic of SIPX on the copper activated ZnS sensor surface is shown in Figure 4-10. Figure 4-10 (a) compares the frequency changes vs. time monitored by QCM-D during the adsorption of SIPX on copper activated ZnS sensor with or without calcium. The dissipation shifts during the adsorption of SIPX were small compared to the frequency shifts ($-\frac{\Delta D_n}{\Delta f_n} < 1 \times 10^{-7}$), hence the mass uptake of SIPX on ZnS sensor surface can be calculated through Sauerbrey equation (Eq. 2-1) and the results are shown in Figure 4-10(b). QCM-D results confirm that SIPX does not adsorb on ZnS sensor surface without copper activation. As shown in Figure 10, the frequency of inactivated ZnS sensor stayed constant with the introduction of 1.25×10^{-5} M SIPX in the system (Figure 4-10(a)-a), as a result, zero SIPX mass uptake on the ZnS sensor surface is observed (Figure 4-10(b)-a). The activation conditions of ZnS sensor by copper has remarkable impact on the adsorption kinetics of SIPX on ZnS. The frequency change or mass uptake due to the adsorption of SIPX on ZnS sensor activated with copper in the absence of calcium (Curve d and e) is almost twice as larger as that in the presence of 800 ppm calcium (Curve b and c) (Figure 4-10). On the other hand, the presence of 800 ppm calcium has negligible impact on the uptake of SIPX on ZnS sensor that activated under the same condition. As shown in Figure 4-10, when ZnS was activated in 800 ppm, the frequency or mass vs. time curves of SIPX in 800 ppm calcium solution (b) is almost overlapping with that in DI water (c). Similarly, curve d is almost overlapping with curve e, where ZnS was activated in DI water. The QCM-D results confirm that the presence of

800 ppm calcium retards the uptake of copper species on ZnS surface and hence the sequence uptake of SIPX.

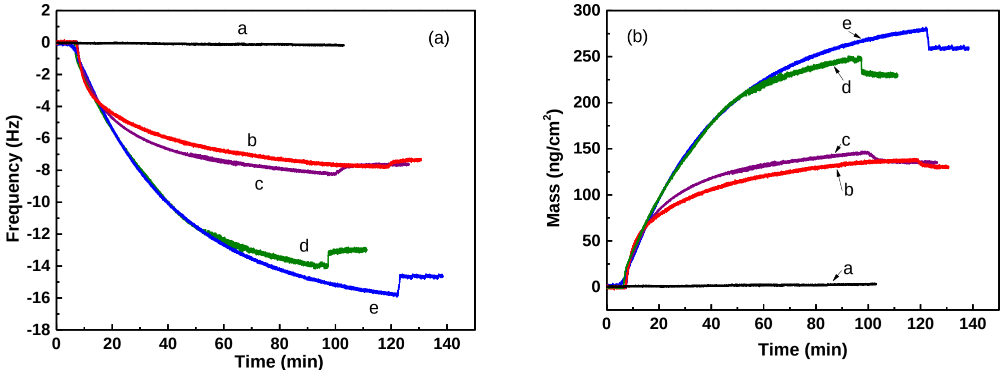

Figure 4-10 QCM-D study on the impact of calcium on the uptake of SIPX on copper activated ZnS at pH 6.5. ((a) frequency shifts monitored by QCM-D during the adsorption of SIPX. (b) mass uptake of SIPX on ZnS sensor surface converted from frequency shifts using Sauerbrey equation. a – adsorption of SIPX in DI water on ZnS sensor without activation; b – adsorption of SIPX in 800 ppm calcium solution on ZnS activated in 800 ppm calcium, c – adsorption of SIPX in DI water on ZnS activated in 800 ppm calcium, d – adsorption of SIPX in 800 ppm calcium solution on ZnS activated in DI water, e – adsorption of SIPX in DI water on ZnS activated in DI water)

It has to be noted that even though trivial change in frequency is observed in the activation of ZnS with copper in the presence of 800 ppm calcium solution (curve b in Figure 4-8), substantial frequency shifts (curve b and c in Figure 4-10) are detected when SIPX is successively pumped into the flow module, indicating that the activation of ZnS with copper at pH 6.5 involves both Cu^{2+} and $CuOH^{+}$.

4.3 Significance in sphalerite flotation

The results presented above have clearly indicated that the presence of calcium or gypsum supersaturated solution significantly impacted the copper activation of sphalerite and hence the sequence adsorption of xanthate. The reduced copper and xanthate uptake could impact the flotation behavior of sphalerite. As shown in Figure 4-11, the flotation recovery of sphalerite in 800 ppm calcium solution and gypsum supersaturated solution reduce about 15% in comparison with that in DI water. As expected, sphalerite minerals cannot be floated without activation (Figure 4-11).

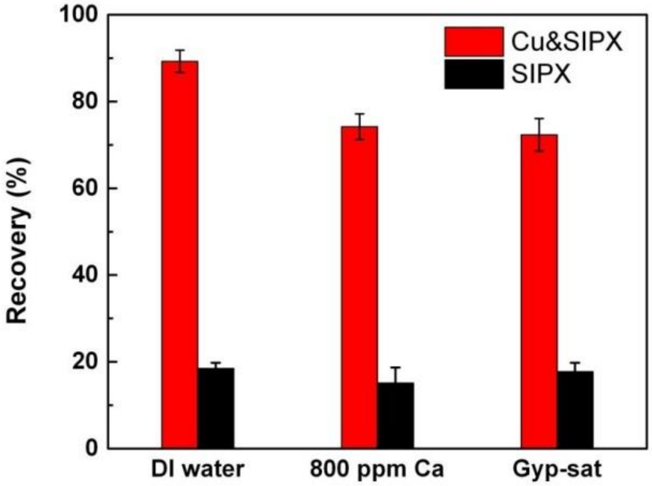

Figure 4-11 Flotation recovery of sphalerite in different solutions at pH 6.5 (Cu: 1.25×10^{-5} M, SIPX: 1.25×10^{-5} M)

Though many activation mechanisms and kinetics have been proposed for the sphalerite activation at neutral and alkaline pHs, the activation of sphalerite process with copper generally involves the following two steps: 1) the surface adsorption of copper species from solution onto minerals surface; 2) activation the surface for collector attachment. Calcium has been reported to be able to adsorb at the ZnS-H_2O interface over a wide pH range, involving the movement of calcium ions into the Stern layer without the release of an equivalent number of protons into the diffuse layer and bulk solution [36]. Our previous XPS results also confirmed that the sphalerite surface was coated with calcium in 800 ppm calcium solution and gypsum supersaturated solution. The adsorption of copper species onto sphalerite surface from bulk solution might be retarded when there is a layer of calcium at the ZnS-H_2O interface. As shown in the schematic diagram of sphalerite activation in the presence of calcium in Figure 4-12, in order to achieve successful activation of sphalerite, the copper species have to firstly move onto the ZnS-H_2O interface. The movement of copper species onto ZnS-H_2O interface depends on the bulk copper concentration as well as the surface charge on sphalerite. In the presence of calcium, the migration of copper species onto ZnS-H_2O interface from the bulk solution is retarded due to competition adsorption between copper species and calcium species. Meanwhile, the adsorption of calcium species leads to a much less negative charge on sphalerite surface, resulting in the decrease of electrostatic attraction between sphalerite surface and copper hydrolysis species in the bulk solution, which also affects the adsorption of copper species. The retardation of copper species migration onto the ZnS-H_2O interface results in the reduction of copper uptake and subsequent SIPX adsorption, which might be responsible for the decrease in flotation recovery.

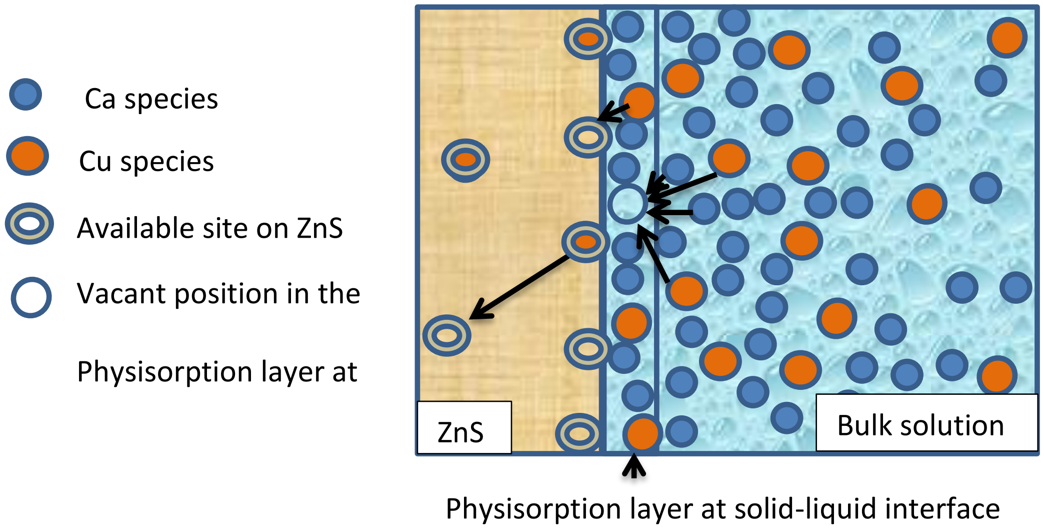

Figure 4-12 Schematic diagram of the activation process in presence of calcium

4.4 Conclusions

Supersaturated of gypsum in recycle water has a significant impact on the interactions between flotation reagents (Cu and SIPX) and sphalerite. The uptake of copper and SIPX is retarded in 800 ppm calcium solution and gypsum supersaturated recycle water. The inhabited Cu and SIPX uptake in gypsum supersaturated solution is more likely attributed to the high calcium concentration, which is responsible for the decreased flotation recovery in the gypsum supersaturated recycle water.

Chapter 5 Impact of Gypsum Supersaturated Solution on the Interactions between Silica and Zinc Sulphide Minerals

5.1 Introduction

Fine mineral particles can aggregate under certain conditions. The aggregation between mineral particles can be beneficial or detrimental to the flotation separation. For instance, the homo-aggregation of fine target mineral particles is desirable while the hetero-aggregation between gangue mineral particles and target mineral particles is detrimental to the selective separation of the target mineral from other minerals. In order to achieve selective flotation separation, it is important to understand and control the interactions between mineral particles in a processing environment.

The study of particle interactions in flotation system has been undergoing for many years. Methods of investigation on mineral interactions have included zeta potential measurements [40, 183-185], viscosity [186-190], turbidity [191, 192], apparent particle size [193, 194], settling tests [183, 184, 194], and AFM force measurements [41, 187, 195-198]. More recently, micro-gravimetric measurements obtained using the quartz crystal microbalance with dissipation (QCM-D) has also been used to evaluate the interactions between particles and clean or functionalized surfaces in aquatic environment [137, 138, 152, 153, 199]. QCM-D has been widely used to monitor the deposition kinetics of polymers [145-147], DNA [148, 149], proteins [150, 151], and nanoparticles [137, 152, 153] or microparticles [154]. In the research of using QCM-D to determine the deposition kinetics of nanoparticles, the mass of nanoparticles deposited on QCM-D sensor surface was related to the measured decrease in the resonance frequency of a QCM-D crystal. Increases in resonance frequency of the QCM-D crystal were observed, however, in the investigation of micro size particles deposition kinetics [154]. Positive frequency shifts occur when the crystal is put into contact with a sufficiently large sphere [200]. The positive frequency shift is due to the increase in the effective *stiffness* of the composite resonator, rather than the mass. Another approach to characterize the particle deposition using the QCM-D is the measurement of the energy dissipation factor. The measurements of nanoparticle deposition onto silica obtained with QCM-D were in relatively good agreement with DLVO predictions [137, 152, 153]. The advantages of using QCM-D to characterize the interactions between mineral surfaces are that it provides real-time in-situ studies, and both quantitative and qualitative results can be obtained.

QCM-D has been proven to be a powerful tool for investigating the influence of environmental conditions on nanoparticle deposition onto clean and functionalized surfaces. However, it has to be noted that QCM-D studies alone might not be able to develop a fundamental understanding of the interactions between the surfaces. Under conditions that the suspended particles aggregate, the actual deposition or attachment kinetics can be obscured by the gravity effect due to the QCM-D setup. The recent QCM-D instruments provided by Q-sense allow the particle suspension to flow on the top of the quartz crystal. When the suspended particles homo-aggregate which resulting in the increase of apparent particle size and density, the particles can deposit on the QCM-D crystal surface by gravity force. Hence, using QCM-D to study the interactions between minerals can sometimes be misleading. In order to obtain reliable results, it is important to improve the QCM-D experiment setup and couple it with other methods such as AFM force measurements, zeta potential tests, and settling test. In this study, we carefully designed the QCM-D setup by placing the QCM-D chamber upside down to make sure the monitored resonance frequency and energy dissipation changes were caused by the real particle attachment.

In flotation system, a variety of uncontrolled species exist in the pulp arising from the water source, involved minerals and deliberate additives. The role of these species on the interactions between minerals in zinc sulphide flotation has received considerable attention. Zeta potential measurements, settling tests, particle size distribution measurements, and direct colloidal force measurements in combination with model predictions have been carried out to study the homo- and hetero- aggregation of zinc sulphide and silicate minerals [30, 38, 40, 41, 187, 191-193, 195-198, 201-203]. The effect of pulp pH, ionic strength, calcium ion, and other additives including activator, depressant and collector on the interactions between silicate minerals, zinc sulphide minerals and, silicate and zinc sulphide minerals has been extensively investigated. Calcium has been proven to have significant effect on the interactions between zinc sulphide and silicate minerals [40, 41]. The calcium concentration used in these previous studies was no more than 0.5 mM (20 ppm). In real zinc sulphide flotation plants especially those practising recycle water, however, the calcium ion concentration in the process water is far more than that and can be as high as up to 20 mM (800 ppm) [28, 45]. In addition, gypsum supersaturated process water has been a concern in the sulphide mineral flotation separation [26-28]. In this study, we focus on the impact of gypsum supersaturated process water on the flotation separation of zinc sulphide and silicate minerals. The purpose of this study is to examine systematically the effect of divalent ions (Ca and Mg) and gypsum supersaturated water on the interactions between zinc sulphide and silica minerals. QCM-D was used to evaluate the deposition behaviour of silica nanoparticles onto ZnS or SiO_2 coated quartz crystal surface over a broad range of divalent ions concentrations and gypsum supersaturated water. To better understand the interactions between silica and zinc sulphide, and silica-silica minerals in the presence of calcium ions, magnesium ions, and gypsum supersaturated water, the colloidal forces between a silica particle and a fractured sphalerite mineral surface, and a silica particle and a silica wafer surface were measured. AFM results and predictions based on DLVO theory were employed to verify the QCM-D observations. The impact of calcium ions, magnesium ions, and gypsum supersaturated water on the flotation selectivity of sphalerite from silica was discussed.

5.2 Results and discussion

5.2.1 Electrokinetic characterization of silica nanoparticles, natural sphalerite, SiO_2 and ZnS sensor

The zeta potentials of silica and sphalerite particles in various concentrations of calcium and magnesium solutions and gypsum supersaturated water were measured using a ZETAPALS (Brookhaven Instruments, NY, USA). The 15 nm silica particles were used for the zeta potential measurement and the - 45 µm sphalerite particles were further ground to about - 5 µm. The reproducibility of the measurement was ± 3 mV determined from repeat experiments. The zeta potential of SiO_2 and ZnS coated quartz sensor was measured using streaming potential method (SurPASS, Anton Paar). The measurements were made at room temperature.

Figure 5-1 shows the zeta potential of silica nanoparticles, natural sphalerite particles, SiO_2 and ZnS sensor in different water chemistries at pH 6.5. In 1 mM KCl solution without calcium or magnesium, the zeta potentials of silica and sphalerite particles are - 26 mV and - 17 mV respectively, which are comparable to values reported previously under similar conditions [40, 114, 180, 181]. The zeta potentials of ZnS coated quartz sensor (- 25 mV) and SiO_2 coated quartz sensor (-50 mV) are slightly more negative than that of natural sphalerite and silica nanoparticles. Such a difference could be a result of different measurement techniques used to measure zeta potentials of sensors and mineral particles. The different crystalline nature between the ZnS or SiO_2 coatings and the mineral particles could also contribute to the observed difference in zeta potentials between ZnS or SiO_2 snesor surfaces and sphalerite or silica particles. In the presence of calcium or magnesium ions, the zeta potentials of silica, sphalerite particles, SiO_2 and ZnS sensors become less negative with increasing concentration of calcium and magnesium ions. Our previouse study indicate that the zeta potentials of silica and sphelrite in the gypusm supersaturated solution are almost idential, - 10 mV. The zeta potential values detemined are used later to interprerate the inetraction forces between silica and sphalerite/ZnS, measured using AFM.

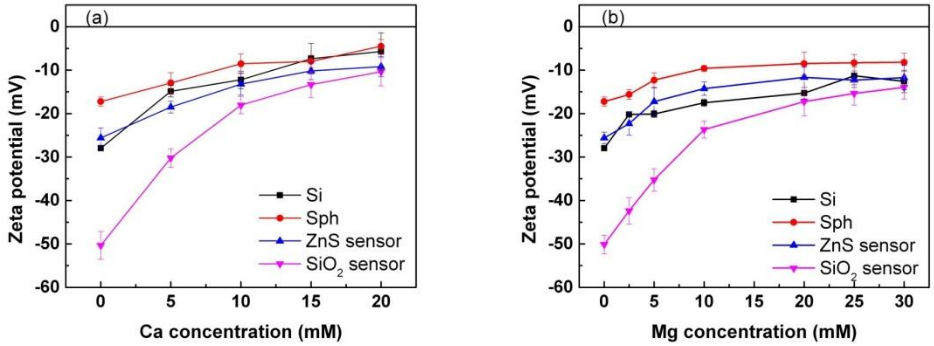

Figure 5-1 Zeta potentials of silica, sphalerite, and ZnS sensor as a function of (a) calcium and (b) magnesium concentration at pH 6.5.

5.2.2 Principle of using QCM-D to study mineral interaction

The idea of using a QCM-D to determine the interactions between minerals is fairly straight forward. The quartz sensor can be coated with desired minerals. Meanwhile, mineral particles can be suspended in desired solutions and injected into the QCM-D modules mounted with desired mineral sensor. The interaction between the mineral sensor and the mineral particles is then evaluated by monitoring the frequency and energy dissipation of the mineral coated quartz crystal sensor. The frequency and dissipation of the mineral sensor would stay constant if there are no mineral particles deposited on the mineral sensor surface. On the other hand, if the mineral particles in the suspension attach onto the mineral sensor surface, the frequency and dissipation of the sensor would shift, depending on the amount of particles deposited on the sensor surface and the structure of the deposited particles. In this way, the interactions between minerals can be determined. An advantage of this method over the zeta potential distribution method [30, 132, 185] to study mineral particle interactions is that it does not have any limitation on surface properties of interacting particles. In fact this method can also study homo-aggregation (silica-silica and sphalerite-sphalerite, for example) as well as hetero-aggregation (silica-sphalerite, for example) for any mineral pairs as long as one of the minerals could be coated on quartz crystal sensors.

Figure 5-2 shows representative QCM-D measurements of the interactions between silica nanoparticles and ZnS sensor surface. In phase 1, a particle-free baseline solution was injected to the QCM-D module. After establishing a baseline, a silica suspension was injected into the QCM-D module (phase 2) until a stable frequency and dissipation signal is established. During this phase 2 period, a decrease in frequency and an increase in dissipation would be observed if silica nanoparticles deposit onto the ZnS sensor surface (Solid lines), in contrast to a constant frequency and dissipation which would indicate the absence of deposition (Dash lines). Over phase 3, the baseline solution of the same IS (ionic strength) and pH is introduced into the flow module to remove the loosely attached particles.

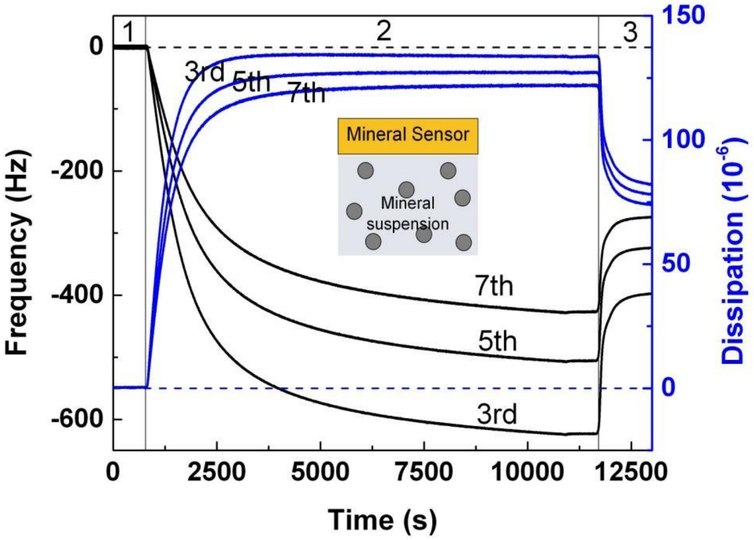

Figure 5-2 Representative frequency and dissipation shifts obtained by QCM-D for deposition of SiO_2 nanoparticles onto ZnS coated QCM-D crystals.

Based on the Sauerbrey relation (Eq. 2-1), the frequency shift (Δf) is proportional to the change in mass (Δm) at the crystal surface, the rate of frequency change (Δf) is equivalent to the rate of mass increase on the crystal surface, i.e., the deposition rate of particles onto the crystal surface. In this way, the silica deposition rate can be determined by calculating the initial slope of the f versus time plot:

$$-f_{n/Slope} = -\frac{d\Delta f_n}{dt} \tag{5-1}$$

Note that the frequency shifts obtained from QCM-D were normalized, divided by the overtone number (n=3, 5, and 7, in this case). This approach has been used in the studies of deposition kinetics of engineering nanoparticles on clean or functionalized surfaces, relying on the Sauerbrey relation (Eq. 2-1) for rigidly adsorbed films [137, 138, 152, 153, 204, 205].

As mentioned early in 2.3.1 of chapter 2, the dissipation provides information on rigidity of the attached materials. A perfectly rigid layer of particles attached onto the crystal surface should yield a zero increase in dissipation (D). However, the deposition of each particle onto the crystal surface can add a similar amount of energy loss which is reflected in dissipation (D) [152]. Based on the suggestion of the manufacture of QCM-D (Q-Sense), the Sauerbrey relation (Eq. 2-1) is applicable when the $-\Delta D_n/\Delta f_n$ ratio is below 1×10^{-7} Hz^{-1} (the adsorbed mass cause a small dissipation compared to the frequency shift). Reviakine et al. [134]

proposed the $-\Delta D_n/\Delta f_n$ threshold value of 4 × 10^{-7} Hz^{-1}. Otherwise, the frequency shifts underestimate the adsorbed mass when the dissipation shifts are too large within the adsorbed film [137, 138]. For this reason, the variation in dissipation change with time ($-\frac{d\Delta D_n}{dt}$) has been used to evaluate the deposition kinetics of particles in some of the cases [137, 138, 152]. Meanwhile, the $-\Delta D_n/\Delta f_n$ ratio has been employed as an indication of the rigidity of homogeneously adsorbed films. In the studies of polymer adsorptions, for instance, the $-\Delta D_n/\Delta f_n$ ratio has been used to study the conformation changes in adsorbed layers [206, 207].

Moreover, the QCM-D E4 system simultaneously measures frequency and dissipation changes at multiple overtones. The different overtones give information about the homogeneity of deposited layers. Variation in frequency and dissipation at different overtones suggest depth heterogeneous in the deposited layers.

5.2.3 QCM-D study on the impact of divalent ions (Ca^{2+} and Mg^{2+}) and gypsum supersaturated solution on mineral interaction

5.2.3.1 In Milli-Q water

Interactions between silica nanoparticles and ZnS or SiO_2 coated sensor surface in Milli-Q water were monitored using a QCM-D. As shown in Figure 5-3, changes in the frequency and dissipation of the ZnS (Figure 5-3a) or SiO_2 (Figure 5-3b) coated sensor are minimal when silica nanoparticle suspension was introduced into the QCM-D chamber and the frequency shifts back to zero when the sensor surface was rinsed with particle-free the baseline solution (Milli-Q water). The small frequency shift is due to the bulk effect when switching the baseline solution into a silica suspension. The QCM-D response indicates the absence of silica nanoparticle deposition onto ZnS or SiO_2 coated sensor surface in Milli-Q water. Note that both silica nanoparticles and ZnS or SiO_2 coated sensor surface carry very negative surface charge in Milli-Q water of pH 6.5. Zeta potential measurement showed that the zeta potentials of silica nanoparticle, and ZnS or SiO_2 coated sensor in 1 mM KCl of pH 6.5 were - 35 mV, - 25 mV and - 50 mV, respectively. The strong electric double layer (EDL) repulsive force between silica nanoparticle and ZnS or SiO_2 coated sensor surface prevents the attachment of silica nanoparticles onto sensor surfaces. The interaction forces between silica and silica or sphalerite in a simple electrolyte solution will be further discussed in section 5.2.3.

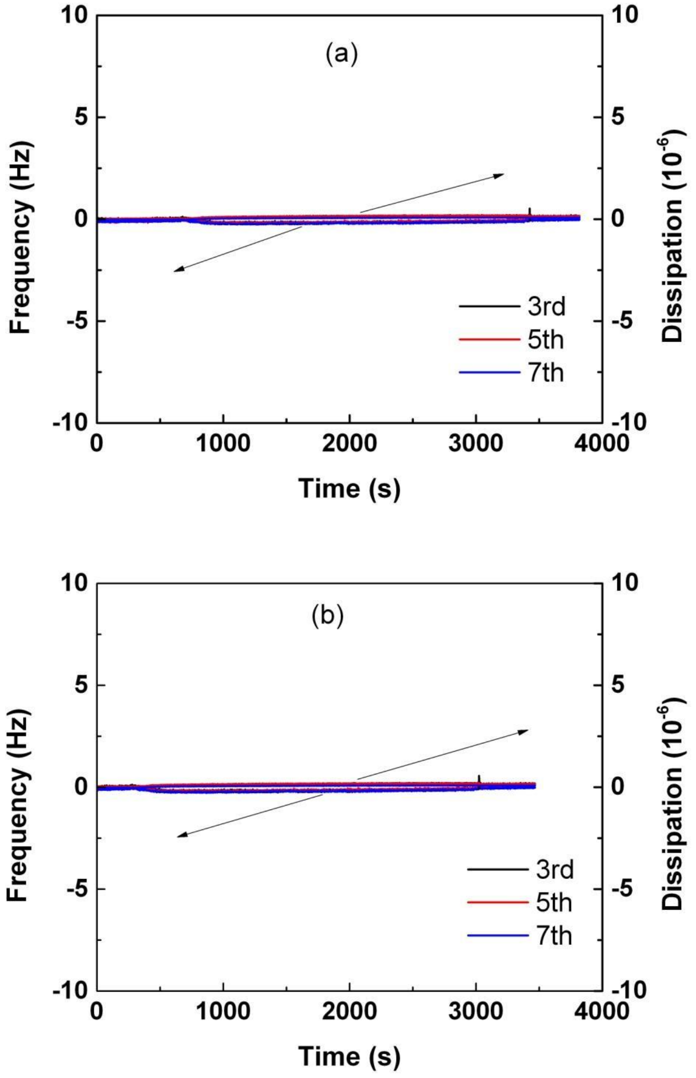

Figure 5-3 QCM-D frequency and dissipation response of 3^rd^, 5^th^, 7^th^ overtone as a function of time of the attachment of silica nanoparticle on (a) ZnS coated sensor and on (b) SiO_2 coated sensor in Milli-Q water of pH 6.5 (baseline solution: Milli-Q water of pH 6.5).

5.2.3.2 Impact of calcium ions

(1) Silica – sphalerite interaction

Deposition of silica nanoparticles on ZnS sensor surface in calcium ion solutions, measured by QCM-D are shown in Figure 5-4. Figure 5-4a shows the representative normalized frequency shifts of third overtone as silica nanoparticles deposit on ZnS surface in $CaCl_2$ solutions of pH 6.5. A greater frequency drop (larger absolute values of (Δf_3)) indicates a larger amount of silica nanoparticles deposited onto the ZnS sensor surface. It is evident that the presence of calcium triggers the deposition of silica nanoparticles onto ZnS sensor surface. As shown in Figure 5-4a, the frequency of ZnS coated sensor in Milli-Q water stays constant, indicating the absence of silica deposition onto ZnS surface. However, in the presence of calcium, frequency drop resulting from the deposition of silica on ZnS surface is observed. The frequency shift (Δf_3) increases with increasing calcium concentration, indicating that more nanoparticles deposited on ZnS sensor surface at a higher calcium concentration in the concentration range tested. It should be noted that in the absence of silica nanoparticles, increasing calcium concentration in the tested range showed a negligible change in frequency of quartz crystal sensors, indicating that the contribution frequency change due to calcium ion adsorption to the frequency change of particle deposition is negligible. The deposition rate determined from the slope of the initial (linear) portion of the normalized frequency (f_3) vs time curve is presented in Figure 5-4b. In the absence of calcium (Milli-Q water), the silica deposition rate on ZnS surface is zero. The deposition rate increases almost linearly with increasing calcium ion concentration. The QCM-D results demonstrate that the presence of calcium ions in a process medium can induce the hetero-aggregation between silica and sphalerite minerals, the degree of which increases with the increase of calcium concentration.

(2) Silica – silica interaction

Figure 5-5 shows the deposition kinetics of silica nanoparticles on SiO_2 coated sensor surfaces as a function of calcium concentration at pH 6.5. Silica nanoparticles do not deposit on the SiO_2 sensor surface in the absence of calcium or low calcium concentration. As shown in Figure 5-5a, the frequency of SiO_2 sensor stayed constant when silica nanoparticles suspended in Milli-Q water or 5 mM of calcium solution of pH 6.5. Deposition of silica nanoparticles on the SiO_2 coated sensor surface is observed when increasing the calcium concentration up to 10 mM. Increase the calcium concentration to 15 mM results in more silica nanoparticle deposition. The deposition of silica nanoparticles does not increase much more with further increasing the calcium concentration to 20 mM (800 ppm). The deposition rate of silica nanoparticles increases with the increase of calcium concentration under the tested calcium concentration range as shown in Figure 5-5b. The QCM-D results indicate that the presence of high calcium ions concentration (up to 10 mM) induces the homo-aggregation between silica and silica. The extent of homo-aggregation increases with the increasing calcium concentration.

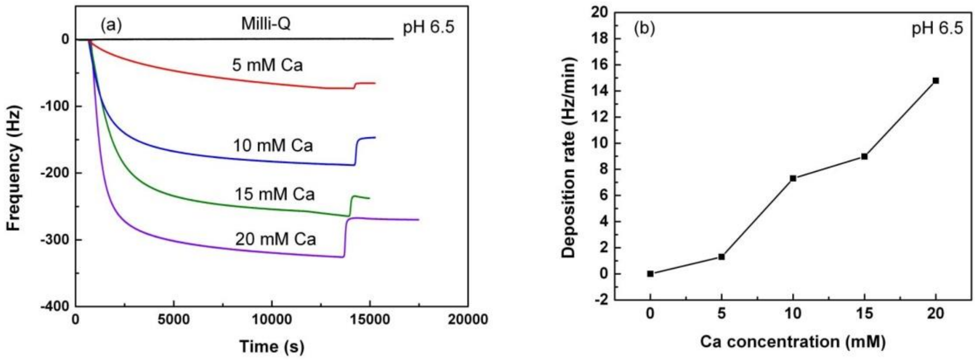

Figure 5-4 Deposition of silica particles on ZnS coated sensor surface as a function of calcium concentration at pH 6.5 ((a) normalized frequency shifts of third overtone as silica nanoparticles deposit on ZnS surface in $CaCl_2$ solutions of different Ca concentration; (b) deposition rate determined from the slope of the initial (linear) portion of the normalized frequency (f_3) vs time curve).

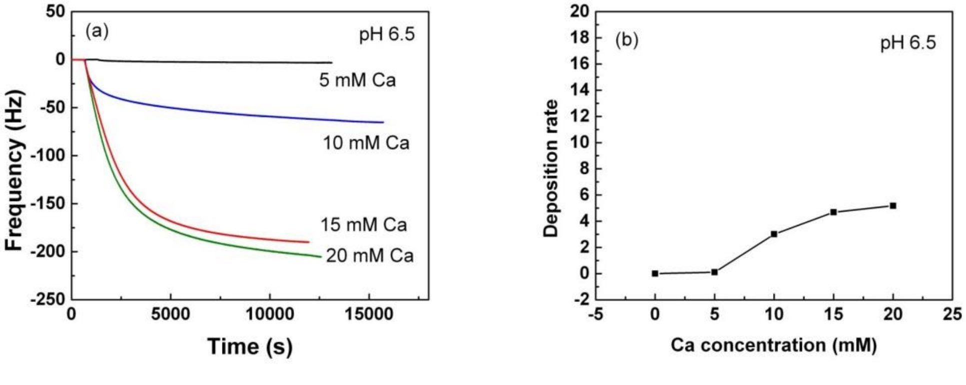

Figure 5-5 Deposition of silica nanoparticles on SiO_2 coated sensor surface as a function of calcium concentration at pH 6.5 ((a) normalized frequency shifts of

third overtone as silica nanoparticles deposit on SiO_2 surface in $CaCl_2$ solutions of different Ca concentration; (b) deposition rate determined from the slope of the initial (linear) portion of the normalized frequency (f_3) vs time curve).

(3) Interpretation of the $-\Delta \boldsymbol{D}_{\boldsymbol{n}}/\Delta \boldsymbol{f}_{\boldsymbol{n}}$ ratio

Dissipation as a function of frequency has been employed to indicate the variation in the adsorption kinetics, layer viscosity, and conformational changes in the adsorbed layers [146, 147, 206-209]. The ratio of dissipation and frequency change ($-\Delta \boldsymbol{D}_{\boldsymbol{n}}/\Delta \boldsymbol{f}_{\boldsymbol{n}}$ ratio) enables the examination of the adsorbed layer properties [136, 204, 210, 211]. The $-\Delta \boldsymbol{D}_{\boldsymbol{n}}/\Delta \boldsymbol{f}_{\boldsymbol{n}}$ ratio has been utilized in the evaluation of layer formation and rigidity of deposited solid particles [135, 204, 211]. The layer thickness should not affect the $-\Delta \boldsymbol{D}_{\boldsymbol{n}}/\Delta \boldsymbol{f}_{\boldsymbol{n}}$ ratio if the deposited particle layer is homogenous [135].

Figure 5-6 shows the $-\Delta \boldsymbol{D}_{\boldsymbol{3}}/\Delta \boldsymbol{f}_{\boldsymbol{3}}$ ratio as a function of time of the deposition of silica nanoparticles on ZnS and SiO_2 sensor surface in various concentrations of calcium. As shown in Figure 5-6, the $-\Delta \boldsymbol{D}_{\boldsymbol{3}}/\Delta \boldsymbol{f}_{\boldsymbol{3}}$ ratios as a function of deposition time for both SiO_2-ZnS (Figure 5-6a) and SiO_2-SiO_2 (Figure 5-6b) pairs are considerable high under all tested calcium concentrations, though they fairly meet the Sauerbrey limit (Reviakine et al.), suggesting that the deposited nanoparticle layer contains much water. Meanwhile, the $-\Delta \boldsymbol{D}_{\boldsymbol{3}}/\Delta \boldsymbol{f}_{\boldsymbol{3}}$ ratios for the deposition of silica nanoparticle on both ZnS and SiO_2 sensor at various calcium concentration decrease with time. The decrease of $-\Delta \boldsymbol{D}_{\boldsymbol{3}}/\Delta \boldsymbol{f}_{\boldsymbol{3}}$ ratio with time indicates changes in the layer coverage and particle distribution along the deposition process [135]. The $-\Delta \boldsymbol{D_3}/\Delta \boldsymbol{f_3}$ ratio vs. time plots in Figure 5-6 implies that the deposited silica nanoparticles layer consists of particle clusters which may not fully cover the sensor surface.

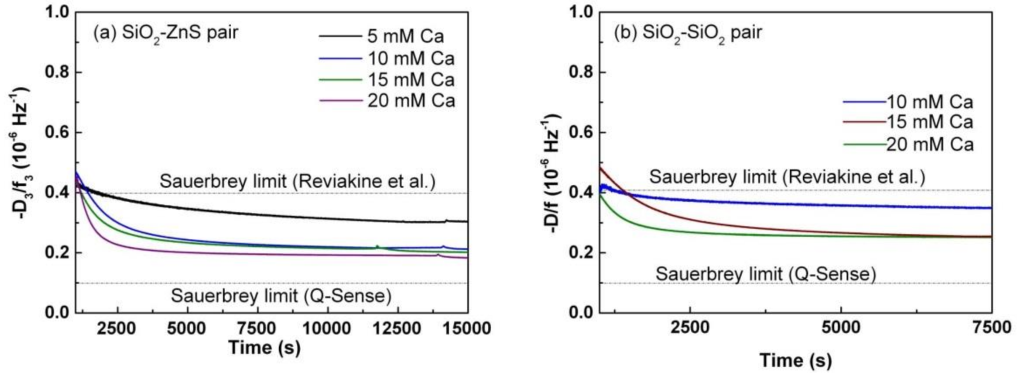

Figure 5-6 The dissipation to frequency ratio of the 3rd overtone as a function of time of the deposition of silica nanoparticle on (a) ZnS and (b) SiO_2 sensor surface in various concentrations of calcium

Comparing the $-\Delta \boldsymbol{D_3}/\Delta \boldsymbol{f_3}$ ratio vs. time in different calcium concentrations, it is evident that the $-\Delta \boldsymbol{D_3}/\Delta \boldsymbol{f_3}$ ratio for both SiO_2-ZnS (Figure 5-6a) and SiO_2-SiO_2 (Figure 5-6b) pairs decreases with the increase of calcium concentration. This suggests that the deposited silica nanoparticles layer on both ZnS and SiO_2 sensor surface become more rigid and homogenous as the increase of calcium concentration. A more rigid particle layer indicates stronger attachment of the deposited particles on a sensor surface.

In the presence of calcium ions, the zeta potentials of silica and sphalerite particles, and ZnS or SiO_2 sensor all become less negative with increasing calcium concentration, resulting in the decrease of electrostatic repulsive force between mineral surfaces. The surface charge on the deposition kinetics of silica nanoparticles on ZnS or SiO_2 coated sensor surfaces will be further discussed in the following section.

5.2.3.3 Impact of Mg ions

(1) Silica-sphalerite interaction

The impact of magnesium on the deposition of silica nanoparticle on ZnS sensor surface is similar to that of calcium. As shown in Figure 5-7, silica deposition on ZnS surface is induced in the presence of magnesium. Increasing the concentration of magnesium increases the deposition rate and the amount of silica particle deposition on ZnS surface. In comparison with the effect of calcium, the impact of magnesium on the deposition kinetic of silica on ZnS sensor is not as dramatic. Under the same concentrations of calcium and magnesium, the magnitude of frequency shifts and deposition rate in the presence of magnesium is smaller than that in the presence of calcium. This observation could be attributed to the less effective surface charge neutralization of magnesium on both silica and sphalerite surface comparing to calcium. As show in Figure 5-1, the shift of zeta potentials of both silica and sphalerite surface caused by the addition of magnesium is much less than that of the addition of calcium.

(2) Silica – silica interaction

Similar to the case of calcium ions, homo-aggregation between silica and silica is triggered in the presence of high concentrations of magnesium ions. As shown in Figure 5-8a, deposition of silica nanoparticles on SiO_2 sensor surface is absent or not significant under low magnesium ion concentration, 24 ppm (1 mM), for example. With increasing the magnesium concentration, however, deposition of silica nanoparticles is observed. The deposition increases with increase magnesium concentration. In comparison with the case of calcium ions, the impact of magnesium on the deposition kinetic of silica on SiO_2 sensor is not quite predominant. The deposition kinetics of silica nanoparticle on SiO_2 sensor surface in the presence of magnesium can be well explained by the surface charge of silica minerals (as discussed in 5.2.1). The presence of magnesium ions neutralizes the negative surface charge of silica (Figure 5-1b), resulting in the decrease in the electrical double layer force (or energy barrier) between silica and silica surface.

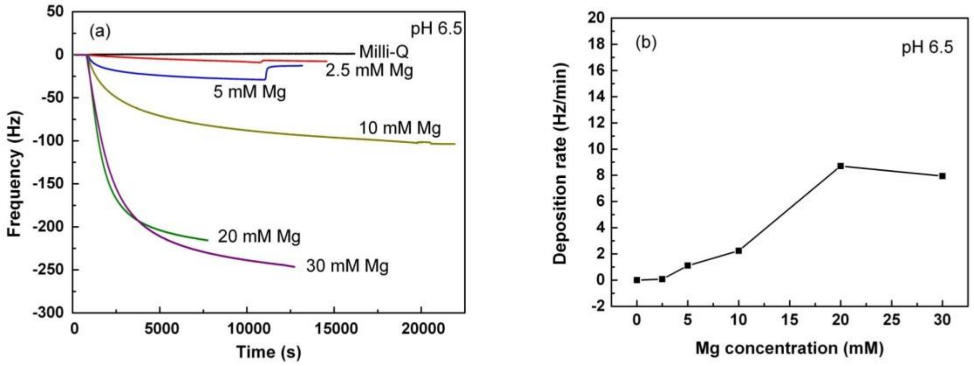

Figure 5-7 Deposition of silica particles on ZnS sensor surface as a function of magnesium concentration at pH 6.5 ((a) normalized frequency shifts of third overtone as silica nanoparticles deposit on ZnS surface in solutions of different Mg concentration; (b) deposition rate determined from the slope of the initial (linear) portion of the normalized frequency (f_3) vs time curve).

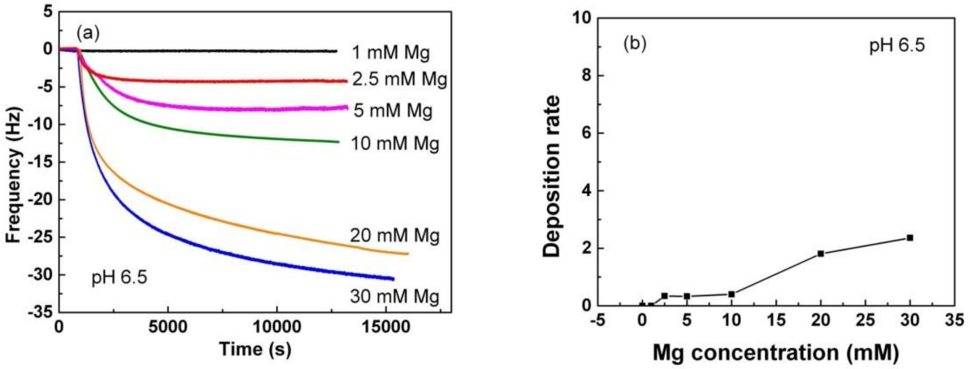

Figure 5-8 Deposition of silica particles on silica sensor surface as a function of magnesium concentration at pH 6.5 ((a) normalized frequency shifts of third overtone as silica nanoparticles deposit on SiO_2 surface in solutions of different

Mg concentration; (b) deposition rate determined from the slope of the initial (linear) portion of the normalized frequency (f_3) vs time curve).

(3) Interpretation of the $-\Delta \boldsymbol{D_n}/\Delta \boldsymbol{f_n}$ ratio

Similar to the calcium solutions, the $-\Delta \boldsymbol{D_3}/\Delta \boldsymbol{f_3}$ ratios (Df-ratio) as a function of deposition time for both SiO_2-ZnS (Figure 5-9a) and SiO_2-SiO_2 (Figure 5-9b) pairs at various magnesium concentrations decrease with time, indicating changes in the layer coverage and particle distribution along the deposition process [135]. In magnesium solutions, the deposited silica nanoparticles layer also consists of particle clusters which may not fully cover the sensor surface. The deposited silica nanoparticles layer on both ZnS and SiO_2 sensor surface become more rigid and homogenous with the increase of magnesium concentration. As shown in Figure 5-9, the $-\Delta \boldsymbol{D_3}/\Delta \boldsymbol{f_3}$ ratios vs. time curves for both SiO_2-ZnS (Figure 5-9a) and SiO_2-SiO_2 (Figure 5-9b) pairs decrease with increase magnesium concentration, suggesting that the attachment of silica nanoparticles on both ZnS and SiO_2 coated sensor surfaces is stronger at higher magnesium concentrations.

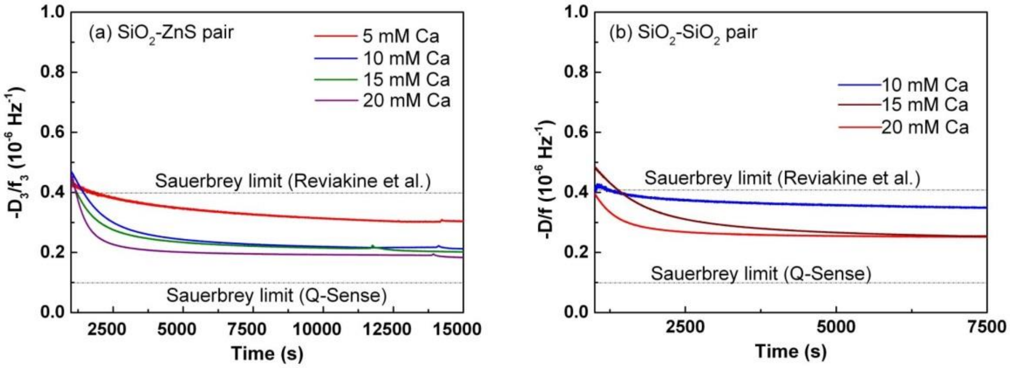

Figure 5-9 The dissipation to frequency ratio of the 3rd overtone as a function of time of the deposition of silica nanoparticle on (a) ZnS and (b) SiO_2 sensor surface in various concentrations of calcium

5.2.3.4 Impact of gypsum supersaturated solution

Supersaturation of water with gypsum has a significant impact on the interactions between silica nanoparticles and ZnS or SiO_2 coated sensor surface (Figure 5-10). In contrast to that of Milli-Q water system, significant frequency shifts were detected on both ZnS (Figure 5-10a) and SiO_2 (Figure 5-10b) coated sensor surface when dispersing the silica nanoparticles in the gypsum supersaturated solution. The substantial maximum changes in frequency, - 620 Hz for ZnS coated sensor and - 525 Hz for SiO_2 coated sensor on the third overtone, indicate a large amount of silica nanoparticles attached onto both ZnS and SiO_2 coated sensor surface. Variations in frequency shifts at different overtones were observed in both silica nanoparticle-ZnS and silica nanoparticle-

SiO_2 pairs, implying the heterogeneous depth distribution of the attached silica nanoparticle layers.

Accompanying with the frequency shifts, phenomenal energy dissipation shifts were observed (Figure 5-10), suggesting the attached silica nanoparticle layer is viscous and contains water. Plotting the QCM-D response of silica nanoparticle attachment as the dissipation to the frequency ratio vs. time shows that the Df-ratio of silica nanoparticle attachment on both ZnS and SiO_2 coated sensor surface decreases with time (Figure 5-11), suggesting the changes in the layer coverage and particle distribution along the silica nanoparticle attachment [135, 211]. The silica nanoparticles attached onto ZnS or SiO_2 coated sensor surface possibly form a layer consisting of particle clusters which do not homogenously cover the sensor surface. It is also noticeable that the Df-ratio of silica nanoparticle deposition on SiO_2 sensor is higher than that of ZnS sensor, indicating the attached silica nanoparticle layer on ZnS sensor surface is more rigid than on SiO_2 sensor. In another word, the attachment of silica nanoparticles on ZnS sensor surface is stronger than those on SiO_2 sensor surface.

It should be noted that the QCM-D response of the adsorption of gypsum supersaturated solution on both ZnS and SiO_2 coated sensor surface is negligible in comparison to that of a silica nanoparticles suspension in gypsum supersaturated solution. Our previous results also showed that gypsum precipitates formed in the gypsum supersaturated solution well dispersed with silica and sphalerite minerals. Nevertheless, the QCM-D results show that the gypsum supersaturated water induces the hetero-aggregation between silica and sphalerite, or slime coating of silica fines on sphalerite mineral surface, and homo-aggregation of fine silica particles. The substantial attachment of silica nanoparticles onto ZnS or SiO_2 coated sensor surface observed in the gypsum supersaturated solution is probably attributed to the compressed electric double layer with the supersaturation of water by gypsum. The zeta potentials of silica nanoparticle and ZnS or SiO_2 coated sensor surface are much less negative in gypsum supersaturated water of pH 6.5, - 10 mV, in comparison with those in 1 mM KCl solution of the same pH.

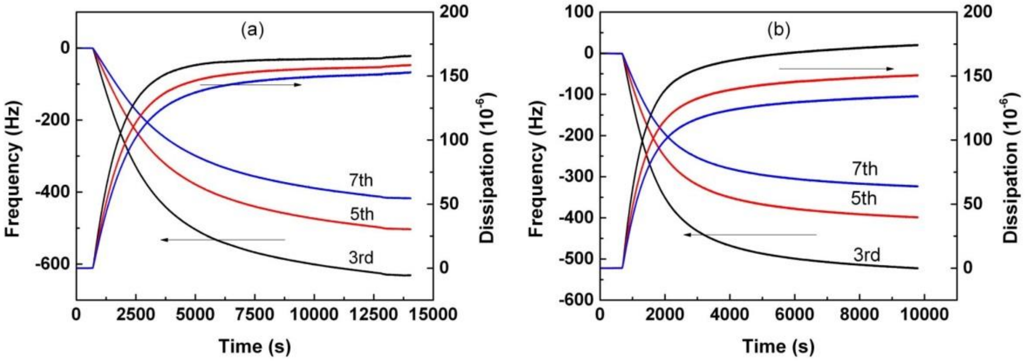

Figure 5-10 QCM-D frequency and dissipation response of 3rd, 5th, 7th overtone as a function of time of the attachment of silica nanoparticle on (a) ZnS coated sensor and on (b) SiO_2 coated sensor in gypsum supersaturated solution of pH 6.5 (baseline solution: gypsum supersaturated solution of pH 6.5).

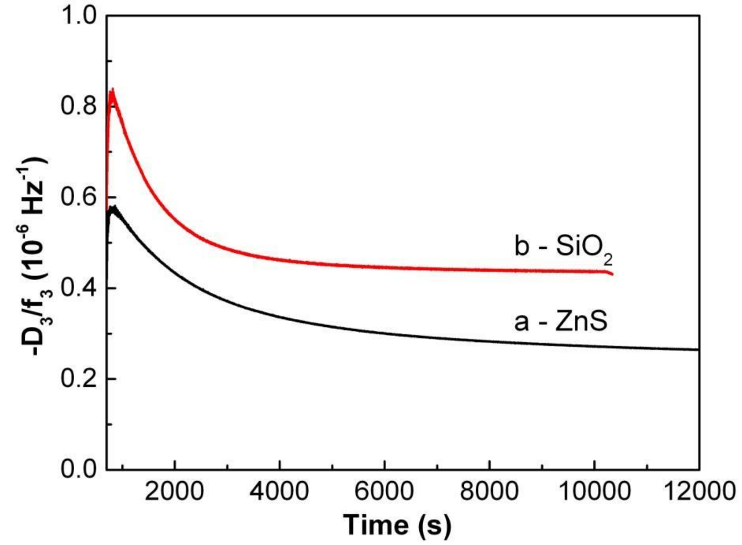

Figure 5-11 The dissipation to frequency ratio of the 3rd overtone as a function of time of the attachment of silica nanoparticle on (a) ZnS coated sensor and on (b) SiO_2 coated sensor in gypsum supersaturated solution of pH 6.5.

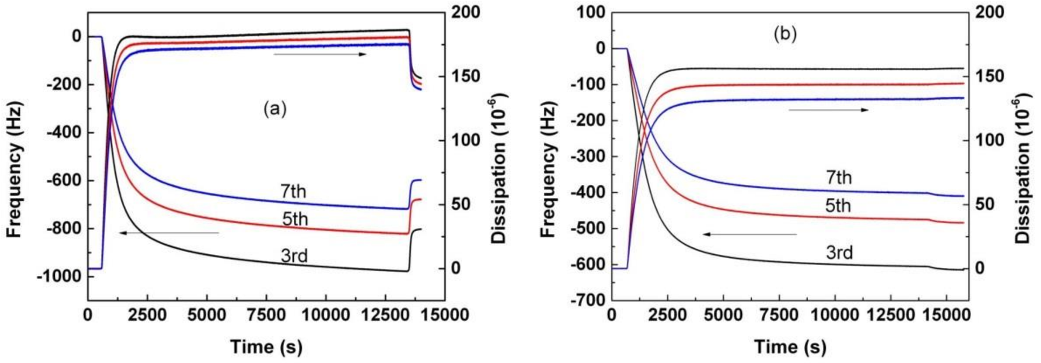

Figure 5-12 QCM-D frequency and dissipation response of 3rd, 5th, 7th overtone as a function of time of the attachment of silica nanoparticle on (a) ZnS coated sensor and on (b) SiO_2 coated sensor in 800 ppm calcium solution of pH 6.5 (baseline solution: 800 ppm calcium solution of pH 6.5).

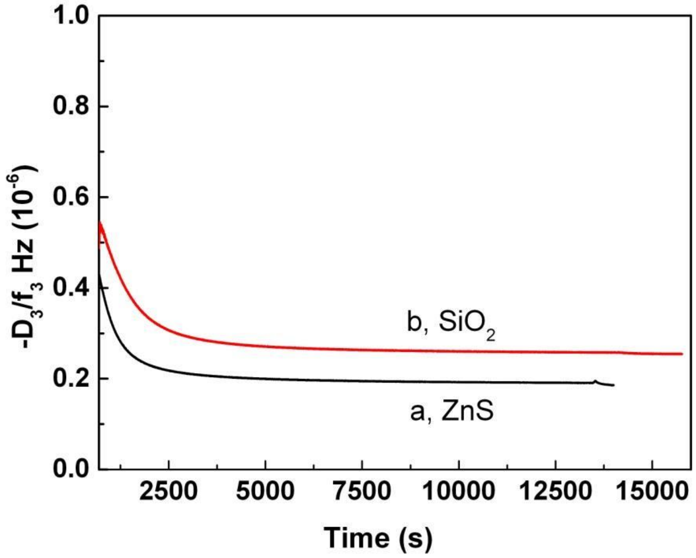

Figure 5-13 The dissipation to frequency ratio of the 3rd overtone as a function of time of the attachment of silica nanoparticle on (a) ZnS coated sensor and on (b) SiO_2 coated sensor in 800 ppm calcium solution of pH 6.5.

The strong hetero-aggregation between silica nanoparticle and ZnS surface, and homo-aggregation between silica nanoparticles and SiO_2 surface is most likely attributed to the high calcium concentration of the gypsum supersaturated solution. As shown in Figure 5-12, strong hetero-aggregation between silica and sphalerite, and homo-aggregation of silica is also found in 800 ppm calcium solution. Dramatic frequency shifts were detected on both ZnS and SiO_2 coated sensor when introducing the silica suspension in an 800 ppm calcium solution of pH 6.5. Again, the attached silica nanoparticles layer shows heterogeneous depth distribution, as variation in the measured overtones were detected (Figure 5-12). The maximum frequency shift of the silica nanoparticle – ZnS sensor pair (-

910 Hz for the 3rd overtone) is higher than that of silica nanoparticle – SiO_2 sensor pair (- 610 Hz for the 3rd overtone), indicating that more silica nanoparticles might have attached on ZnS coated sensor surface than on SiO_2 sensor surface. Meanwhile, an increase in frequency was observed when switching the silica suspension into a particle free baseline solution (800 ppm calcium solution of pH 6.5), indicating the detachment of silica nanoparticles from ZnS coated sensor surface. This phenomenon was not observed in the gypsum supersaturated system (Figure 5-11) and silica nanoparticle – SiO_2 sensor pair in 800 ppm calcium solution (Figure 5-12b). The Df-ratio of silica nanoparticle layer attached to both ZnS and SiO_2 coated sensor surface in the 800 ppm calcium solution also decreases with time (Figure 5-13). Similar to the gypsum supersaturated solution system, the attached silica nanoparticle layer consisting of particle clusters which do not homogeneously cover the sensor surfaces.

It is obvious that the QCM-D responses of the deposition of silica nanoparticles on ZnS and SiO_2 coated sensor surface in gypsum supersaturated solution (Figure 5-10 and 5-11) and in the 800 ppm calcium solution (Figure 5-12 and 5-13) are very similar, though slightly higher frequency shifts were observed in the 800 ppm calcium solution. Moreover, our previous results has shown that the QCM-D responses of the adsorption of gypsum supersaturated solution on ZnS and SiO_2 coated sensor surface were almost identical to that in the 800 ppm calcium solution. Zeta potential measurement also showed that the zeta potentials of silica nanoparticles, ZnS and SiO_2 coated sensor surfaces are almost the same, around -10 mV. Therefore, it is safe to conclude that the deposition of silica nanoparticles on the ZnS and SiO_2 coated sensor surface is mainly attributed to the high calcium concentration in the gypsum supersaturated solution.

5.2.4 AFM force measurement and DLVO fitting

5.2.4.1 Impact of calcium ions

The silica deposition kinetics on ZnS or SiO_2 coated sensor surface can be well explained by the results of colloidal force measurements and DLVO interpretation, as shown in Figure 5-14 and 5-15. At pH 6.5, a repulsive long range force profile is obtained in the absence of calcium (1 mM KCl solution), without noticeable adhesion when separating the two surfaces in contact (Figure 5-14a). The AFM force profile can be well fitted by the electrostatic double layer force (EDL) between a silica particle and a sphalerite surface (Solid line in Figure 5-14a), indicating that the EDL force dominates the long range forces between the silica particle and sphalerite surface in 1 mM of KCl solution. The addition of calcium has a significant effect on the force profile between a silica particle and a fractured sphalerite surface. The repulsive EDL force decreases dramatically in the presence of 1 mM calcium solution. Further increasing the calcium concentration results in the diminishment of repulsive EDL force and force profiles of attractive van der Waals forces (vdW) are observed. As shown in Figure 5-14a, the force profile between the silica and sphalerite surfaces changes from repulsive to attractive when increase calcium concentration from 1 mM to 2.5 mM. Meanwhile, the adhesion force between silica and sphalerite surfaces is observed in the presence of calcium, which increases with the increase of calcium concentration (Figure 5-14b).

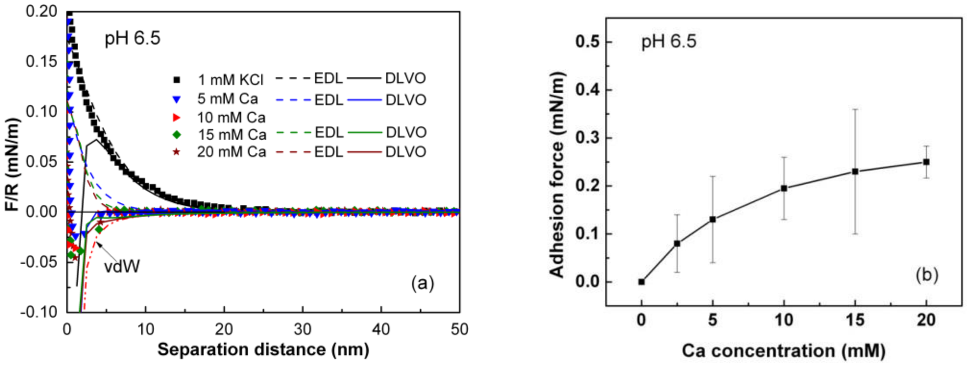

Figure 5-14 Normalized interaction forces between silica and sphalerite surfaces in calcium ion solutions of different concentrations at pH 6.5 (The solid curves are theoretical fitting of DLVO theory. The EDL curves (dash lines) are obtained by numerical solution of the nonlinear Poisson-Boltzmann equation under the constant surface potential boundary conditions. The fitted Stern potential values of the silica and sphalerite are ψ_{Si} - 35 mV, ψ_{Sp} - 15 mV for 1 mM KCl of pH 6.5; ψ_{Si} - 15 mV, ψ_{Sp} - 12 mV for 5 mM Ca of pH 6.5, ψ_{Si} - 10 mV, ψ_{Sp} - 10 mV for 15 mM and 20 mM Ca of pH 6.5. Hamaker constant of 1.0 × 10^{-20} J is used to calculate the van der Waals forces (red dash dot dot line)).

Similar to the silica – sphalerite system, the presence of calcium ion affects the interaction forces between silica and silica surfaces (Figure 5-15). In the absence of calcium (Milli-Q water or 1 mM KCl), silica surface carries negative charge at pH 6.5 (Figure 5-1). The repulsive EDL force dominates the interactions between silica surfaces, resulting in zero silica deposition onto the SiO_2 sensor surface (Figure 5-5). With the addition of calcium, surface charge of silica is neutralized and screened with the increase of calcium concentration. Consequently, the long range EDL repulsive force decreases or disappears. As shown in Figure 5-15a, a long range repulsive force profile is obtained between a silica particle and a silica wafer surface in 1 mM KCl solution of pH 6.5. The magnitude of long range repulsive force decreases dramatically in the presence of 5 mM calcium ions due to the compression of EDL on silica surface. Further increase the calcium ion concentration results in the further EDL compression. As a result, the long range repulsive force decreases and disappears, and vdW attraction force is measured by AFM force measure when the calcium concentration is increased up to 15 mM or 20 mM. Adhesion force is found between silica surfaces in the presence of high calcium concentration (above 5 mM) (Figure 5-15b). The adhesion force between the silica surfaces increases with increasing calcium concentration.

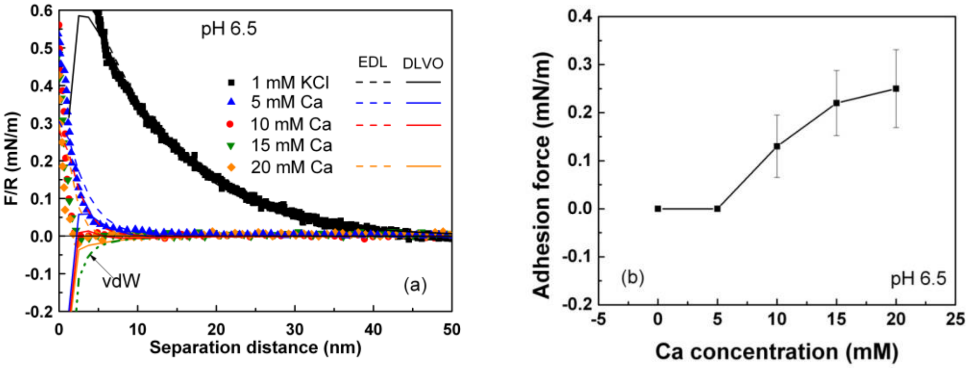

Figure 5-15 Normalized interaction forces between silica surfaces as a function of separation distance in different concentrations of calcium solution of pH 6.5 (The EDL curves (dash lines) are theoretical fitting obtained by numerical solution of the nonlinear Poisson-Boltzmann equation calculated under constant potential boundary conditions. Solid lines are classic DLVO fittings. The fitted values of the silica surface potential are - 55 mV for 1 mM KCl, - 15 mV for 5 mM Ca, -12 mV for 10 mM Ca, and -10 mV for 20 mM Ca. Hamaker constant of 8.5 × 10^{-21} J is used for the van der Waals force fitting (the green dash dot dot line))

Clearly, the addition of calcium ions compresses the EDL, resulting in the reduction of the electrostatic repulsive force. The vdW attractive force overcomes the electrostatic repulsive force resulting in the increases of overall attractive force. The reduction of repulsive force is attributed to the screening effect of increasing electrolyte concentration and surface charge neutralization at the sphalerite and the silica surface. As discussed in 5.2.1, both silica and sphalerite carry negative charge at pH 6.5 in the absence of calcium. The zeta potentials of silica nanoparticles and ZnS or SiO_2 sensor shift to less negative values when increasing the calcium concentration. The zeta potentials of silica and ZnS or SiO_2 sensors are compressed to near zero when increasing the calcium concentration to 20 mM. Therefore, in the absence of calcium (Milli-Q water or 1 mM KCl), repulsive electrostatic force dominate the silica nanoparticle-ZnS surface interaction, resulting in zero deposition. In contrast, in the presence of calcium, the long range electrostatic repulsive force decreases or disappears due to surface charge neutralization and EDL compression and the attractive vdW force becomes dominate, resulting in the deposition of silica nanoparticles onto ZnS sensor surface. The EDL of both silica and sphalerite mineral surfaces is more compressed with the increase of calcium concentration. Hence, the overall attractive force increases resulting in a stronger attachment between silica and sphalerite or silica minerals. In another word, a more rigid particle deposition layer can be obtained in the QCM-D deposition measurement.

5.2.4.2 Impact of Mg ions

The effect of magnesium ions on the interactions between a silica particle and a fractured sphalerite surface or a silica wafer surface is similar to that of calcium at pH 6.5. As shown in Figure 5-16, attractive force profiles are obtained between a silica particle and a fractured sphalerite surface in the presence of 2.5 mM magnesium ions. The attractive force profiles are in great agreement with the fitted vdW force. Adhesion force, which is absent between silica and sphalerite surfaces, is detected in the magnesium solutions. The adhesion force between silica and sphalerite surfaces increase with increasing magnesium concentration. The AFM results and DLVO interpretation well explain the impact of magnesium on the silica deposition kinetic on ZnS surface. The same as to the effect of calcium, the addition of magnesium reduces the electrostatic repulsive force resulting in overall attraction due to the van der Waals attractive force. The attraction force and adhesion force measured in the presence of magnesium contributes to the silica deposition on ZnS surface.

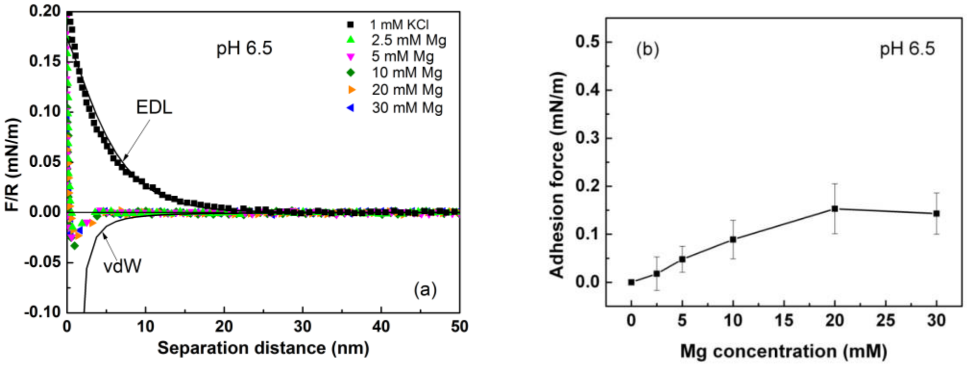

Figure 5-16 Normalized interaction forces between silica and sphalerite surfaces in different concentrations of magnesium solution of pH 6.5 (The solid curves are theoretical fitting obtained by numerical solution of the nonlinear Poisson-Boltzmann equation calculated under constant potential boundary conditions. The fitted values of the silica and sphalerite surface potential are

ψsi - 35 mV, ψsp - 15 mV for 1 mM KCl of pH 6.5. Hamark constant of 1.0 × 10^{-20} J is used for the van der Waals force fitting).

The colloidal forces between a silica particle and a silica wafer surface obtained by direct AFM force measurement in different magnesium concentration of pH 6.5 are shown in Figure 5-17. As show in the Figure 5-17a, the addition of magnesium ions reduces the repulsion force between the silica surfaces. The repulsive force profiles are in good agreement with the fitted EDL force, indicating that the repulsive force obtained by the AFM force measurement is mainly attributed to the EDL force between the silica surfaces (solid lines in Figure 5-17a). Small attractive force profiles are observed when increasing the magnesium concentration up to 20 mM. The attractive force profiles are mainly attributed to the vdW force between the silica surfaces (solid line in Figure 5-17a). Meanwhile, the adhesion force is detected between the mineral surfaces, which increase slightly with increasing magnesium concentration. The colloidal forces between silica surfaces (Figure 5-17) can well explain the deposition kinetics of silica nanoparticle on SiO_2 sensor surface in the presence of magnesium. The presence of magnesium ions neutralizes the negative surface charge of silica (Figure 5-1b), resulting in the decrease in the EDL force (or energy barrier) between silica and silica surface (Figure 5-17a). Hence, the vdW force becomes dominate between silica mineral surfaces, which induces the deposition of silica nanoparticles onto the sensor surface.

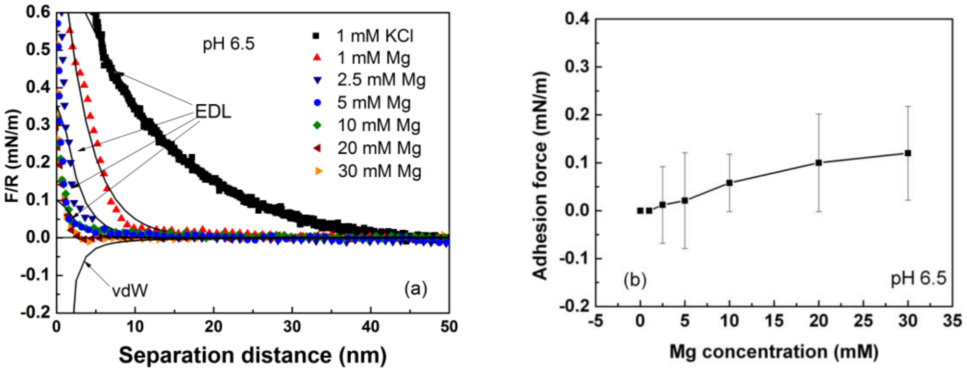

Figure 5-17 Normalized interaction forces between silica surfaces as a function of separation distance in different concentrations of magnesium solution of pH 6.5. (The solid curves are theoretical fitting obtained by numerical solution of the nonlinear Poisson-Boltzmann equation calculated under constant potential boundary conditions. The fitted values of the silica surface potential are $\psi_{Si\_particle}$ - 35 mV, ψ_{Si_wafer} - 55 mV for 1 mM KCl; $\psi_{Si\_particle} = \psi_{Si\_wafer}$ = - 35 mV for 1 mM Mg; $\psi_{Si\_particle} = \psi_{Si\_wafer}$ = - 25 mV for 2.5 mM Mg; $\psi_{Si\_particle} = \psi_{Si\_wafer}$ = - 18 mV for 5 mM Mg. Hamaker constant of 8.5×10^{-21} J is used for the van der Waals force fitting).

5.2.4.3 Gypsum supersaturated water

Figure 5-18 compares the colloidal interaction forces between a silica particle and a fractured sphalerite or a silica wafer surface in 1 mM KCl solution with those in gypsum supersaturated solution and 800 ppm calcium solution at pH 6.5. As shown in Figure 5-18a, a repulsive long range force profile is obtained in 1 mM KCl solution of pH 6.5, without noticeable adhesion when separating the two surfaces in contact. The AFM force profile can be well fitted by the electrostatic double layer force (EDL) between a silica particle and a sphalerite surface (Solid line in Figure 5-18a), indicating that the EDL force dominates the long range forces between the silica particle and sphalerite surface in 1 mM of KCl solution. In contrast to the 1 mM KCl solution, attractive force profiles, which can be well fitted by the van der Waals (vdW) force, are obtained between the silica and sphalerite surfaces in both 800 ppm calcium solution and gypsum supersaturated solution. Meanwhile, adhesion force was detected between silica and sphalerite surfaces in both 800 ppm calcium solution and gypsum supersaturated solution.

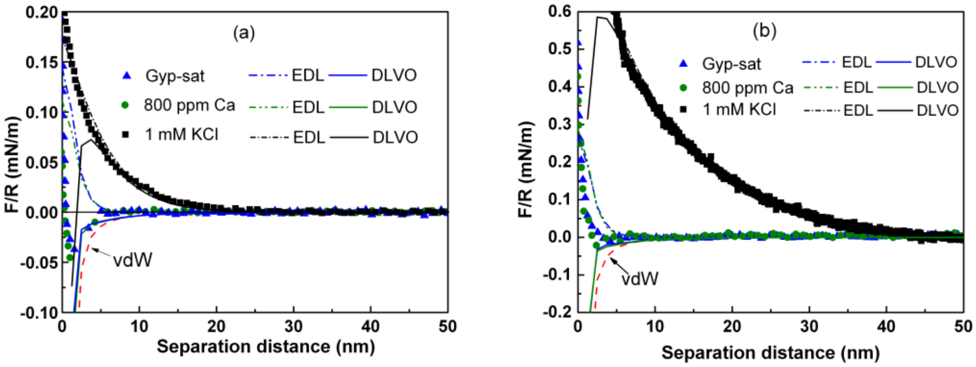

Figure 5-18 Normalized interaction force between (a) silica and sphalerite, and (b) silica and silica surfaces as a function of separation distance in different water chemistry at pH 6.5 (The EDL curves are theoretical fitting of DLVO theory obtained by numerical solution of the nonlinear Poisson-Boltzmann equation under the constant surface potential boundary conditions. The fitted

Stern potential values of the silica and sphalerite are $\psi_{Si\_particle}$ - 35 mV, ψ_{Si_wafer} - 55 mV, ψ_{Sp} - 25 mV for 1 mM KCl of pH 6.5; Hamaker constant of 1.0 × 10^{-20} J and 8.5 × 10^{-21} J are used for calculating the van der Waals force for silica-sphalerite and silica-silica respectively).

Similarly to the silica – sphalerite interactions, the force profile between a silica particle and a silica wafer surface in 1 mM KCl solution is repulsive without adhesion in contact (Figure 5-18b). The long range repulsive force profile obtained by the AFM force measurement is attributed to the EDL force. As shown in Figure 5-18b, the AFM force profile between the silica surfaces in 1 mM KCl is in great agreement with the EDL fitting. In 800 ppm calcium solution and gypsum supersaturated solution, the long range repulsive force between the silica surfaces disappeared, and attractive vdW force are detected instead.

The QCM-D response of the silica nanoparticles deposition measurements on ZnS and SiO_2 coated sensor surface in gypsum supersaturated solution can be well explained by the results of AFM colloidal force measurements and DLVO interpretation. In Milli-Q water or 1 mM KCl solution, the repulsive EDL force dominates the interactions between silica and sphalerite or silica surfaces, resulting in zero silica attachment onto the SiO_2 sensor surface (Figure 5-3). In both 800 ppm calcium and gypsum supersaturated solutions, the repulsive force between silica and sphalerite or silica surfaces is suppressed due to the screening effect of the increased electrolyte concentration and the surface charge neutralization on both sphalerite and silica surface. As discussed earlier, the zeta potentials of silica and sphalerite minerals become identical and are compressed to near zero (- 10 mV) in both 800 ppm calcium and gypsum supersaturated solutions. Hence, the vdW force becomes dominate between the mineral surfaces, resulting in tremendous attachment of silica nanoparticles on both ZnS and SiO_2 coated sensor surface. Furthermore, the colloidal force profile between silica and sphalerite or silica surfaces obtained in the gypsum supersaturated solution almost overlaps with that obtained in 800 ppm calcium solution. The AFM results further confirm that the hetero-aggregation between silica and sphalerite and the homo-aggregation of silica induced in the gypsum supersaturated solution is mainly attributed to the high calcium concentration of the gypsum supersaturated solution.

5.3 Significance in sphalerite flotation

The motivation of this study is trying to understand the cause of silicate gangue minerals misplacement in the zinc concentrates observed in the gypsum supersaturated process water. Clearly, hetero-aggregation between silica and sphalerite in the gypsum supersaturated water is significant; the presence of calcium and magnesium can induce the hetero-aggregation between silica and sphalerite minerals. Hetero-aggregation between silica and sphalerite minerals leads to slime coating of silica on sphalerite surface. As shown in Figure 5-9, the ZnS coated QCM-D sensor surface was fully covered by silica nanoparticles after the deposition experiment in 20 mM calcium solution of pH 6.5. It is noted that the attached particle layer is heterogonous and clusters of silica nanoparticles are observed on the ZnS sensor surface, which is probably due to the homo-aggregation of silica nanoparticles.

The hetero-aggregation between silica and sphalerite could cause the reduction of sphalerite flotation recovery and promote silica contamination in the zinc concentrate. Figure 5-10 shows the impact of calcium and gypsum supersaturated water on the flotation selectivity of sphalerite from silica. In Milli-Q water, the flotation recovery of sphalerite is up to 90% with less than 10% of silica entrainment. However, in 20 mM calcium solution and gypsum supersaturated solution, the flotation recovery of sphalerite in the concentrate decreases to less than 80%; meanwhile, misplacement of silica in the zinc concentrates increases up to 20%. It has to be noted that the presence of calcium and gypsum supersaturated solution retarded the uptake of copper and xanthate on sphalerite, which could also be responsible for the reduced flotation recovery.

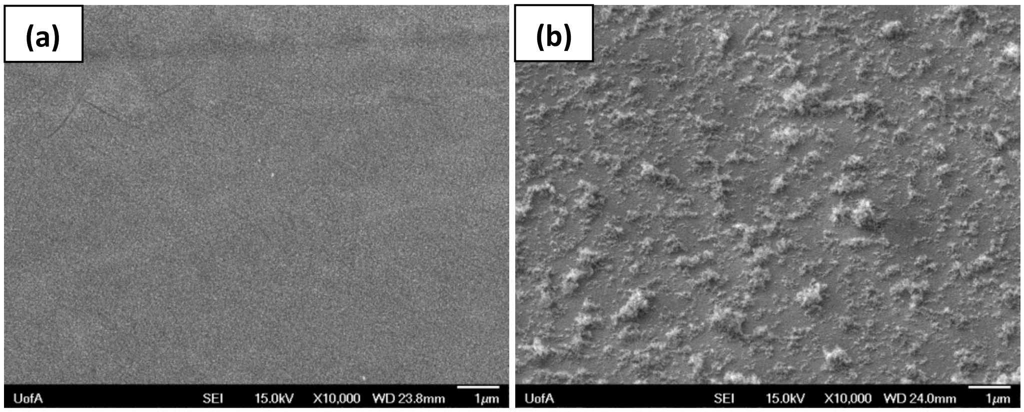

Figure 5-19 SEM images of ZnS coated QCM-D sensor (a) before and (b) after silica nanoparticle deposition in 20 mM calcium solution of pH 6.5.

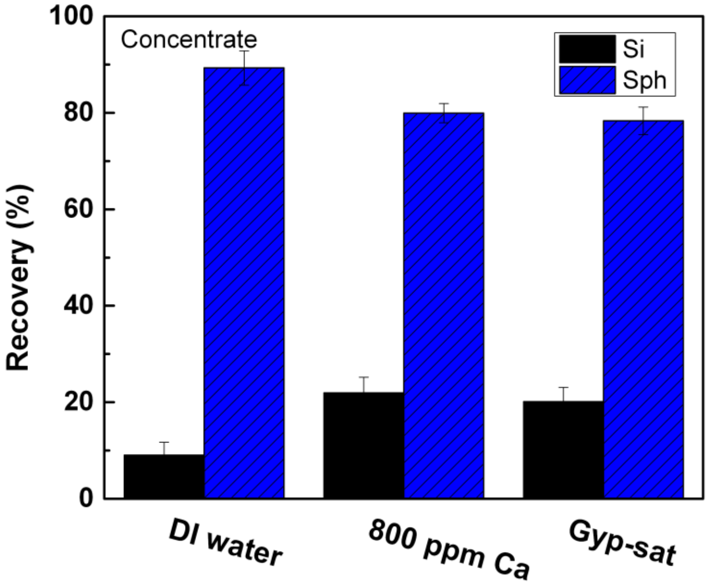

Figure 5-20 Flotation selectivity of sphalerite from silica in different solutions

5.4 Conclusions

QCM-D is proven to be a powerful tool to study the interactions between minerals. At pH 6.5, the deposition of silica on ZnS or SiO_2 coated QCM-D sensor is minimal in Miili-Q water. The presence of calcium, magnesium, and gypsum supersaturated water induces the deposition of silica on ZnS or SiO_2 sensor surface. The deposition rate increases with increasing calcium and magnesium concentration.

The surface force between a silica sphere and a fractured sphalerite surface in the supporting electrolyte solutions are repulsive with no adhesion in contact at both pH 6.5 and 10. The addition of calcium and magnesium reduces the long-range repulsive force, resulting in an overall attractive van der Waals force between silica and sphalerite. Adhesion force is found in the presence of calcium and magnesium, which increases with the increasing of calcium and magnesium concentration. Attractive force and adhesion force are also found in the gypsum supersaturated solution. Similar surface force results are obtained between silica surfaces in the presence of calcium and magnesium, and in gypsum supersaturated solution.

The presence of calcium, magnesium and gypsum supersaturated water promotes the hetero-aggregation between silica and sphalerite minerals, resulting in the reduction of flotation selectivity. The poor flotation selectivity of sphalerite from silica in the gypsum supersaturated water is mainly attributed to the high calcium concentration of the gypsum supersaturated water.

Chapter 6 Approaches of Improving the Flotation Recovery and Selectivity of Sphalerite in the Gypsum Supersaturated Water

6.1 Introduction

One of lead/zinc mines recycles treated water from the tailings impoundment back into the flotation process. Water reclaimed from the tailings impoundment is treated using a high density sludge process prior to its recycle. The process water is supersaturated with respect to calcium sulphate and is implicated in scaling of the slurry transport pipe in the concentration. The calcium concentration in the process water and reclaim water in The lead/zinc mine is reported 840 ppm and 560 ppm, while the sulphate concentration is 2400 ppm and 2861 ppm, respectively. The gypsum supersaturated process water has detrimental impact on the zinc flotation circuit at the lead/zinc mine.

The high calcium concentration in the gypsum supersaturated process water has been believed to be responsible for the poor flotation recovery and selectivity at the zinc flotation circuit. Our previous chapters showed that the gypsum supersaturated solution had significant impact on the surface properties of silica and sphalerite mineral. Even though gypsum precipitated neither grew on mineral surface nor hetero-aggregated with mineral, the surface charge of silica and sphalerite minerals become identical due to the discriminate adsorption of calcium. The adsorption of copper and xanthate on sphalerite surface was retarded in the presence of 800 calcium ions and gypsum supersaturated solutions. It has been reported that calcium could specifically adsorb at ZnS-H_2O interface [179], which reduced the exchange rate with activating ions, copper, in the case of sphalerite flotation [36], resulting in a decrease in recovery. The presence of calcium and gypsum supersaturation in process water also induced the hetero-aggregation between silica and sphalerite minerals, which is responsible for the poor flotation selectivity. Calcium ion has been proven to have significant effect on the interactions between zinc sulphide and silicate minerals [40, 41]. The presence of calcium and gypsum supersaturated process water led to a decrease of repulsive electrical double layer force, which is responsible for the hetero-aggregation between sphalerite and silicate gangue minerals.

One of the effective approaches to eliminate the detrimental effect of calcium ion or gypsum supersaturated process water on sphalerite flotation is to add carbonate (e. g. soda ash) to precipitate calcium ions as calcium carbonate as well as converting calcium sulphate to calcium carbonate. The addition of soda ash has been proven to be effective in Hilton concentrator [27] and in sphalerite flotation [45].

In this study, three approaches of eliminating the adverse impact of gypsum supersaturated solutions on the flotation of sphalerite were investigated and evaluated. Since calcium has been demonstrated to be the main cause of the flotation problem in sphalerite, it is therefore of great interest to study the flotation behavior of silica and sphalerite, both alone and mixture, in the gypsum supersaturated solutions before and after calcium removal with sodium carbonate or bicarbonate. Our previous studies have confirmed that the gypsum supersaturated solution retards the adsorption of copper and xanthate on sphalerite surface. Hence, increasing the dosage of copper and xanthate or conditioning the minerals with copper and xanthate prior to exposing in the gypsum supersaturated process water (Pre-hydrophobic conditioning) may also improve the flotation of sphalerite. Micro-flotation was conducted to evaluate the potential of those approaches of improving the flotation performance of sphalerite in gypsum supersaturated solutions.

6.2 Results and discussion

6.2.1 Flotation behavior of silica and sphalerite in gypsum supersaturated water

Gypsum supersaturated solutions have significant effect on the flotation behavior of silica and sphalerite. Figure 6-1 presents the recovery of sphalerite single mineral flotation in different water chemistry. Sphalerite cannot be floated with xanthate without the activation of copper, as it has been expected. As shown in Figure 6-1, the flotation recovery of sphalerite is up to 90% in DI water. When float the sphalerite in the gypsum supersaturated solutions, however, the flotation recovery of sphalerite drops to about 70%. Similar reduction in flotation recovery of sphalerite is also observed in 800 ppm calcium solution. Our previous study has shown that the presence of high calcium concentration retarded the uptake of copper and xanthate on sphalerite surface, which is responsible for the decreased flotation recovery observed in the gypsum supersaturated solutions and 800 ppm calcium solution. On the other hand, good flotation recovery can be obtained in calcite saturated solution where the calcium concentration is much lower.

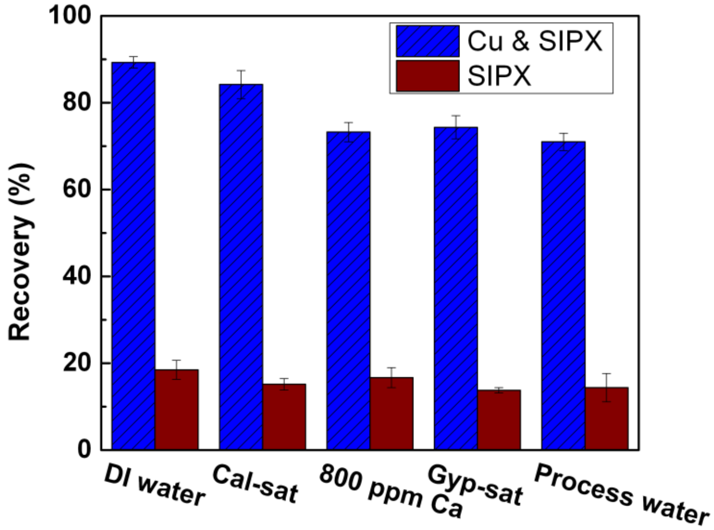

Figure 6-1 Flotation recovery of sphalerite in different solutions at pH 6.5 (Cu: 1.25×10^{-5} mol/L, SIPX: 1.25×10^{-5} mol/L).

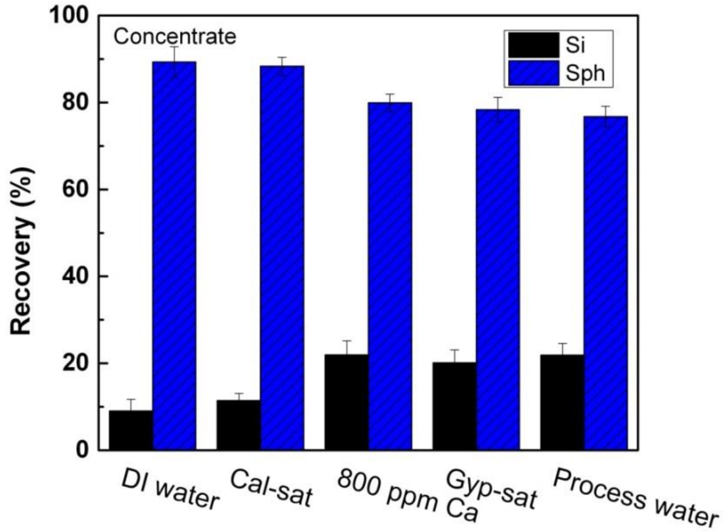

Figure 6-2 Flotation selectivity of sphalerite in different solutions at pH 6.5 (Cu: 1.25×10^{-5} mol/L, SIPX: 1.25×10^{-5} mol/L).

Figure 6-2 shows the recovery of sphalerite and silica in the flotation of sphalerite and silica mixture in different water chemistry. Good flotation selectivity is obtained in both DI water and calcite saturated solution. As shown in Figure 6-2, in DI water and calcite saturated solution, the flotation recovery of sphalerite in the concentrate remains to 90%, while the entrainment of silica is about 10%. In the gypsum supersaturated solutions and 800 ppm calcium solution, on the other hand, decreased flotation selectivity of sphalerite from silica is observe. The flotation recovery of sphalerite drops about 15% while the misplacement of silica in the sphalerite concentrate rises up to 20%. The presence of high calcium concentration and gypsum supersaturated solution induces the hetero-aggregation between sphalerite and silica minerals, as it has been demonstrated in our previous QCM-D and AFM studies, resulting the misreporting of silica in the flotation concentrate.

Flotation results of sphalerite single mineral and a mixture of silica and sphalerite minerals demonstrate that the gypsum supersaturated solutions decrease the flotation recovery and selectivity of sphalerite. The poor sphalerite flotation recovery observed in the gypsum supersaturated solutions is attributed to the high calcium concentration in those solutions. Good flotation recovery and selectivity is possible to be achieved by converting gypsum supersaturated solution to calcite saturated solution.

6.2.2 Removal of calcium by the addition of sodium carbonate

As discussed previously, the high calcium concentration in the gypsum supersaturated solutions is responsible for the poor flotation recovery and selectivity of sphalerite. As practiced in the real industry [27, 45], an effective approach to eliminate the detrimental effect of both calcium ions and calcium sulphate precipitates on flotation is to add carbonate (e. g. soda ash) to precipitate calcium ions as calcium carbonate or convert calcium sulphate to calcium carbonate. In this study, sodium carbonate was used to remove and control the calcium concentration of the gypsum supersaturated water. The amount of sodium carbonate addition was calculated depending on the calcium concentration of the gypsum supersaturated solutions. The solutions were conditioned with sodium carbonate for 30 min and the precipitates were removed by filtration. The pH of the solutions after sodium carbonate treatment is about 9.5. The solutions were then adjusted to pH 6.5 and filtered again. The calcium concentration of the gypsum supersaturated solutions after the sodium carbonate treatment is less than 20 ppm. Flotation of sphalerite single mineral and a mixture of silica and sphalerite were conducted to investigate the effect of calcium removal on the flotation recovery and selectivity of sphalerite in the solutions and the results are shown in Figure 6-3 and 6-4.

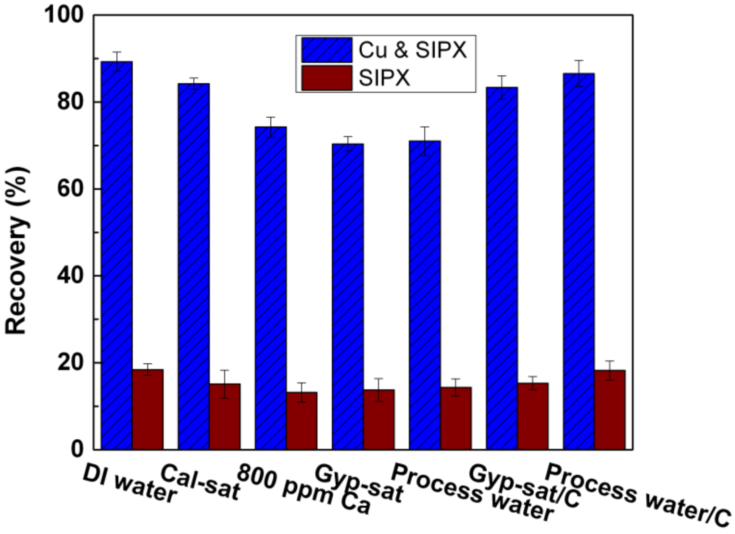

Figure 6-3 Effect of carbonate addition on the flotation recovery of sphalerite in gypsum supersaturated solutions at pH 6.5 (Cu: 1.25×10^{-5} mol/L, SIPX: 1.25×10^{-5} mol/L).

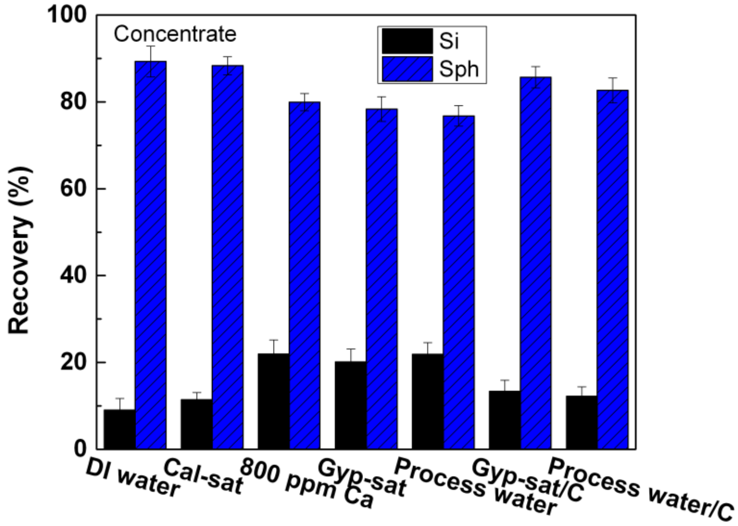

Figure 6-4 Effect of carbonate addition on the flotation selectivity of sphalerite in gypsum supersaturated solutions at pH 6.5(Cu: 1.25×10^{-5} mol/L, SIPX: 1.25×10^{-5} mol/L).

Figure 6-3 presents the single mineral flotation of sphalerite in the gypsum supersaturated solutions with and without sodium carbonate treatment. The addition of sodium carbonate can significantly improve the flotation recovery of sphalerite in the gypsum supersaturated solutions. After the sodium carbonate treatment, the flotation recovery of sphalerite increase up to 90%. The flotation results of the silica and sphalerite mixture system show an improvement of the flotation recovery of sphalerite as well (Figure 6-4). The flotation recovery of sphalerite increases from 70% to 85% after the sodium carbonate treatment. Silica entrainment in the sphalerite concentration reduces to 10%. The results demonstrate that the removal of calcium ions from the gypsum supersaturated solutions can significantly improve the flotation recovery and selectivity of sphalerite.

The addition of the sodium carbonate removes most of the calcium ions from the gypsum supersaturated solutions. The removal of calcium cleans the mineral surface. Figure 6-5 shows the XPS results of silica and sphalerite conditioned in the gypsum supersaturated solution with and without sodium carbonate treatment. As show in the Figure, strong Ca 2p signals at 346 eV is found on both silica and sphalerite surfaces after conditioned in the gypsum supersaturated solution. Calcium was also found on those mineral surfaces after conditioned in 800 ppm solution. The Ca 2p signals vanish from both silica and sphalerite mineral surfaces after treating the gypsum supersaturated solution with sodium carbonate, indicating much cleaner surfaces.

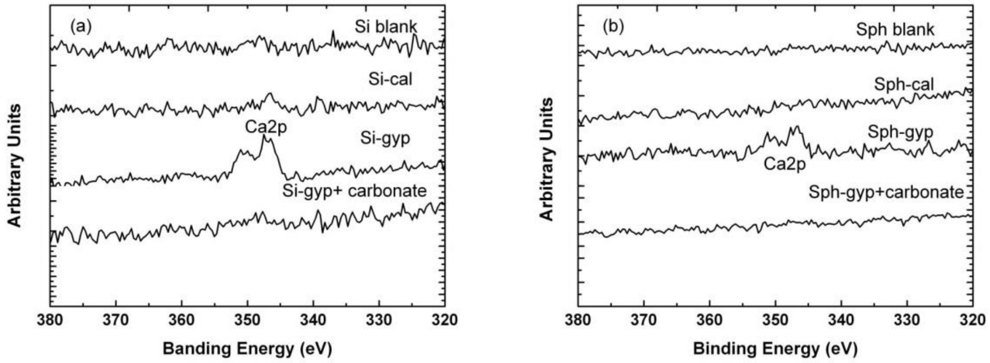

Figure 6-5 XPS narrow scan Ca2p spectra for a) silica and b) sphalerite particles treated with Milli-Q water, calcite-supersaturated solution, gypsum-supersaturated solution and gypsum-supersaturated solution with the treatment of sodium carbonate or bicarbonate.

6.2.3 Increasing flotation reagents

The presence of high calcium concentration in the gypsum supersaturated solutions retards the activation of sphalerite with copper and hence the sequence adsorption of xanthate on sphalerite surface. In this part of work, the potential of improving the flotation performance of sphalerite in gypsum supersaturated solution by increasing the dosage of flotation reagents: activator, copper, and collector, SIPX, is evaluated and the results are shown in Figure 6-6 and 6-7.

Single mineral flotation results indicate that the flotation recovery of sphalerite in the gypsum supersaturated solutions can be improved by simply increasing the flotation reagents (Figure 6-6). In both gypsum supersaturated solution and simulated process water, the flotation recovery of sphalerite increases up to 80% when increasing the dosage of copper and SIPX to 2×10^{-5} mol/L. Further increasing the flotation reagents' dosage, the flotation recovery of sphalerite can reach to more than 90%.

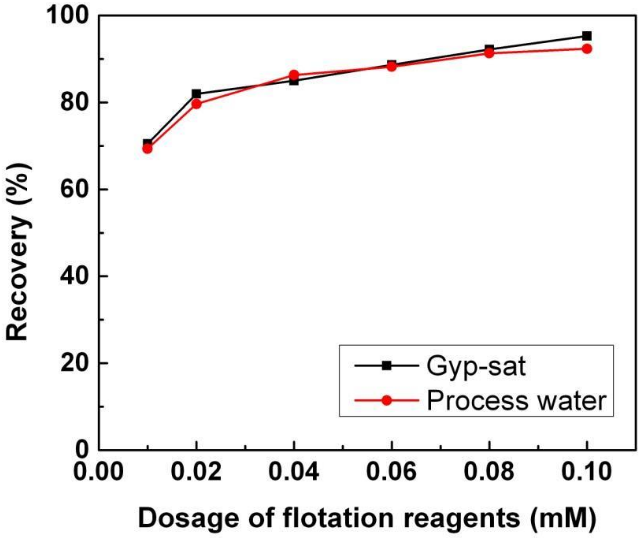

Figure 6-6 Effect of increasing the dosage flotation reagents on the flotation recovery of sphalerite in gypsum supersaturated solutions at pH 6.5.

Increasing flotation reagents has limited effect on the flotation selectivity of sphalerite from silica. As shown in Figure 6-7, when mixing sphalerite with silica, the flotation recovery of sphalerite in the concentration only marginally increased with the increasing of copper and SIPX addition up to 1×10^{-4} mol/L. Meanwhile, the misreport of silica in the concentrate remains as high as those with lower copper and SIPX addition. Simply increase the flotation reagents cannot reduce the hetero-aggregation between silica and sphalerite. Moreover, the presence of copper and xanthate could enhance the hetero-aggregation between silica and sphalerite. The presence of copper and xanthate has been found to be able to trigger an attractive non-DLVO force between silica and ZnS

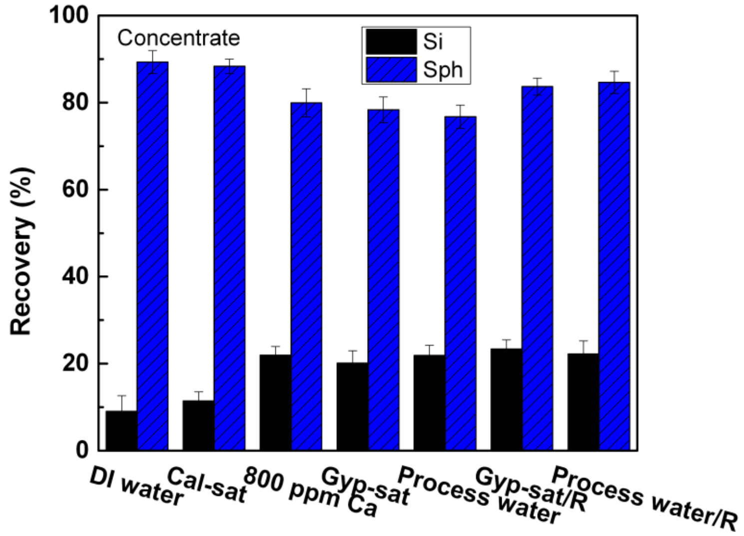

Figure 6-7 Effect of increase flotation reagents on the flotation selectivity of sphalerite in gypsum supersaturated solutions at pH 6.5 (Cu: 1.25×10^{-5} mol/L, SIPX: 1.25×10^{-5} mol/L, for the Gyp-sat/R, Reclaim water/R, and Process water/R: Cu: 1×10^{-4} mol/L, SIPX: 1×10^{-4} mol/L).

6.2.4 Pre-hydrophobic conditioning

The high calcium concentration in the gypsum supersaturated solutions has been proven to be responsible for the poor flotation recovery and selectivity of sphalerite. If conditioning the minerals with flotation reagents prior to their exposing in the gypsum supersaturated solutions (pre-hydrophobic treatment), the flotation performance of sphalerite could be improved. Figure 6-8 and 6-9 compare the flotation results of sphalerite single mineral and a mixture of silica and sphalerite minerals with and without pre-hydrophobic treatment. The single mineral flotation results confirm our hypnosis. With the pre-hydrophobic treatment, the flotation recovery of sphalerite in the gypsum supersaturated solutions improves dramatically. Pre-hydrophobic treatment has limited effect on improving the flotation selectivity of sphalerite from silica. As shown in Figure 6-9, the flotation recovery of sphalerite in the gypsum supersaturated solutions increases slightly with the pre-hydrophobic treatment. However, the misplacement of silica in the concentrate is not improved. Again, the poor selectivity is attributed to the hetero-aggregation between silica and sphalerite mineral (slime coating). The pro-hydrophobic treatment may induce an attractive non-DLVO force between silica and sphalerite.

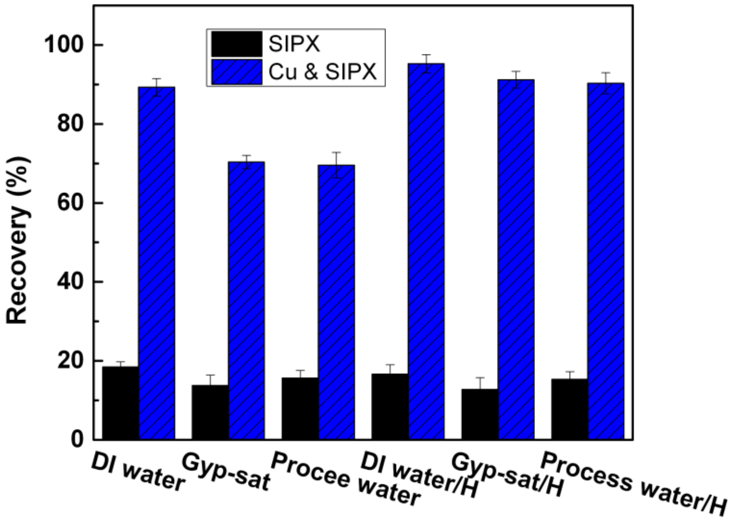

Figure 6-8 Effect of the pre-hydrophobic treatment on the flotation recovery of sphalerite in gypsum supersaturated solutions at pH 6.5(Cu: 1.25×10^{-5} mol/L, SIPX: 1.25×10^{-5} mol/L).

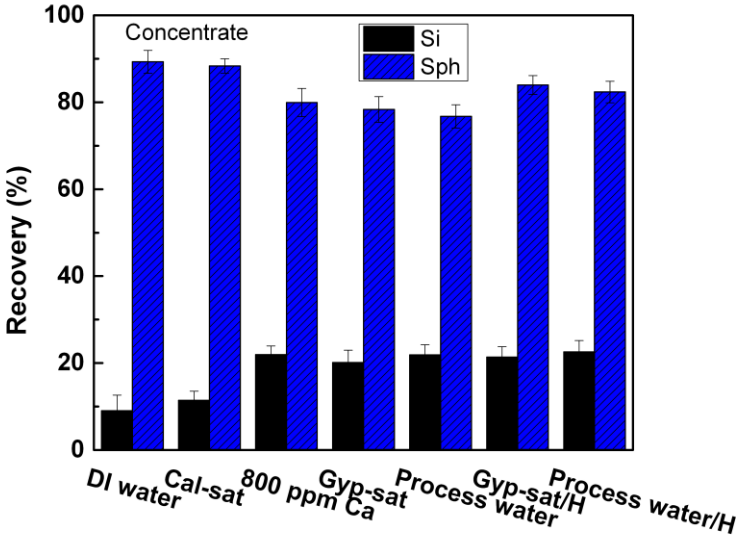

Figure 6-9 Effect of pro-hydrophobic conditioning on the flotation selectivity of sphalerite in gypsum supersaturated solutions at pH 6.5 (Cu: 1.25×10^{-5} mol/L, SIPX: 1.25×10^{-5} mol/L).

6.2.5 Examination of silica and sphalerite minerals in real process water

In order to verify that our lab-scale findings can be extended to the real mineral flotation process system, the impact of real process water on silica and sphalerite mineral surfaces was examined. Silica (- 30 µm) and sphalerite (- 45 µm) pure minerals with similar particle size to that of zinc flotation circuit were send to A lead/zinc mine. The minerals were conditioned in the Real process water following the procedures described in Chapter 2 (Section 2.4.4) and analyzed using SEM.

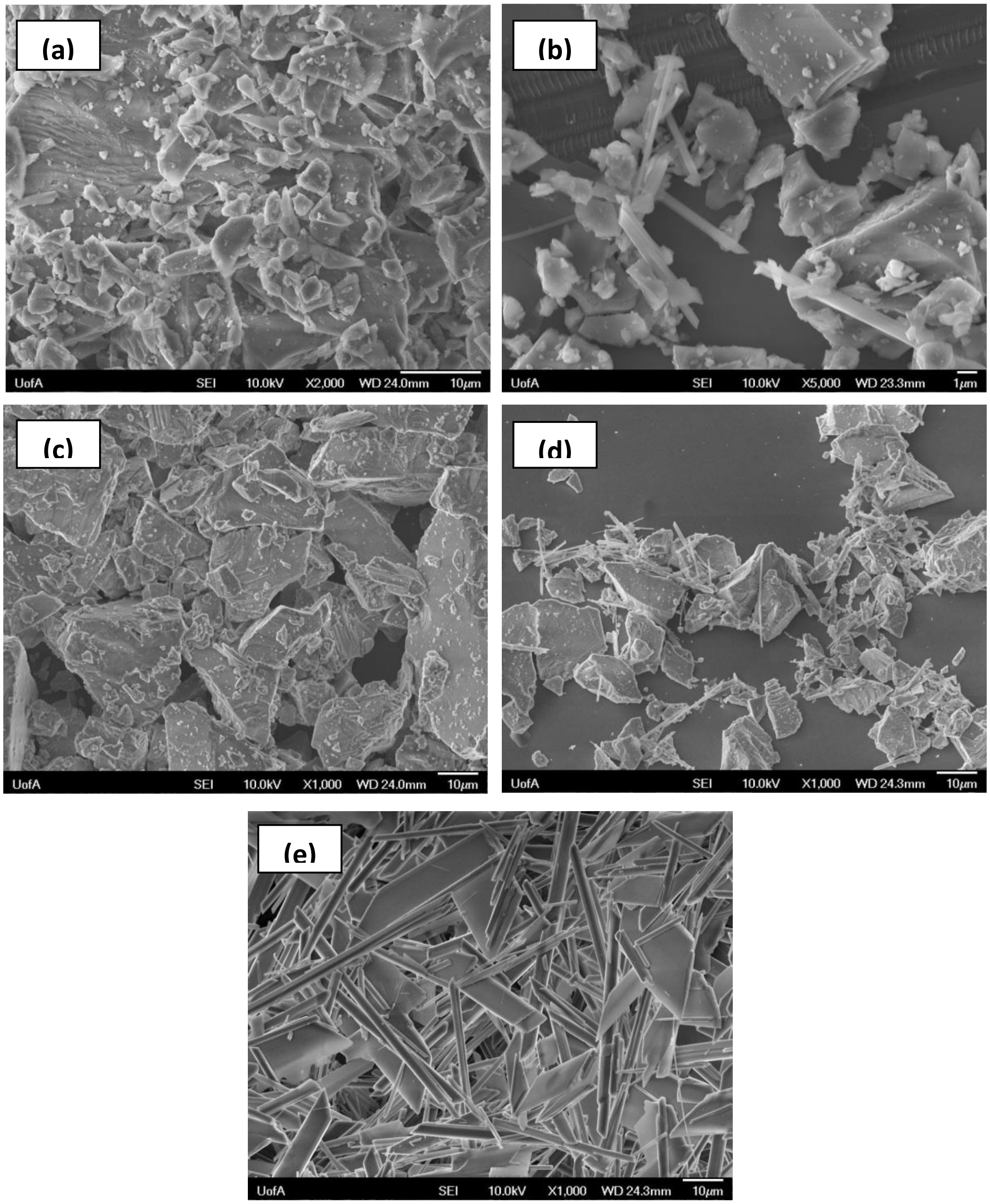

Figure 6-10 Typical SEM micrographs of a) Silica conditioned in water, b) Silica conditioned in process water, c) Sphalerite conditioned in water, d) Sphalerite conditioned in process water, and e) Gypsum precipitates from gypsum supersaturated solution.

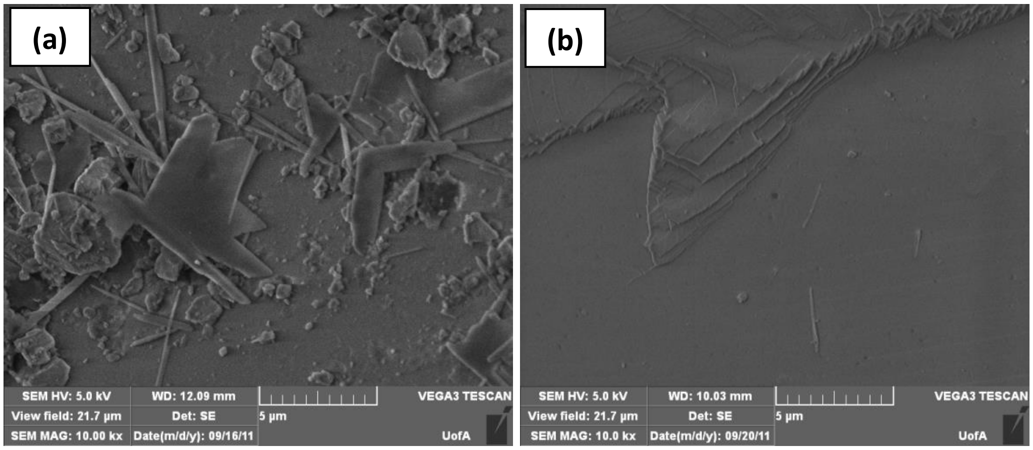

Figure 6-11 Typical SEM micrographs of sphalerite conditioned in process water before (a) and after (b) 5 min sonication in ethanol.

The SEM images of silica and sphalerite before and after conditioned in the Real process water are shown in Figure 6-10. It is evident that gypsum precipitates are found in the silica and sphalerite minerals after conditioned in the Real process water. However, the gypsum precipitates can be easily removed from the mineral surface. As shown in Figure 6-11, after 5 minutes sonication treatment, the sphalerite mineral surface becomes clean with only a few needle-shape gypsum precipitates. These results are in great agreement with our previous results that obtained from the gypsum supersaturated solution model system.

6.3 Conclusions

Gypsum supersaturated solution have adverse impacts on the flotation performance of sphalerite. Poorer flotation recovery and selectivity is observed in gypsum supersaturated solution as well as 800 ppm calcium solution.

The removal of the calcium from the gypsum supersaturated solutions by the addition of sodium carbonate can significantly improve the flotation recovery and selectivity of sphalerite. Simply increasing the dosage of flotation reagents or conditioning the minerals with flotation reagents prior to their exposing in the gypsum supersaturated solution can improve the recovery of sphalerite but not selectivity.

Chapter 7 Conclusions and Future Work

7.1 Concluding remarks

Water quality is one of the critical factors that influence flotation performance of minerals. In sulphide mineral flotation, the process water is commonly gypsum saturated or supersaturated due to the dissolving of minerals, deliberate chemical reagents addition, and the source of water. Saturation or supersaturation of gypsum in process water is believed to be detrimental to the flotation performance of sulphide minerals. In order to achieve effective improvement of flotation performance of sulphide minerals in gypsum saturated or supersaturated process water, it is essential to gain a fundamental understanding of how gypsum saturation or supersaturation impacts the flotation process of minerals. In the past few decades, considerable studies have been carried out regarding to the sulphide mineral flotation problems in gypsum saturated or supersaturated process water. The depression mechanisms of gypsum saturated or supersaturated process water on the flotation of sulphide minerals, however, are not quite well understood. For example, controversy results on whether gypsum precipitates on minerals surfaces and whether gypsum saturated or supersaturated solution affects mineral activation have been reported. In this study, a gypsum supersaturated solution is used to systematically study its impact on the surface properties of silica and sphalerite minerals, the adsorption of flotation reagents on sphalerite mineral surface, and the interactions between mineral particles.

1) Impact of gypsum supersaturated solution on the surface properties of silica and sphalerite minerals

Gypsum supersaturated solution has significant effects on the surface properties of silica and sphalerite minerals. First of all, the surface charges of both silica and sphalerite minerals are neutralized and screened in the gypsum supersaturated solution. The zeta potentials of silica and sphalerite, which are distinctive in simple supporting electrolyte solutions, become identical in gypsum supersaturated solutions. Under the particular experimental conditions carried out in this study, gypsum coating on silica or sphalerite mineral surfaces is proven to be absent. Gypsum crystals are found to precipitate in the bulk gypsum supersaturated solution. The gypsum precipitates do not hetero-aggregate with silica or sphalerite mineral particles in gypsum supersaturated solutions due to the hydration force. Large hydration force is found between a silica particle and a cleaved natural gypsum crystal surface in a gypsum saturated solution through direct colloidal force measurement using an atomic force microscopy (AFM). The changes of surface properties of silica and sphalerite minerals in the gypsum supersaturated solution are mainly attributed to the high calcium concentrations of the gypsum supersaturated solution. The zeta potentials of silica and sphalerite minerals are identical in the presence of 800 ppm calcium which are similar to those in the gypsum supersaturated solution. Silica and sphalerite minerals surfaces are indiscriminately coated with calcium in both 800 ppm calcium solution and gypsum supersaturated solution. Surface oxidation of pure sphalerite minerals after conditioning in gypsum supersaturated solution is insignificant.

2) Impact of gypsum supersaturated solution on the uptake of copper and SIPX on sphalerite

Sphalerite activation by copper and the subsequence xanthate adsorption on sphalerite mineral surface are substantially affected in the gypsum supersaturated solution under near neutral pH. In comparison with Milli-Q water system, the supersaturation of water by gypsum retards the adsorption of copper and hence the sequence xanthate adsorption on sphalerite. The retardation of copper and xanthate adsorption on sphalerite is also observed by the addition of 800 ppm calcium. The adsorption of calcium is identified to compete with copper species for the reactive surface sites of the sphalerite, resulting in the reduction in copper and xanthate uptake and hence flotation recovery of sphalerite.

3) Impact of gypsum supersaturated solution on the interactions between silica and sphalerite minerals

The presence of calcium, magnesium, or gypsum supersaturated water triggers the hetero-aggregation between silica and sphalerite minerals, and the homo-aggregation of silica particles. QCM-D measurement, which is proven to be a powerful tool to study the interactions between minerals, indicated the deposition of silica nanoparticles on ZnS or SiO_2 coated QCM-D quartz sensor surface in the presence of high calcium or magnesium concentration and in gypsum supersaturated solutions. The deposition rate increases with the increase of calcium or magnesium concentration under the tested range. Direct colloidal force measurement by AFM showed that the addition of calcium or magnesium reduces the long-range repulsive force, resulting in an overall attractive van der Waals force between silica-sphalerite and silica-silica. Adhesion force is found in the presence of calcium and magnesium, which increases with the increasing of calcium and magnesium concentration. Attractive force and adhesion force are also found in the gypsum supersaturated solution. The presence of calcium, magnesium and gypsum supersaturated water promotes the hetero-aggregation between silica and sphalerite minerals, resulting in the reduction of flotation selectivity. The poor flotation selectivity of sphalerite from silica in the gypsum supersaturated water is mainly attributed to the high calcium concentration of the gypsum supersaturated water.

4) Approaches of eliminating the adverse impact of gypsum supersaturated solution on the flotation performance of sphalerite

Gypsum supersaturated solution have adverse impact on the flotation performance of sphalerite. Poorer flotation recovery and selectivity is observed in gypsum supersaturated solutions as well as 800 ppm calcium solution. Treating the gypsum supersaturated solutions with sodium carbonate can effectively eliminate its adverse impact on the flotation of sphalerite. The addition of sodium carbonate removes most of the calcium ions leading to a clean mineral surface, which significantly improves the flotation recovery and selectivity of sphalerite. Simply increasing the dosage of flotation reagents (copper and xanthate) or conditioning the minerals with flotation reagents (copper and xanthate) prior to their exposing in the gypsum supersaturated solution can marginally improve the flotation recovery of sphalerite but has limited ability in improving the flotation selectivity of sphalerite.

7.2 Major contributions to original knowledge

1) This thesis presents systematic research on the impact of gypsum supersaturation in process water on mineral surfaces, interactions between minerals and flotation reagents, and interactions between minerals. Flotation recovery and selectivity problems of sphalerite pure mineral in gypsum supersaturated process water have been identified.

2) Surface analysis methods are established to study the surface properties of minerals in a gypsum supersaturated environment. Through mineral surface

properties studies, questions regarding whether gypsum would scale on mineral surfaces has been clarified in model gypsum supersaturated solution system.

3) The poor flotation performance of sphalerite in the gypsum supersaturated process water has been determined to be attributed to the high calcium ion concentration in gypsum supersaturated process water. The high calcium ion concentration retards the activation of sphalerite and the sequence collector adsorption. Furthermore, the high calcium concentration in gypsum supersaturated process water induces the slime coating of fine gangue mineral particles (quartz) on sphalerite mineral surfaces.

4) A novel method of using a QCM-D to apply in-situ studies on mineral interactions under flotation related conditions has been developed in this thesis. It has been proven to be a powerful tool to investigate the homo-aggregation and hetero-aggregation for mineral systems.

5) This thesis developed a better understanding of the Zn flotation recovery and selectivity problems at Zinc mines operated in gypsum supersaturated process water. Potential approaches to mitigate the adverse impact of gypsum supersaturation in process water on sphalerite flotation have been proposed and evaluated.

7.3 Suggestions for future work

1) Study the gypsum scaling on silica and sphalerite minerals with the involvement of grinding process. It is possible that the grinding process generates surface active sites on mineral surface which can induce the nucleation of gypsum. Meanwhile, the temperature on mineral surfaces could change during grinding which can also trigger the nucleation of gypsum. It would be interesting to examine the mineral surfaces with SEM, XPS or Auger after grinding in gypsum supersaturated process water.

2) Research the gypsum scaling on silica and sphalerite mineral surfaces with the consideration of temperature. For example, characterize mineral surfaces after conditioning in gypsum supersaturated process water with the increase of temperature from 0 ^{o}C to 40 ^{o}C. QCM-D could be one of the best techniques to study the gypsum scaling on silica or sphalerite mineral surface under different temperature.

3) Investigate the impact of gypsum supersaturated process water on the electrochemical reactions on copper activated sphalerite mineral surface under flotation related conditions.

References

1. Espinosa-Gomez, R.; Finch, J. A.; Laplante, A. R., Effects of the type of water on the selective flotation of pyrochlore from niobec. *Colloids and Surfaces* **1987,** *26* (0), 333-350.

2. Rao, S. R.; Espinosa-Gomez, R.; Finch, J. A.; Biss, R., Effects of water chemistry on the flotation of pyrochlore and silicate minerals. *Minerals Engineering* **1988,** *1* (3), 189-202.

3. Rao, S. R.; Finch, J. A., A review of water re-use in flotation. *Minerals Engineering* **1989,** *2* (1), 65-85.

4. Ikumapayi, F.; Makitalo, M.; Johansson, B.; Rao, K. H., Recycling of process water in sulphide flotation: Effect of calcium and sulphate ions on flotation of galena. *Minerals Engineering* **2012,** *39*, 77-88.

5. Chen, J. m.; Liu, R. q.; Sun, W.; Qiu, G. z., Effect of mineral processing wastewater on flotation of sulfide minerals. *Transactions of Nonferrous Metals Society of China (English Edition)* **2009,** *19* (2), 454-457.

6. Farrokhpay, S.; Zanin, M., An investigation into the effect of water quality on froth stability. *Advanced Powder Technology* **2012,** *23* (4), 493-497.

7. Shackleton, N. J.; Malysiak, V.; De Vaux, D.; Plint, N., Water quality - A comparative study between moncheite and pentlandite in mixture with pyroxene. *Minerals Engineering* **2012,** *36-38*, 53-64.

8. Shackleton, N. J.; Malysiak, V.; De Vaux, D.; Plint, N., Effect of cations, anions, and ionic strength on the flotation of pentlandite-pyroxene mixtures. In *Water in Mineral Processing - Proceedings of the 1st International Symposium*, **2012**; pp 197-210.

9. Liu, D.; Somasundaran, P.; Vasudevan, T. V.; Harris, C. C., Role of pH and dissolved mineral species in Pittsburgh no. 8 coal flotation system - II. Separation of pyrite and non-pyritic minerals from coal. *International Journal of Mineral Processing* **1994,** *41* (3-4), 215-225.

10. Vasudevan, M.; Bhambhani, T.; Nagaraj, D. R.; Farinato, R. S., Impact of dissolved gangue species and fine colloidal matter in process water on flotation performance. In *Water in Mineral Processing - Proceedings of the 1st International Symposium*, **2012**; pp 247-259.

11. King, P. H.; Chu, A. M. W.; Chu, E. C. L.; Amy, G. L. *Reuse of municipal effluent in mineral flotation* **1983**.

12. Sekiguchi, I.; Fijigaki, S.; Yamaguchi, Y.; Takamori, T., Water recycling in mineral processing (1st report): continuous operation tests of closed circuit system *Nihon Kogyokaishi* **1984,** *100* (1152), 79-85.

13. Levay, G., Schumann, R. , A systematic approach to water quality management in the minerals processing industry. In *Proceeding of Water in Mining*, Melbourne, Australian, **2006**; pp 251-259.

14. Levay, G.; Smart, R. S. C.; Skinner, W. M., The impact of water quality on flotation performance. *Journal of The South African Institute of Mining and Metallurgy* **2001,** *101* (2), 69-75.

15. Schumann, R.; Levay, G.; Dunne, R.; Hart, S., Managing process water quality in base metal sufide flotation. In *Proceeding of Water in Mining*, Melbourne, **2003**; pp 251-259.

16. Coetzer, G.; Du Preez, H. S.; Bredenhann, R., Influence of water resources and metal ions on galena flotation of Rosh Pinah ore. *Journal of The South African Institute of Mining and Metallurgy* **2003,** *103* (3), 193-201.

17. Ozkan, S. G.; Acar, A., Investigation of impact of water type on borate ore flotation. *Water Research* **2004,** *38* (7), 1773-1778.

18. Broman, P. G., Water reuse at sulphide ore concentrators in Sweden: practice, experience and current developments. In *Complex Sulphide Ores Conference*, Rome, **1980**; pp 28-39.

19. Hoover, M. R., Water chemistry effects in the flotation of sulphide ores - a review and discussion for molybdenite. **1980**; pp 100-112.

20. Ikumapayi, F.; Makitalo, M.; Johansson, B.; Rao, K. H., Recycling process water in sulfide flotation, Part a: Effect of calcium and sulfate on sphalerite recovery. *Minerals and Metallurgical Processing* **2012,** *29* (4), 183-191.

21. Brown, E. T., Water for a sustainable minerals industry - A review. In *Proceedings Water in Mining*, The Australasian Institute of Mining and Metallurgy: Melbourne, **2003**; pp 3-14.

22. Bicak, O.; Ekmekci, Z.; Can, M.; Ozturk, Y., The effect of water chemistry on froth stability and surface chemistry of the flotation of a Cu-Zn sulfide ore. *International Journal of Mineral Processing* **2012,** *102-103*, 32-37.

23. Muzenda, E., An investigation into the effect of water quality on flotation performance. *Proceedings of World Academy of Science, Engineering and Technology* **2010,** *70*, 237-241.

24. Johnson, N. W., Issues in maximisation of recycling of water in a mineral processing plant. In *Proceedings Water in Mining*, The Australasian Institute of Mining and Metallurgy: Melbourne, **2003**; pp 239-246.

25. Liu, L.; Rao, S. R.; Finch, J. A., Technical note laboratory study of effect of recycle water on flotation of a Cu/Zn sulphide ore. *Minerals Engineering* **1993,** *6* (11), 1183-1190.

26. Grano, S. R.; Johnson, N. W.; Ralston, J., Control of the solution interaction of metabisulphite and ethyl xanthate in the flotation of the Hilton ore of Mount Isa Mines Limited, Australia. *Minerals Engineering* **1997,** *10* (1), 17-39.

27. Grano, S. R., Wong, P.L.M., Skinner, W., Johnson, N.W., Ralston, J. , Detection and control of calcium sulphate precipitation in the lead circuit of the Hilton concentrator of Mount Isa Mines Limited, Australia. In *XIX International Mineral Processing Conference*, Colorado, **1995**; Vol. 3, pp 171-179.

28. Grano, S. R.; Lauder, D. W.; Johnson, N. W.; Ralston, J., An investigation of galena recovery problems in the Hilton concentrator of Mount Isa mines limited, Australia. *Minerals Engineering* **1997,** *10* (10), 1139-1163.

29. Wei, Y.; Sandenbergh, R. F. In *Evaluation of absorbents as a means to control the influence of heavy metal ions on the flotation of a complex sulfide ore*, Brisbane, QLD, Australia, Australasian Institute of Mining and Metallurgy: Brisbane, QLD, Australia, **2005**; 1057-1063.

30. Beauchamp, R. M.; Choung, J. W.; Xu, Z., Mineral particles interactions in gypsum-supersaturated process water. In *The 6th UBC-McGill-UA International Symposium, 45th Annual Conference of Metallurgists of CIM*, Xu, Z.; Liu, Q., Eds. Montreal, **2006**; 101-116.

31. Woodcock, J. T., Jones, M. H. *Oxygen concentrations, redox potentials, xanthate residuals and other parameters in flotation plant pulps*; Institution of Mining and Metallurgy: London, **1970**; 439-468.

32. Rao, S. R., *Surface Chemistry of Froth Flotation*. Kluwer Academic/Plenum Publishers, New York: **2004**; Vol. 2.

33. Liu, Q.; Zhang, Y., Effect of calcium ions and citric acid on the flotation separation of chalcopyrite from galena using dextrin. *Minerals Engineering* **2000,** *13* (13), 1405-1416.

34. James, R. O.; Healy, T. W., Adsorption of hydrolyzable metal ions at the oxide-water interface. *Journal of Colloid and Interface Science* **1972,** *40* (1), 42-64.

35. Gandin, A. M.; Charles, W. D., Adsorption of calcium and sodium on pyrite. *Mining Engineering* **1953,** *5*, 195-200.

36. Moignard, M. S., James, R. O. Healy, T. W., Adsorption of calcium at the zinc sulphide-water interface. *Aust. J. Chem.* **1977,** (33), 733-740.

37. Rashchi, F.; Xu, Z.; Finch, J. A., Adsorption on silica in Pb- and Ca-SO_4-CO_3 systems. *Colloids and Surfaces A: Physicochemical and Engineering Aspects* **1998,** *132* (2-3), 159-171.

38. Sui, C.; Rashchi, F.; Xu, Z.; Kim, J.; Nesset, J. E.; Finch, J. A., Interactions in the sphalerite-Ca-SO_4-CO_3 systems. *Colloids and Surfaces A: Physicochemical and Engineering Aspects* **1998,** *137* (1-3), 69-77.

39. Lascelles, D.; Finch, J. A.; Sui, C., Depressant action of Ca and Mg on flotation of Cu activated sphalerite. *Canadian Metallurgical Quarterly* **2003,** *42* (2), 133-140.

40. DiFeo, A.; Finch, J. A.; Xu, Z., Sphalerite-silica interactions: Effect of pH and calcium ions. *International Journal of Mineral Processing* **2001,** *61* (1), 57-71.

41. Xu, Z.; Chi, R.; Difeo, T.; Finch, J. A., Surface forces between sphalerite and silica particles in aqueous solutions. *Journal of Adhesion Science and Technology* **2000,** *14* (14), 1813-1827.

42. Lauder, D. W.; Rohner, P.; Burford, B. D.; Johnson, N. W., Transfer of zinc from LGM concentrate to zinc concentrate at the Hilton concentrator of Mount Iso Mines Limited. *Proceedings of Australasian Institute of Mining and Metallurgy* **1994,** *2*, 14-20.

43. Cullinan, V. J. Improving the flotation response of fine galena. University of South Australia, **1999**.

44. Martell, A. E.; Smith, R. M., *Critical stability constants*. Plenum Press: New York, **1976**; Vol 4.

45. Nesset, J. E.; Sui, C.; Kim, J. Y.; Cooper, M.; Li, M.; Chryssoulis, S. L., The effect of soda ash and lime as pH modifiers in sphalerite flotation. In *30th Annual CMP Meeting*, Ottawa, **1998**; 460-481.

46. Fahiminia, F.; Watkinson, A. P.; Epstein, N., Early events in the precipitation fouling of calcium sulpfate dihydrate under sensible heating conditions. *Canadian Journal of Chemical Engineering* **2007,** *85* (5), 679-691.

47. Hoang, T. A.; Ang, H. M.; Rohl, A. L., Effects of temperature on the scaling of calcium sulphate in pipes. *Powder Technology* **2007,** *179* (1-2), 31-37.

48. Shams El Din, A. M.; El-Dahshan, M. E.; Mohammed, R. A., Scale formation in flash chambers of high-temperature MSF distillers. *Desalination* **2005,** *177* (1-3), 241-258.

49. Seewoo, S.; Van Hille, R.; Lewis, A., Aspects of gypsum precipitation in scaling waters. *Hydrometallurgy* **2004,** *75* (1-4), 135-146.

50. Greenlee, L. F.; Lawler, D. F.; Freeman, B. D.; Marrot, B.; Moulin, P., Reverse osmosis desalination: Water sources, technology, and today's challenges. *Water Research* **2009,** *43* (9), 2317-2348.

51. Hasson, D.; Drak, A.; Semiat, R., Inception of $CaSO_4$ scaling on RO membranes at various water recovery levels. *Desalination* **2001,** *139* (1-3), 73-81.

52. Lambert, B.; Schaffer, R. J., Studies of precipitated solids. Part II. Calcium sulphate. *Journal of the Chemical Society (Resumed)* **1926,** *129*, 2648-2655.

53. Sudmalis, M.; Sheikholeslami, R., Coprecipitation of $CaCO_3$ and $CaSO_4$. *Canadian Journal of Chemical Engineering* **2000,** *78* (1), 21-31.

54. Agamaliev, M. M.; Krikun, M. M.; Nasibov, A. G., Solubility of calcium sulphate in concentrates of mineralized waters. *Khimiya i Tekhnologiya Vody* **1993,** *15* (1), 44-50.

55. Dutrizac, J. E., Calcium sulphate solubilities in simulated zinc processing solutions. *Hydrometallurgy* **2002,** *65* (2-3), 109-135.

56. Flint, O., Increased solubility of calcium sulphate in sea water containing hydrochloric acid. *Desalination* **1968,** *4* (3), 328-335.

57. Furby, E.; Glueckauf, E.; McDonald, L. A., The solubility of calcium sulphate in sodium chloride and sea salt solutions. *Desalination* **1968,** *4* (2), 264-276.

58. Gardner, A. W.; Glueckauf, E., Thermodynamic data of the calcium sulphate solution process between 0 and 200 °C. *Transactions of the Faraday Society* **1970,** *66*, 1081-1086.

59. Klepetsanis, P. G.; Dalas, E.; Koutsoukos, P. G., Role of Temperature in the Spontaneous Precipitation of Calcium Sulfate Dihydrate. *Langmuir* **1999,** *15* (4), 1534-1540.

60. Alimi, F.; Elfil, H.; Gadri, A., Kinetics of the precipitation of calcium sulfate dihydrate in a desalination unit. *Desalination* **2003,** *158* (1-3), 9-16.

61. Randolph, A. D. *Calcium sulfite and calcium sulfate crystallization: final report. kinetics of calcium sulfite crystallization and predictions of crystal-size distribution*; 2; 1986.

62. Chong, T. H.; Sheikholeslami, R., Thermodynamics and kinetics for mixed calcium carbonate and calcium sulfate precipitation. *Chemical Engineering Science* **2001,** *56* (18), 5391-5400.

63. Feldmann, T.; Demopoulos, G. P., The crystal growth kinetics of alpha calcium sulfate hemihydrate in concentrated $CaCl_2$ - HCl solutions. *Journal of Crystal Growth* **2012,** *351* (1), 9-18.

64. Gill, J. S.; Nancollas, G. H., Kinetics of growth of calcium sulfate crystals at heated metal surfaces. *Journal of Crystal Growth* **1980,** *48* (1), 34-40.

65. Kan, A. T.; Fu, G.; Fan, C.; Tomson, M. B.; Shen, D., Quantitative evaluation of calcium sulfate precipitation kinetics in the presence and absence

of scale inhibitors. In *Proceedings - SPE International Symposium on Oilfield Chemistry*, 2009; Vol. 1, 485-503.

66. Klepetsanis, P. G.; Koutsoukos, P. G., Kinetics of calcium sulfate formation in aqueous media: Effect of organophosphorus compounds. *Journal of Crystal Growth* **1998,** *193* (1-2), 156-163.

67. Linnikov, O. D., Investigation of the initial period of sulphate scale formation. Part 1. Kinetics and mechanism of calcium sulphate surface nucleation at its crystallization on a heat-exchange surface. *Desalination* **1999,** *122* (1), 1-14.

68. Linnikov, O. D., Investigation of the initial period of sulphate scale formation Part 2. Kinetics of calcium sulphate crystal growth at its crystallization on a heat-exchange surface. *Desalination* **2000,** *128* (1), 35-46.

69. Liu, S. T.; Nancollas, G. H., The kinetics of crystal growth of calcium sulfate dihydrate. *Journal of Crystal Growth* **1970,** *6* (3), 281-289.

70. Sandhya, S.; Sureshbabu, S.; Varma, H. K.; Komath, M., Nucleation kinetics of the formation of low dimensional calcium sulfate dihydrate crystals in isopropyl alcohol medium. *Crystal Research and Technology* **2012,** *47* (7), 780-792.

71. Sheikholeslami, R.; Ong, H. W. K., Kinetics and thermodynamics of calcium carbonate and calcium sulfate at salinities up to 1.5 M. *Desalination* **2003,** *157* (1-3), 217-234.

72. Vainshtein, I. A.; Safullin, N. S.; Kudenko, G. A.; Luk'yanova, V. L., Kinetics of the controlled crystallization of clacium sulfate. *Journal of applied chemistry of the USSR* **1985,** *58* (9 pt 1), 1798-1802.

73. Amjad, Z., Calcium sulfate dihydrate (gypsum) scale formation on heat exchanger surfaces: The influence of scale inhibitors. *Journal of Colloid and Interface Science* **1988,** *123* (2), 523-536.

74. Farshad, F. F.; Linsley, J.; Kuznetsov, O.; Vargas, S., The effects of magnetic treatment on calcium sulfate scale formation. In *SPE Western Regional/AAPG Pacific Section Joint Meeting*, **2002**; 519-527.

75. Graham, G. M.; Boak, L. S.; Sorbie, K. S., Influence of formation calcium on the effectiveness of generically different barium sulphate oilfield scale inhibitors. In *Proceedings - SPE International Symposium on Oilfield Chemistry*, **1997**; 611-626.

76. Hoang, T. A.; Ang, H. M.; Rohl, A. L., Investigation into the effects of phosphonic inhibitors on the formation of calcium sulfate scales. *Desalination and Water Treatment* **2011,** *29* (1-3), 294-301.

77. Jamialahmadi, M.; Mueller-Steinhagen, H., Reduction of calcium sulfate scale formation during nucleate boiling by addition of EDTA. *Heat Transfer Engineering* **1991,** *12* (4), 19-26.

78. Linnikov, O. D.; Posbereznyi, V. L., Effect of ioms and paf-13A complexing agents on formation of calcium sulfate deposits during evaporation of mineralized water. *Soviet journal of water chemistry and technology* **1989,** *11* (2), 77-79.

79. Luo, K.; Li, C.; Xiang, L.; Li, H.; Ning, P., Influence of temperature and solution composition on the formation of calcium sulfates. *Particuology* **2010,** *8* (3), 240-244.

80. Martynowicz, E. T. M. J.; Witkamp, G. J.; Van Rosmalen, G. M., The effect of aluminium fluoride on the formation of calcium sulfate hydrates. *Hydrometallurgy* **1996,** *41* (2-3), 171-186.

81. Shimabayashi, S.; Nakagaki, M., Effect of chondroitin sulfate on the precipitate formation of calcium phosphate in water. *Chemical & pharmaceutical bulletin* **1985,** *33* (9), 3589-3594.

82. Tourneret, L.; Berger, F.; Mavon, C.; Chambaudet, A., Calcium sulphate formation during the heat-up period: Some essential parameters. *Applied Clay Science* **1999,** *14* (5-6), 299-317.

83. Le Gouellec, Y. A.; Elimelech, M., Calcium sulfate (gypsum) scaling in nanofiltration of agricultural drainage water. *Journal of Membrane Science* **2002,** *205* (1-2), 279-291.

84. Hoang, T. A.; Ang, H. M.; Rohl, A. L.; Jeffrey, M. I., A study of gypsum scale formation using quartz crystal microbalance. *Developments in Chemical Engineering and Mineral Processing* **2006,** *14* (1-2), 313-321.

85. Lin, N. H.; Shih, W.-Y.; Lyster, E.; Cohen, Y., Crystallization of calcium sulfate on polymeric surfaces. *Journal of Colloid and Interface Science* **2011,** *356* (2), 790-797.

86. Seidell, A.; Linke, W. F., *Solubilities: Inorganic and metal-organic compounds*. American Chemical Society: **1958**.

87. Marshall, W. L.; Slusher, R., Thermodynamics of calcium sulfate dihydrate in aqueous sodium chloride solutions, 0 - 110 °C. *Journal of Physical Chemistry* **1966,** *70* (12), 4015-4027.

88. Seidell, A., *Solubilities of Inorganic and Organic Compounds: A Compilation of Quantitative Solubility Data from the Periodical Literature*. D. Van Nostrand Company: **1919**.

89. Mersmann, A., *Crystallization Technology Handbook*. Marcel Dekker Inc.: New York, 2001.

90. Hina, A.; Nancollas, G. H., Precipitation and dissolution of alkaline earth sulfates: Kinetics and surface energy. *Reviews in Mineralogy and Geochemistry* **2000,** *40*, 276-301.

91. Zhang, J.; Nancollas, G. H., Mechanisms of growth and dissolution of sparingly soluble salts. *Reviews in Mineralogy and Geochemistry* **1990b,** (23), 365-396.

92. Gill, J. S.; Nancollas, G. H., The growth of gypsum crystals on barite and calcite. *Desalination* **1979,** *29* (3), 247-254.

93. Nielsen, A. E., *Kinetics of precipitation*. Pergamon Press: New York, **1964**.

94. Turnbull, D., Kinetics of solidification of supercooled liquid mercury droplets. *The Journal of Chemical Physics* **1952,** *20* (3), 411-424.

95. Wu, W.; Nancollas, G. H., Interfacial free energies and crystallization in aqueous media. *Journal of Colloid and Interface Science* **1996,** *182* (2), 365-373.

96. Van Oss, C. J., *Interfacial forces in aqueous media*. Taylor & Francis: **2006**.

97. Van Oss, C. J., Use of the combined Lifshitz-van der Waals and Lewis acid-base approaches in determining the apolar and polar contributions to surface and interfacial tensions and free energies. *Journal of Adhesion Science and Technology* **2002,** *16* (6), 669-677.

98. Van Oss, C. J.; Chaudhury, M. K.; Good, R. J., Interfacial Lifshitz-van der Waals and polar interactions in macroscopic systems. *Chemical Reviews* **1988,** *88* (6), 927-941.

99. Wu, W.; Giese Jr, R. F.; Van Oss, C. J., Evaluation of the Lifshitz-van der Waals/acid-base approach to determine surface tension components. *Langmuir* **1995,** *11* (1), 379-382.

100. Klassen, V. I.; Mokrousov, V. A., *An introduction to the theory of flotation*. Butterworths: 1963.

101. Dixon, D. R., Photochemical reactions at the ZnS-H_2O interface. *Transactions of the Society of Mining Engineers* **1975,** *258*, 81-88.

102. Maust, E. E.; Richardson, P. E., *Electrophysical considerations of the activation of sphalerite for flotation*. U.S. Dept. of the Interior, Bureau of Mines: **1976**; Vol. 8018.

103. King, R. P., *Principles of Flotation*. South African Institute of Mining and Metallurgy: Johannesburg, **1982**.

104. Finkelstein, N. P.; Allison, S. A., *The chemistry of activation, deactivation and depression in the flotation of zinc sulfide: a review*. New York, **1976**; Vol. 1, 414-457.

105. Finkelstein, N. P., The activation of sulphide minerals for flotation: A review. *International Journal of Mineral Processing* **1997,** *52* (2-3), 81-120.

106. Chandra, A. P.; Gerson, A. R., A review of the fundamental studies of the copper activation mechanisms for selective flotation of the sulfide minerals, sphalerite and pyrite. *Advances in Colloid and Interface Science* **2009,** *145* (1-2), 97-110.

107. Ralston, J.; Healy, T. W., Activation of zinc sulphide with Cu $^{2+}$, Cd $^{2+}$ and Pb $^{2+}$ - 1. activation in weakly acidic media. *International Journal of Mineral Processing* **1980,** *7* (3), 175-201.

108. Teng, F.; Liu, Q.; Zeng, H., In situ kinetic study of zinc sulfide activation using a quartz crystal microbalance with dissipation (QCM-D). *Journal of Colloid and Interface Science* **2012,** *368* (1), 512-520.

109. Jain, S.; Fuerstenau, D. W., *Flotation of Sulphide Minerals*. Elsevier: Amsterdam, 1985.

110. Girczys, J.; Laskowski, J.; Lekki, J., Copper activation studies with sphalerite. *Canadian Metallurgical Quarterly* **1972,** *11*, 553-558.

111. Laskowski, J. S.; Liu, Q.; Zhan, Y., Sphalerite activation: Flotation and electrokinetic studies. *Minerals Engineering* **1997,** *10* (8), 787-802.

112. Prestidge, C. A.; Skinner, W. M.; Ralston, J.; Smart, R. S. C., Copper(II) activation and cyanide deactivation of zinc sulphide under mildly alkaline conditions. *Applied Surface Science* **1997,** *108* (3), 333-344.

113. Gerson, A. R.; Lange, A. G.; Prince, K. E.; Smart, R. S. C., The mechanism of copper activation of sphalerite. *Applied Surface Science* **1999,** *137* (1-4), 207-223.

114. Pattrick, R. A. D.; England, K. E. R.; Charnock, J. M.; Mosselmans, J. F. W., Copper activation of sphalerite and its reaction with xanthate in relation to flotation: an X-ray absorption spectroscopy (reflection extended X-ray absorption fine structure) investigation. *International Journal of Mineral Processing* **1999,** *55* (4), 247-265.

115. Leppinen, J. O., FTIR and flotation investigation of the adsorption of ethyl xanthate on activated and non-activated sulfide minerals. *International Journal of Mineral Processing* **1990,** *30* (3-4), 245-263.

116. Popov, S. R.; Vučinić, D. R., The ethylxanthate adsorption on copper-activated sphalerite under flotation-related conditions in alkaline media. *International Journal of Mineral Processing* **1990,** *30* (3-4), 229-244.

117. Kartio, I. J.; Basilio, C. I.; Yoon, R. H., An XPS study of sphalerite activation by copper. *Langmuir* **1998,** *14* (18), 5274-5278.

118. Lascelles, D.; Sui, C. C.; Finch, J. A.; Butler, I. S., Copper ion mobility in sphalerite activation. *Colloids and Surfaces A: Physicochemical and Engineering Aspects* **2001,** *186* (3), 163-172.

119. Rashchi, F.; Sui, C.; Finch, J. A., Sphalerite activation and surface Pb ion concentration. *International Journal of Mineral Processing* **2002,** *67* (1-4), 43-58.

120. Sutherland, K. L.; Wark, I. W., *Principles of flotation*. Australasian Institute of Mining and Metallurgy: **1955**.

121. Steininger, J., The depression of sphalerite and pyrite by basic complexes of copper and sulfhydryl flotation collector. *Mining and Metallurgic Engineering* **1968,** (March), 34-14.

122. Solecki, J.; Komosa, A.; Szczypa, J., Copper ion activatin of synthetic sphalerite with various iron contents. *International Journal of Mineral Processing* **1979,** *6* (3), 221-228.

123. Szczypa, J.; Solecki, J.; Komosa, A., Effect of surface oxidation and iron contents on xanthate ions adsorption of synthetic sphalerites. *International Journal of Mineral Processing* **1980,** *7* (2), 151-157.

124. Boulton, A.; Fornasiero, D.; Ralston, J., Effect of iron content in sphalerite on flotation. *Minerals Engineering* **2005,** *18* (11), 1120-1122.

125. Harmer, S. L.; Mierczynska-Vasilev, A.; Beattie, D. A.; Shapter, J. G., The effect of bulk iron concentration and heterogeneities on the copper activation of sphalerite. *Minerals Engineering* **2008,** *21* (12-14), 1005-1012.

126. Hunter, R. J., *Zeta potential in colloid science: principles and applications*. Acadamic Press INC.: San Diego, 1981.

127. Hunter, R. J., *Foundations of colloid science*. Oxford University Press: New York, 2001.

128. Shaw, D. J., *Introduction to Colloid and Surface Chemistry*. 4th ed.; Butterworth Heinemann Publishing: 1992.

129. Liu, J.; Xu, Z.; Masliyah, J., Role of fine clays in bitumen extraction from oil sands. *AIChE Journal* **2004,** *50* (8), 1917-1927.

130. Liu, J.; Xu, Z.; Masliyah, J., Interaction between bitumen and fines in oil sands extraction system: Implication to bitumen recovery. *Canadian Journal of Chemical Engineering* **2004,** *82* (4), 655-666.

131. Liu, J.; Xu, Z.; Masliyah, J., Interaction forces in bitumen extraction from oil sands. *Journal of Colloid and Interface Science* **2005,** *287* (2), 507-520.

132. Liu, J.; Zhou, Z.; Xu, Z.; Masliyah, J., Bitumen-clay interactions in aqueous media studied by zeta potential distribution measurement. *Journal of Colloid and Interface Science* **2002,** *252* (2), 409-418.

133. Sauerbrey, G., Verwendung von Schwingquarzen zur Wägung dünner Schichten und zur Mikrowägung. *Zeitschrift für Physik* **1959,** *155* (2), 206-222.

134. Reviakine, I.; Johannsmann, D.; Richter, R. P., Hearing what you cannot see and visualizing what you hear: Interpreting quartz crystal microbalance data from solvated interfaces. *Analytical Chemistry* **2011,** *83* (23), 8838-8848.

135. Tellechea, E.; Johannsmann, D.; Steinmetz, N. F.; Richter, R. P.; Reviakine, I., Model-independent analysis of QCM data on colloidal particle adsorption. *Langmuir* **2009,** *25* (9), 5177-5184.

136. Du, B.; Johannsmann, D., Operation of the quartz crystal microbalance in liquids: Derivation of the elastic compliance of a film from the ratio of bandwidth shift and frequency shift. *Langmuir* **2004,** *20* (7), 2809-2812.

137. Fatisson, J.; Ghoshal, S.; Tufenkji, N., Deposition of carboxymethylcellulose-coated zero-valent iron nanoparticles onto silica: Roles of solution chemistry and organic molecules. *Langmuir* **2010,** *26* (15), 12832-12840.

138. Yi, P.; Chen, K. L., Influence of surface oxidation on the aggregation and deposition kinetics of multiwalled carbon nanotubes in monovalent and divalent electrolytes. *Langmuir* **2011,** *27* (7), 3588-3599.

139. Johannsmann, D.; Reviakine, I.; Richter, R. P., Dissipation in films of adsorbed nanospheres studied by quartz crystal microbalance (QCM). *Analytical Chemistry* **2009,** *81* (19), 8167-8176.

140. Kunze, M.; Shull, K. R.; Johannsmann, D., Quartz crystal microbalance studies of the contact between soft, viscoelastic solids. *Langmuir* **2006,** *22* (1), 169-173.

141. Vittorias, E.; Kappl, M.; Butt, H. J.; Johannsmann, D., Studying mechanical microcontacts of fine particles with the quartz crystal microbalance. *Powder Technology* **2010,** *203* (3), 489-502.

142. Johannsmann, D., Viscoelastic analysis of organic thin films on quartz resonators. *Macromolecular Chemistry and Physics* **1999,** *200* (3), 501-516.

143. Johannsmann, D.; Mathauer, K.; Wegner, G.; Knoll, W., Viscoelastic properties of thin films probed with a quartz-crystal resonator. *Physical Review B* **1992,** *46* (12), 7808-7815.

144. Johannsmann, D., Viscoelastic, mechanical, and dielectric measurements on complex samples with the quartz crystal microbalance. *Physical Chemistry Chemical Physics* **2008,** *10* (31), 4516-4534.

145. Sakai, K.; Smith, E. G.; Webber, G. B.; Baker, M.; Wanless, E. J.; Bütün, V.; Armes, S. P.; Biggs, S., Characterizing the pH-responsive behavior of thin films of

diblock copolymer micelles at the silica/aqueous solution interface. *Langmuir* **2006,** *22* (20), 8435-8442.

146. Irwin, E. F.; Ho, J. E.; Kane, S. R.; Healy, K. E., Analysis of interpenetrating polymer networks via quartz crystal microbalance with dissipation monitoring. *Langmuir* **2005,** *21* (12), 5529-5536.

147. Olanya, G.; Iruthayaraj, J.; Poptoshev, E.; Makuska, R.; Vareikis, A.; Claesson, P. M., Adsorption characteristics of bottle-brush polymers on silica: Effect of side chain and charge density. *Langmuir* **2008,** *24* (10), 5341-5349.

148. Nguyen, T. H.; Elimelech, M., Adsorption of plasmid DNA to a natural organic matter-coated silica surface: Kinetics, conformation, and reversibility. *Langmuir* **2007,** *23* (6), 3273-3279.

149. Xu, J.; Liu, K. W.; Matthews, K. S.; Biswal, S. L., Monitoring DNA binding to Escherichia coli lactose repressor using quartz crystal microbalance with dissipation. *Langmuir* **2011,** *27* (8), 4900-4905.

150. Kaufman, E. D.; Belyea, J.; Johnson, M. C.; Nicholson, Z. M.; Ricks, J. L.; Shah, P. K.; Bayless, M.; Pettersson, T.; Feldotö, Z.; Blomberg, E.; Claesson, P.; Franzen, S., Probing protein adsorption onto mercaptoundecanoic acid stabilized gold nanoparticles and surfaces by quartz crystal microbalance and zeta-potential measurements. *Langmuir* **2007,** *23* (11), 6053-6062.

151. Fraser, S. J.; Mulet, X.; Martin, L.; Praporski, S.; Mechler, A.; Hartley, P. G.; Polyzos, A.; Separovic, F., Surface immobilization of bio-functionalized cubosomes: Sensing of proteins by quartz crystal microbalance. *Langmuir* **2012,** *28* (1), 620-627.

152. Fatisson, M.; Domingos, R. F.; Wilkinson, K. J.; Tufenkji, N., Deposition of TiO_2 nanoparticles onto silica measured using a quartz crystal microbalance with dissipation monitoring. *Langmuir* **2009,** *25* (11), 6062-6069.

153. Jiang, X.; Tong, M.; Li, H.; Yang, K., Deposition kinetics of zinc oxide nanoparticles on natural organic matter coated silica surfaces. *Journal of Colloid and Interface Science* **2010,** *350* (2), 427-434.

154. Pomorska, A.; Shchukin, D.; Hammond, R.; Cooper, M. A.; Grundmeier, G.; Johannsmann, D., Positive frequency shifts observed upon adsorbing micron-sized solid objects to a quartz crystal microbalance from the liquid phase. *Analytical Chemistry* **2010,** *82* (6), 2237-2242.

155. Bining, G.; Rohrer, H., Scanning tunneling microscopy. *Helvetica Physica Acta* **1982,** (55), 726-735.

156. Binnig, G.; Quate, C. F.; Gerber, C., Atomic force microscope. *Physical Review Letters* **1986,** *56* (9), 930-933.

157. Ducker, W. A.; Senden, T. J.; Pashley, R. M., Direct measurement of colloidal forces using an atomic force microscope. *Nature* **1991,** *353* (6341), 239-241.

158. Ducker, W. A.; Senden, T. J.; Pashley, R. M., Measurement of forces in liquids using a force microscope. *Langmuir* **1992,** *8* (7), 1831-1836.

159. Israelachvili, J. N., *Intermolecular and Surface Forces: Revised Third Edition*. Elsevier Science: 2011.

160. Hunter, R. J., *Introduction to modern colloid science*. Oxford University Press: 1994.

161. Cao, M.; Liu, Q., Reexamining the functions of zinc sulfate as a selective depressant in differential sulfide flotation - The role of coagulation. *Journal of Colloid and Interface Science* **2006,** *301* (2), 523-531.

162. Duarte, A. C. P.; Grano, S. R., Mechanism for the recovery of silicate gangue minerals in the flotation of ultrafine sphalerite. *Minerals Engineering* **2007,** *20* (8), 766-775.

163. Kaggwa, G. B.; Nalam, P. C.; Kilpatrick, J. I.; Spencer, N. D.; Jarvis, S. P., Impact of hydrophilic/hydrophobic surface chemistry on hydration forces in the absence of confinement. *Langmuir* **2012,** *28* (16), 6589-6594.

164. Kralchevsky, P. A.; Danov, K. D.; Basheva, E. S., Hydration force due to the reduced screening of the electrostatic repulsion in few-nanometer-thick films. *Current Opinion in Colloid and Interface Science* **2011,** *16* (6), 517-524.

165. Leng, Y., Hydration force between mica surfaces in aqueous KCl electrolyte solution. *Langmuir* **2012,** *28* (12), 5339-5349.

166. Pashley, R. M.; Quirk, J. P., The effect of cation valency on DLVO and hydration forces between macroscopic sheets of muscovite mica in relation to clay swelling. *Colloids and Surfaces* **1984,** *9* (1), 1-17.

167. Valle-Delgado, J. J.; Molina-Bolívar, J. A.; Galisteo-González, F.; Gálvez-Ruiz, M. J.; Feiler, A.; Rutland, M. W., Hydration forces between silica surfaces: Experimental data and predictions from different theories. *Journal of Chemical Physics* **2005,** *123* (3).

168. Yoon, R. H.; Vivek, S., Effects of short-chain alcohols and pyridine on the hydration forces between silica surfaces. *Journal of Colloid and Interface Science* **1998,** *204* (1), 179-186.

169. Hina, A.; Nancollas, G. H.; Grynpas, M., Surface induced constant composition crystal growth kinetics studies. The brushite-gypsum system. *Journal of Crystal Growth* **2001,** *223* (1-2), 213-224.

170. Tao, J.; Pan, H.; Zhai, H.; Wang, J.; Li, L.; Wu, J.; Jiang, W.; Xu, X.; Tang, R., Controls of tricalcium phosphate single-crystal formation from its amorphous precursor by interfacial energy. *Crystal Growth and Design* **2009,** *9* (7), 3154-3160.

171. van Oss, C. J., Acid-base interfacial interactions in aqueous media. *Colloids and Surfaces A: Physicochemical and Engineering Aspects* **1993,** *78* (C), 1-49.

172. Teng, F. Understanding zinc sulfide activation mechanism and impact of calcium sulfate in sphalerite flotation. MR89982, University of Alberta (Canada), Ann Arbor, 2012.

173. Fuerstenau, D. W., Activation and deactivation in the flotation of sulfide minerals. *Information Circular - United States, Bureau of Mines* **1980**, 100-120.

174. Kivitova, N. V.; Eliseev, N. I.; Kal'nishevskaya, L. N., Special features of the activation of sphalerite in copper sulfate solutions. *Izvestiya Vysshikh Uchebnykh Zavedenij. Tsvetnaya Metallurgiya* **1987,** (1), 12-16.

175. Plichon, V.; Rollat, N., Application of mirage spectroscopy: Zinc sulphide activation by copper ions used in flotation processing. *International Journal of Mineral Processing* **1990,** *28* (1-2), 99-108.

176. Ralston, J.; Healy, T. W., Activation of zinc sulphide with Cu $^{2+}$, Cd $^{2+}$ and Pb $^{2+}$ - 2. activation in neutral and weakly alkaline media. *International Journal of Mineral Processing* **1980,** *7* (3), 203-217.

177. Sui, C. C.; Lee, D.; Casuge, A.; Finch, J. A., Comparison of the activation of sphalerite by copper and lead. *Minerals and Metallurgical Processing* **1999,** *16* (3), 53-61.

178. Wark, E. E.; Wark, I. W., The physical chemistry of flotation. VIII: The process of activation. *Journal of Physical Chemistry* **1936,** *40* (6), 799-810.

179. Duran, J. D. G.; Guindo, M. C.; Delgado, A. V.; Gonzalez-Caballero, F., Stability of monodisperse zinc sulfide colloidal dispersions. *Langmuir* **1995,** *11* (10), 3648-3655.

180. Fornasiero, D.; Ralston, J., Effect of surface oxide/hydroxide products on the collectorless flotation of copper-activated sphalerite. *International Journal of Mineral Processing* **2006,** *78* (4), 231-237.

181. Kuyumcu, H. Z.; Pinka, J.; Bielig, T., A novel process for sorting fine-sized sulphide minerals by biocoagulation. *Transactions of Nonferrous Metals Society of China (English Edition)* **2008,** *18* (6), 1473-1479.

182. Wang, D. Z.; Hu, Y. H., *Solution Cheminstry of Flotation*. Hunan science and technology publisher Changsha, **1988**.

183. Vergouw, J. M.; Difeo, A.; Xu, Z.; Finch, J. A., An agglomeration study of sulphide minerals using zeta potential and settling rate. Part II: Sphalerite/pyrite and sphalerite/galena. *Minerals Engineering* **1998,** *11* (7), 605-614.

184. Vergouw, J. M.; Difeo, A.; Xu, Z.; Finch, J. A., An agglomeration study of sulphide minerals using zeta-potential and settling rate. Part I: Pyrite and galena. *Minerals Engineering* **1998,** *11* (2), 159-169.

185. Xu, Z.; Liu, J.; Choung, J. W.; Zhou, Z., Electrokinetic study of clay interactions with coal in flotation. *International Journal of Mineral Processing* **2003,** *68* (1-4), 183-196.

186. Ametov, I.; Prestidge, C. A., Hydrophobic interactions in concentrated colloidal suspensions: A rheological investigation. *Journal of Physical Chemistry B* **2004,** *108* (32), 12116-12122.

187. Muster, T. H.; Toikka, G.; Hayes, R. A.; Prestidge, C. A.; Ralston, J., Interactions between zinc sulphide particles under flotation-related conditions. *Colloids and Surfaces A: Physicochemical and Engineering Aspects* **1996,** *106* (2-3), 203-211.

188. Prestidge, C. A., Rheological investigations of galena particle interactions. *Colloids and Surfaces A: Physicochemical and Engineering Aspects* **1997,** *126* (2-3), 75-83.

189. Muster, T. H.; Prestidge, C. A., Rheological investigations of sulphide mineral slurries. *Minerals Engineering* **1995,** *8* (12), 1541-1555.

190. Prestidge, C. A., Rheological investigations of ultrafine galena particle slurries under flotation-related conditions. *International Journal of Mineral Processing* **1997,** *51* (1-4), 241-254.

191. El-Ammouri, E.; Mirnezami, M.; Lascelles, D.; Finch, J. A., Aggregation index and a methodology to study role of magnesium in aggregation of sulphide slurries. *CIM Bulletin* **2002,** *95* (1066), 67-72.

192. Mirnezami, M.; Restrepo, L.; Finch, J. A., Aggregation of sphalerite: Role of zinc ions. *Journal of Colloid and Interface Science* **2003,** *259* (1), 36-42.

193. Lange, A. G.; Skinner, W. M.; Smart, R. S. C., Fine:Coarse particle interactions and aggregation in sphalerite flotation. *Minerals Engineering* **1997,** *10* (7), 681-693.

194. Franks, G. V.; Li, H.; O'Shea, J. P.; Qiao, G. G., Temperature responsive polymers as multiple function reagents in mineral processing. *Advanced Powder Technology* **2009,** *20* (3), 273-279.

195. Atkins, D. T.; Pashley, R. M., Surface forces between ZnS and mica in aqueous electrolytes. *Langmuir* **1993,** *9* (8), 2232-2236.

196. Liu, J.; Xu, Z., Role of flotation reagents in tuning colloidal forces for sphalerite-silica separation. *Canadian Metallurgical Quarterly* **2007,** *46* (3), 329-340.

197. Toikka, G.; Hayes, R. A.; Ralston, J., Surface forces between spherical ZnS particles in aqueous electrolyte. *Langmuir* **1996,** *12* (16), 3783-3788.

198. Toikka, G.; Hayes, R. A.; Ralston, J., Surface forces between zinc sulfide and silica in aqueous electrolyte. *Colloids and Surfaces A: Physicochemical and Engineering Aspects* **1998,** *141* (1), 3-8.

199. Xu, D.; Hodges, C.; Ding, Y.; Biggs, S.; Brooker, A.; York, D., Adsorption kinetics of laponite and ludox silica nanoparticles onto a deposited poly(diallyldimethylammonium chloride) layer measured by a quartz crystal microbalance and optical reflectometry. *Langmuir* **2010,** *26* (23), 18105-18112.

200. Dybwad, G. L., A sensitive new method for the determination of adhesive bonding between a particle and a substrate. *Journal of Applied Physics* **1985,** *58* (7), 2789-2790.

201. Ren, H.; Ning, J.; Song, G., Study on the interaction in Silica-Sphalerite-Mixture (Silica:Sphalerite = 4:1)-calcium carbonate systems. *Advanced Materials Research* **2012,** *524-527*, 1105-1108.

202. Ren, H.; Song, G.; Ji, F., Effect on electrochemical properties for calcium ions in Silica-Sphalerite-Mixture (Silica: Sphalerite = 4:1) systems. *Advanced Materials Research* **2012,** *524-527*, 971-974.

203. Ren, H.; Yang, X.; Song, G., Study on the interaction in Silica-Sphalerite-Mixture (Silica:Sphalerite = 4:1)-Gypsum systems. *Advanced Materials Research* **2012,** *524-527*, 1101-1104.

204. Quevedo, I. R.; Olsson, A. L. J.; Tufenkji, N., Deposition kinetics of quantum dots and polystyrene latex nanoparticles onto alumina: Role of water chemistry and particle coating. *Environmental Science and Technology* **2013,** *47* (5), 2212-2220.

205. Liu, X.; Chen, G.; Su, C., Influence of collector surface composition and water chemistry on the deposition of cerium dioxide nanoparticles: QCM-D and column experiment approaches. *Environmental Science and Technology* **2012,** *46* (12), 6681-6688.

206. Alagha, L.; Wang, S.; Xu, Z.; Masliyah, J., Adsorption kinetics of a novel organic-inorganic hybrid polymer on silica and alumina studied by quartz crystal microbalance. *Journal of Physical Chemistry C* **2011,** *115* (31), 15390-15402.

207. Alagha, L.; Wang, S.; Yan, L.; Xu, Z.; Masliyah, J., Probing adsorption of polyacrylamide-based polymers on anisotropic basal planes of kaolinite using quartz crystal microbalance. *Langmuir* **2013,** *29* (12), 3989-3998.

208. Hook, F.; Rodahl, M.; Brzezinski, P.; Kasemo, B., Energy dissipation kinetics for protein and antibody-antigen adsorption under shear oscillation on a quartz crystal microbalance. *Langmuir* **1998,** *14* (4), 729-734.

209. Hook, F.; Brzezinski, P.; Rodahl, M.; Kasemo, B. *Structural changes in hemoglobin during adsorption to solid surfaces: Effects of pH, ionic strength and ligand binding*; 1997.

210. Plunkett, M. A.; Wang, Z.; Rutland, M. W.; Johannsmann, D., Adsorption of pNIPAM layers on hydrophobic gold surfaces, measured in situ by QCM and SPR. *Langmuir* **2003,** *19* (17), 6837-6844.

211. Nypelö, T.; Pynnönen, H.; Österberg, M.; Paltakari, J.; Laine, J., Interactions between inorganic nanoparticles and cellulose nanofibrils. *Cellulose* **2012,** *19* (3), 779-792.